INVESTIGATING THE EFFECT OF CHRONIC MUSCLE USE AND DISUSE ON INNATE IMMUNE SIGNALING IN SKELETAL MUSCLE

PRIYANKA KHEMRAJ

A THESIS SUBMITTED TO THE FACULTY OF GRADUATE STUDIES IN PARTIAL FULFILLMENT OF THE REQUIREMENTS FOR THE DEGREE OF

MASTER OF SCIENCE

GRADUATE PROGRAM IN KINESIOLOGY AND HEALTH SCIENCE

YORK UNIVERSITY

TORONTO, ONTARIO

OCTOBER 2024

ABSTRACT

Skeletal muscle health is highly dependent on the intricate mitochondrial reticulum that exhibits high levels of adaptability. It is now recognized that mitochondrial perturbations can activate innate immune pathways, such as the NLRP3 inflammasome complex, by augmenting the response against damage-associated molecular patterns (DAMPs). The objective of this study was to investigate how various metabolic conditions affect innate immune activation and mitochondrial health within skeletal muscle, which has not been fully elucidated. To investigate this, we assessed innate immune signaling pathways and mitochondrial parameters within a model of muscle denervation and an aging model combined with endurance training. Our results suggest that NLRP3 inflammasome signaling is responsive to alterations in skeletal muscle activity and can be attenuated with chronic endurance training. Furthermore, we highlight a differential response to exercise with aged muscle in innate immune signaling. This work aims to further the understanding of innate immune signaling pathways within skeletal muscle, which can potentially highlight therapeutic targets to regulate its activation under divergent metabolic conditions.

ACKNOWLEDGEMENTS

First and foremost, I would like to dedicate this master's thesis to my incredible parents. Mom and Dad, thank you for being my biggest cheerleaders and encouraging me to follow all my dreams and aspirations. Your belief in me and immense support has shaped who I am today, and for that, I will always consider myself lucky.

To my brothers Ravi, Suneal, and Ajay. Thank you for being the best role models that I could ask for and continuing to inspire me every step of the way. You all have always shown me the value of hard work while also finding the fun in every opportunity. To Dushinka and Hinal, thank you for being the most amazing sisters and helping me grow into the person I am today.

To my supervisor, Dr. David Hood, thank you for everything. Entering my MSc., I could not have predicted all the amazing opportunities and personal growth that I have gained throughout the past two years. I want to thank you for your unwavering mentorship and for always pushing me to strive for excellence, which I will keep with me in all my future endeavors.

To all my wonderful friends who have supported me through this journey. To my Skype Sisters, Sarrah and Sanjani, thank you for always listening to my long conference presentations and endless lab stories. Last but most definitely not least, to my amazing lab mates. I want to thank all of you for your continuous support and assistance which has made this journey truly memorable. I am privileged to have worked alongside such an amazing group of people, and I look forward to seeing all the incredible achievements you will all accomplish in your bright futures. To Sabrina and Victoria, my Hood Rats, thank you for becoming my home away from home over the past two years. From our snack runs to conference adventures and research discussions, you guys were always there to help me grow as a scientist while also filling the journey with laughter along the way. I will always cherish the bonds that we have formed, and I look forward to our future adventures.

TABLE OF CONTENTS

LIST OF FIGURES

CHAPTER 1: REVIEW OF LITERATURE

CHAPTER 2: MANUSCRIPT

APPENDIX B: SUPPLEMENTARY DATA

LIST OF TABLES

CHAPTER 2: MANUSCRIPT

APPENDIX A: SAMPLE DATA AND STATISTICAL ANALYSES

DENERVATION STUDY

LIST OF ABBREVIATIONS

ΔΨ	Mitochondrial membrane potential
4-HNE	4-hydroxynoneal
8-OHdG	8-hydroxy-2′-deoxyguanosine
ADP	Adenosine diphosphate
AIF	Apoptosis Inducing Factor
AMP	Adenosine monophosphate
AMPK	AMP-activated protein kinase
ANOVA	Analysis of variance
ANT	Adenine Nucleotide Translocator
ASC	Apoptosis-associated speck-like protein
ATP	Adenosine triphosphate
BMDM	Bone-marrow derived macrophages
BNIP3	BCL2/adenovirus E1B 19-kDa protein-interacting protein 3
CaMK	$Ca^{2+/}$calmodulin-dependent protein kinase
CARD	Caspase activation and recruitment domain
CCA	Chronic contractile activity
CLR	C-type lectin receptors
cGAS	Cyclic GMP-AMP synthase
cGAMP	Cyclic guanosine monophosphate–adenosine monophosphate
COPII	Coatomer protein complex II
COX	Cytochrome c oxidase
COX-I	Cytochrome c oxidase subunit I
COX-IV	Cytochrome c oxidase subunit IV
Cyto	Cytosolic
DAMP	Damage-associated molecular pattern
Den	Denervation
DNA	Deoxyribonucleic acid
dsDNA	Double-stranded DNA
DRP1	Dynamin-related protein 1
EDL	Extensor digitorum longus
ETC	Electron Transport Chain
FIS1	Mitochondrial fission 1
FUNDC1	Fun14 domain containing 1
GAPDH	Glyceraldehyde-3-Phosphate Dehydrogenase
GSDMD	Gasdermin-D
GSDMD-N	Gasdermin-D N-terminal fragment
GTPase	Guanine nucleotide-binding proteins
H_2O_2	Hydrogen Peroxide
IL-1β	Interleukin-1β
IL-6	Interleukin 6
IMF	Intermyofibrillar
IRF	Interferon-regulatory factor
KO	Knockout
kDa	Kilodaltons
LC3-II	Microtubule-associated proteins 1A/1B light chain 3A II

LPS	Lipopolysaccharide
LRR	Leucine-Rich Repeat
mtDAMP	Mitochondrial DAMP
mtDNA	Mitochondrial DNA
mPTP	Mitochondrial permeability transition pore
mtROS	Mitochondrial-derived Reactive Oxygen Species
Mfn1/2	Mitofusin-1/2
NACHT	Central nucleotide-binding and oligomerization domain
NF-κB	Nuclear factor-kappa B
NLR	NOD-like receptor
NLRP3	NOD-like Receptor Pyrin Domain Containing 3
NOD	Nucleotide-binding oligomerization domain-like receptors
NOX	NADPH Oxidases
NRF-1	Nuclear Respiratory Factor-1
NuGEMPs	Nuclear genes encoding mitochondrial proteins
O^{2-}	Superoxide Anion
OH^{-}	Hydroxyl radical
OPA1	Optic Atrophy 1
p38 MAPK	p38 mitogen-activated protein kinase
PAMP	Pathogen-associated molecular pattern
PRR	Pattern Recognition Receptor
PGC-1α	Peroxisome Proliferator-activated receptor-gamma coactivator
PINK1	PTEN-induced putative kinase 1
PPARγ	Peroxisome proliferator-activated receptor γ
PYD	Pyrin Domain
qPCR	Quantitative polymerase chain reaction
RLR	Rig-I-like receptor
ROS	Reactive oxygen species
RNA	Ribonucleic Acid
rRNA	Ribosomal RNA
RyR1	Ryanodine Receptor 1
SS	Subsarcolemmal
STING	Stimulator of interferon genes
TA	Tibialis Anterior
TBK1	Tank-binding kinase 1
TCA	Tricarboxylic Acid Cycle
TFAM	Mitochondrial Transcription Factor A
TFEB	Transcription factor EB
TLR	Toll-like receptor
TNF-α	Tumor Necrosis Factor-α
tRNA	Transfer RNA
TXNIP	Thioredoxin-Interacting Protein
VDAC	Voltage-dependent anion channel
VWR	Voluntary Wheel Running
WT	Wild type

CHAPTER 1: REVIEW OF LITERATURE

1. Skeletal Muscle Physiology

1.1. Skeletal Muscle Structure and Function

Skeletal muscle is a dynamic organ that comprises approximately 40% of total body mass and plays an essential role in many functions including locomotion, whole-body metabolism, and force production (1). At the micro level, a well-established characteristic of skeletal muscle is the highly organized arrangement of multinucleated myofibers, contributing to its striated appearance. Each myofiber is comprised of adjacent sarcomeres, which serve as the functional unit of muscle by facilitating muscle excitability and contractility (1). Following an excitatory stimulus, action potentials are propagated through the neuromuscular junction and along the sarcolemmal membrane, which subsequently promotes free calcium release from the sarcoplasmic reticulum into the intramuscular space through ryanodine receptor 1 (RyR1). Through the process termed "excitation-contraction coupling", calcium release and ATP hydrolysis promote the formation of actin-myosin cross bridges, which ultimately allows sarcomere shortening and muscle contraction (1). Once the excitatory action potential subsides, the reuptake of calcium into the sarcoplasmic reticulum through passive diffusion or active calcium pumps, facilitates muscle relaxation (1).

1.2. Skeletal Muscle Fiber Types

While the process of muscle contraction is fundamentally similar within skeletal muscle, many other factors can influence the biochemical and contractile characteristics of a myofiber. As a result, skeletal muscle can be classified as either slow-twitch or fast-twitch, depending on their functional properties. Type I fibers or slow-twitch oxidative muscle fibers contain large volumes of mitochondria which leads to a highly oxidative muscle phenotype characterized by increased aerobic respiration and fatigue resistance. However, type I fibers also possess a small cross-sectional area and motor unit size, which allows for easy recruitment but reduces the maximal

force production. Skeletal muscle also contains fast-twitch muscle fibers which can be further divided into two categories: fast-twitch oxidative (Type IIa) and fast-twitch glycolytic (Type IIb/x). In contrast to type I fibers, Type IIb/x fibers have large cross-sectional areas and motor unit sizes, which facilitates high force production and rapid contractility. However, due to their low mitochondrial volume, they possess an increased reliance on glycolytic respiration and are highly fatigable. Type IIa fibers express intermediate characteristics that fall between the Type I and Type IIb/x extremes (2). The overall phenotype of a particular muscle is dependent on its relative composition of muscle fibers. Glycolytic muscles such as the quadriceps produce large amounts of power due to the high percentage of Type IIx fibers, while highly oxidative muscles such as the soleus are primarily comprised of Type I fibers. The proportions of these myofibers determine the aerobic capacity and force capacity of the muscle and play a role in adaptations to chronic use and disuse. In general, chronic endurance training induces a shift in the fiber type makeup towards a more oxidative composition that is characterized by a large increase in Type I fibers relative to the changes in Type II fibers, resulting in a larger type I/II ratio (3). On the other hand, disuse stimuli such as aging lead to detriments in muscle force production and myofiber size, particularly affecting Type II fibers (4, 5).

2. Skeletal Muscle Mitochondria

2.1. Mitochondrial Structure and Function

In addition to its contractile properties, skeletal muscle is being increasingly investigated in its ability to adapt to various metabolic demands, which can be partially attributed to the complex network of mitochondria that strongly regulate muscle metabolism. Mitochondria, commonly referred to as the powerhouse of the cell, are metabolic hubs that regulate a multitude of diverse functions including energy production, calcium handling, and apoptotic signaling (6). Diverse

tissues and cell types rely on mitochondria for energy turnover as the site of metabolic processes including the tricarboxylic acid cycle (TCA), β-oxidation and aerobic respiration. The organelle is comprised of a double-membrane system, resulting in the compartmentalization of various spaces within the mitochondria that each contribute to its tightly regulated function (7). While the outer mitochondrial membrane is highly permeable and allows the free movement of small molecules into the intermembrane space, the inner mitochondrial membrane is highly selective and organized into dense cristae that are critical to mitochondrial function and energy production (7). Due to the tightly regulated movement of ions across the inner membrane, an electrochemical gradient is established between the intermembrane space and the enclosed mitochondrial matrix, which facilitates processes such as the import of nuclear-encoded proteins and aerobic respiration via the electron transport chain (ETC) (6, 8). The ETC is comprised of four multiprotein complexes (Complex I, II, III, and IV) that are bound to the inner membrane of the mitochondria and two mobile electron carriers (Cytochrome C and Ubiquinone) found within the intermembrane space. In a controlled manner, electrons are shuttled through the four protein complexes through a series of redox reactions, until they are ultimately reduced to H_2O at Complex IV by consuming O_2. Importantly, electron movement is coupled to the pumping of protons into the intermembrane space at complexes I, III, and IV, which generates a negative membrane potential within the mitochondrial matrix. This established proton gradient is essential to energy production, as it drives the process of chemiosmosis and promotes the synthesis of the cellular currency ATP, at Complex V (9).

Due to the multifaceted functions of mitochondria in adapting to specific cellular demands, mitochondrial morphology can vary depending on the tissue type or location within the cell. Skeletal muscle mitochondria often exist in a networked reticulum, that is further classified into

two subpopulations that differ in both structural and biochemical properties (10, 11). Subsarcolemmal (SS) mitochondria are closely localized beneath the sarcolemmal membrane, exhibiting a rounded and compact structure. Due to their location, SS mitochondria are often implicated in supplying energy to membrane-related processes such as protein import and assembly, and channel-mediated ion transport (12). In contrast, intermyofibrillar (IMF) mitochondria are located between the myofibrils and exhibit a networked phenotype, enabling them to provide ATP to sustain skeletal muscle contraction (12).

2.2. Reactive Oxygen Species (ROS)

Reactive oxygen species (ROS) are highly reactive, unstable molecules that contain oxygen. They can be categorized as either radical oxygen species including superoxide anions (O^{2-}) and hydroxyl radicals (OH^{-}), or non-radical oxygen derivatives such as hydrogen peroxide (H_2O_2) (13). Throughout the 1980s, the production of ROS was exclusively considered a cytotoxic stressor due to its implications in various pathologies, however, later works began to highlight the generation of ROS as potentially beneficial signaling molecules that could influence skeletal muscle adaptations (14, 15). In 1982, Davies et al. demonstrated that the production of excessive ROS and free radicals from skeletal muscle following exhaustive exercise contributed to impaired mitochondrial function through the oxidation of cellular components such as lipids and proteins (16). This work emphasized the importance of controlling ROS production to yield beneficial adaptations, while also mitigating the harmful consequences of excessive oxidative stress. It is now well-known that ROS can be endogenously generated from various sources within skeletal muscle including NADPH oxidases (NOX) and the mitochondria. The ETC has been implicated as a major producer of O^{2-}, which can occur in response to increased backpressure on the ETC during both active and basal respiration, leading to electron leakage from the respiratory

complexes or promoting the incomplete reduction of oxygen within the terminal step of aerobic respiration (13, 17, 18). Catalyzed by superoxide dismutase or spontaneously produced, O^{2-} can then be converted into H_2O_2, which serves as a commonly used measure of ROS production in practical experimental analysis. Within muscle, ROS can act as an important second messenger through the regulation of cellular kinases such as the p38 MAPKs, which is involved in mitochondrial biogenesis and apoptotic signaling. Furthermore, this can also propagate inflammatory signaling through the positive and negative regulation of the transcription factor NF-κB, by directly influencing its nuclear translocation and DNA-binding affinity (19, 20). Due to their high reactivity, ROS can also oxidize various biomolecules including lipids, proteins, and DNA. For example, free radicals can target various membrane phospholipids leading to the accumulation of lipid peroxidation byproducts such as 4-hydroxynoneal (4-HNE), which has been shown to form covalent adducts to induce protein and skeletal muscle dysfunction (21, 22). Furthermore, ROS has also been shown to oxidize nucleic acids such as mtDNA, which is especially susceptible to oxidative damage due to the lack of protective histones. This can lead to mtDNA mutations and the propagation of several pro-inflammatory pathways through the release of oxidized mtDNA (23, 24).

2.3. The Mitochondrial Genome

Apart from its structural qualities, mitochondria uniquely possess their own genome which is independent of the nuclear genome. This discovery was first made in 1963 through electron microscopy when fibrous structures were identified within the mitochondrion that were structurally similar to nucleic acid structures (25). Shortly after in 1967, Margulis introduced what is now called the endosymbiotic theory of mitochondrial origin, which suggested that mitochondria originally existed as free-living prokaryotic cells that eventually developed a mutually beneficial

relationship with eukaryotic cells (26). Following its complete sequencing in 1981, mtDNA has been identified as circular double-stranded DNA that is approximately 16.6kb in size and is often differentiated from the nuclear genome due to an absence of histones and introns. It contains 37 genes, encoding 22 tRNAs, 2 rRNAs, and 13 protein subunits of the electron transport chain that work in conjunction with the nuclear-encoded proteins to support mitochondrial functioning (27). A commonly recognized nuclear-encoded protein is TFAM, which is highly involved in several aspects of mtDNA processing. TFAM has been shown to play an essential role in the compacting of mtDNA into protein-DNA complexes termed mitochondrial nucleoids, which allows for improved stability and control of mitochondrial gene expression and replication (28, 29). During mtDNA replication, the binding of TFAM to mtDNA aids in unwinding of the DNA strands to allow other proteins such as DNA Polymerase γ and the mitochondrial helicase TWINKLE to initiate DNA replication (30–32). In addition, TFAM also plays an essential role in the initiation of mtDNA transcription which is mediated by its binding and subsequent recruitment of transcription machinery including TFB2M and mitochondrial RNA Polymerase (POLRMT). Moreover, other transcription factors such as p53 interact with mitochondrial DNA to promote the transcription of mitochondrial genes (33, 34).

2.4. Mitochondrial Quality Control

Due to the imperative role of mitochondria in skeletal muscle health and functioning, the maintenance of the mitochondrial reticulum is critical. As a result, the mitochondrial network undergoes constant remodelling through a series of processes collectively referred to as "mitochondrial quality control", which allow mitochondria to adapt to various metabolic demands. The synthesis of new mitochondria, referred to as mitochondrial biogenesis, is reliant on the complex interplay of numerous signaling pathways. A variety of stimuli such as increased Ca^{2+}

release, AMP/ATP ratio, and ROS, can lead to the activation of several kinases including CAMK, AMPK and p38. These signaling cascades all ultimately converge on the phosphorylation and subsequent activation of PGC-1α. PGC-1α is a transcriptional co-activator that is commonly known as the "master regulator of mitochondrial biogenesis", due to its ability to associate with numerous transcription factors such as NRF-1, p53, and PPARγ, and promote the expression of nuclear genes encoding mitochondrial proteins (NuGEMPs) (35)**.** This process supports the generation of new mitochondria through the production of essential proteins such as import machinery, ETC components, and proteins involved in regulating the mitochondrial genome such as TFAM (35). Once new mitochondria are produced, the reticular structure of skeletal muscle mitochondria requires specific processes to control its subsequent expansion and division. Mitochondrial fusion refers to the elongation of the reticulum and is highly regulated through the GTPases, Mfn1/2 and OPA1, which are responsible for the fusion of the outer and inner mitochondrial membrane respectively. The fusion of multiple mitochondria promotes increased aerobic respiration efficiency due to the sharing of metabolites and resources (36, 37). However, in certain cases of metabolic stress, segments of the mitochondrial network can become poorly functional, which is characterized by reductions in membrane potential, inefficient aerobic respiration, and excessive production of ROS. Thus, to retain the integrity of the mitochondrial network, these mitochondria need to be separated from the reticulum and subsequently degraded through the processes of mitochondrial fission and mitophagy. Mitochondrial fission promotes the segregation of abnormally functioning mitochondria from the mitochondrial reticulum and is coordinated by the GTPase DRP1, and its associated mitochondrial receptor, FIS-1 (36, 37). This delicate balance between mitochondrial fission and fusion is often used to assess changes in the morphology of the mitochondrial reticulum and its degree of fragmentation. Lastly, if

mitochondrial dysfunction cannot be resolved, the mitochondria are destined for degradation through the process of mitophagy. Mitophagy is a complex process that can be initiated by several signaling cascades, however, the most discussed mitophagy system is mediated by the proteins PINK1 and Parkin (38). Briefly, throughout this process, PINK1 accumulates on the outer mitochondrial membrane which promotes the recruitment of the E3 ubiquitin ligase Parkin. This promotes the tagging of mitochondrial proteins via ubiquitination and subsequent recruitment of the adaptor protein p62, which can interact with the LC3-II receptor on the autophagosome to engulf the dysfunctional mitochondria. Following this, receptors on the autophagosome can interact with the lysosomal membrane, allowing for fusion and subsequent mitochondrial degradation and cellular recycling. However, it is important to note that there are other mitophagy systems such as receptor-mediated mitophagy coordinated by proteins such as NIX, BNIP3, and FUNDC1, which work in conjunction to maintain the integrity of the mitochondrial pool by directly interacting with lysosome receptor, LC3-II (39).

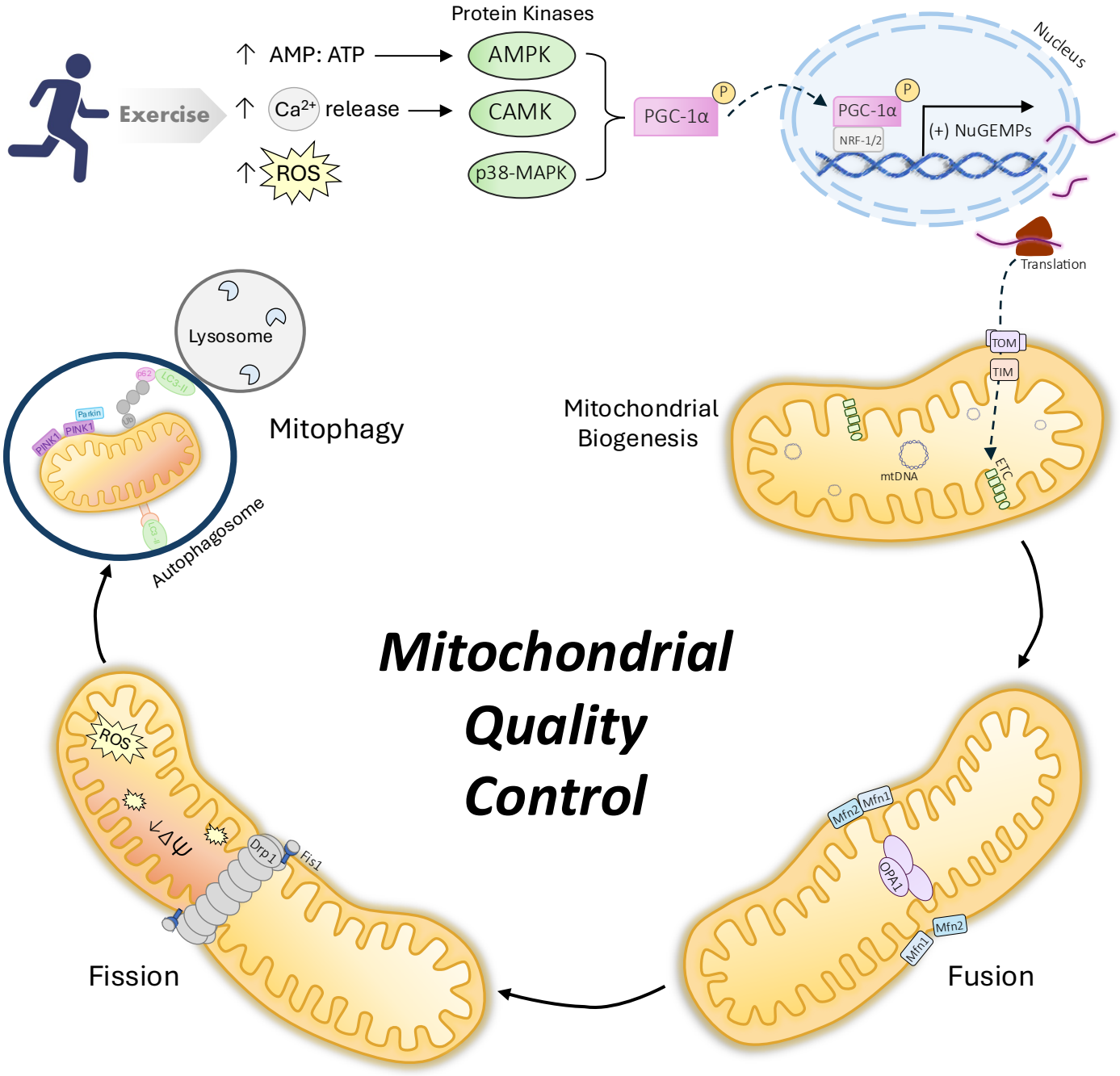
Protein Kinases
Exercise
AMP: ATP
Ca2+ release
ROS
AMPK
CAMK
p38-MAPK
PGC-1α
P
Nucleus
PGC-1α
NRF-1/2
(+) NuGEMPs
Translation
TOM
TIM
Mitochondrial Biogenesis
mtDNA
ETC
Lysosome
Mitophagy
p62
LC3-II
Parkin
PINK1
Autophagosome
Mitochondrial Quality Control
ROS
ΔΨ
Drp1
Fis1
Fission
Mfn2
Mfn1
OPA1
Fusion

Figure 1: Mitochondrial maintenance and quality control processes. The health and functioning of the mitochondrial pool are reliant on a series of quality control processes including mitochondrial biogenesis, fusion, fission, and mitophagy. While these dynamic processes happen simultaneously, the drive towards a particular process can be mediated by several stimuli such as exercise. Following muscle contraction, several cellular perturbations occur including increases in the AMP: ATP ratio, increased cytosolic calcium release from the sarcoplasmic reticulum, and the transient production of ROS. These molecules act as important regulators of mitochondrial maintenance by activating signaling kinases AMPK, CAMK, and p38-MAPK, respectively. Activation of these kinases converge on the phosphorylation and subsequent nuclear translocation of PGC-1α, which co-activates various transcription factors including NRF-1/2 to promote the transcription of NuGEMPs. Following transcription and translation, these proteins can be imported via mitochondrial import machinery to support the biogenesis of new mitochondria. To elongate the mitochondrial reticulum and enhance cellular respiration, mitochondria can undergo the process of fusion which is mediated by Mfn1/2 and OPA1 for fusion of the outer and inner membranes, respectively. While the expansion of the reticulum is critical, mitochondrial health is equally reliant on processes that aid in the removal of dysfunctional mitochondria, that are characterized by a loss of membrane potential ($\Delta\Psi$), impaired import and respiration, and an excessive production of ROS. To segregate these mitochondria from the remainder of the reticulum, the process of mitochondrial fission is induced through the recruitment of DRP1 via the mitophagy receptor, FIS1. Lastly, these abnormally functioning mitochondria become destined for cellular degradation through the process of mitophagy which allows for the breakdown of mitochondrial proteins via hydrolytic proteases located within the lysosomes, to allow for the recycling of monomers to support other cellular processes.

2.5. Mitochondrial-Mediated Apoptosis

Apart from its primary role as an energy-producing organelle, mitochondria also play a central role in mediating several processes including mitochondrial-mediated apoptosis. While there are several forms of targeted cell death, apoptosis functions as a programmed process of cell death which is characterized by DNA fragmentation, cellular shrinking, and a lack of inflammatory activation (40). The involvement of the mitochondria in regulated cell death was originally investigated by Wang and colleagues (41) and plays an important role in the elimination of damaged or harmful cells. Under dysfunctional conditions, an accumulation of pro-apoptotic stimuli such as oxidative stress, DNA damage, or calcium influx can initiate mitochondrial-mediated apoptosis through the opening of the mitochondrial permeability transition pore (mPTP) (42). The pore is thought to consist of several mitochondrial proteins including the outer membrane voltage-dependent anion channel (VDAC), the inner membrane adenine nucleotide translocator (ANT), and the matrix protein Cyclophilin D (43), although the specific composition remains a topic of debate. The opening of the mPTP is highly regulated by the delicate balance of Bcl-2 family proteins including the anti-apoptotic Bcl-2, and the pro-apoptotic Bax and Bak. Upon activation, Bax and Bak oligomerize into the mitochondrial outer membrane and promote permeabilization and the subsequent release of pro-apoptotic factors including cytochrome C and AIF (44). Cytochrome C release is a pivotal activator of the apoptosome protein complex and the downstream initiator caspase-9 and effector caspase-3, which ultimately lead to DNA fragmentation and cellular degradation to execute apoptosis (44). Due to the unique multinucleated structure of skeletal myofibers, the induction of apoptosis results in the death of individual myonuclei as opposed to the entire myofiber. Consequently, myonuclei that undergo nuclear

fragmentation due to cell-mediated apoptosis can no longer contribute as a site of active gene expression and often lead to localized skeletal muscle atrophy.

3. Plasticity of Skeletal Muscle Mitochondria: The good and the bad

One of the most notable features of skeletal muscle is its ability to adapt to various metabolic demands, which can be partially attributed to the highly plastic nature of the mitochondrial reticulum and various quality control processes. However, depending on the stimulus and metabolic perturbations present, the mitochondrial pool can undergo both beneficial and maladaptive changes, which ultimately impact the skeletal muscle phenotype.

3.1. Chronic Endurance Exercise

To assess endurance exercise within rodent models, various models can be employed to induce exercise adaptations including treadmill training, chronic contractile activity (CCA), and voluntary wheel running. While treadmill training and CCA provide a consistent exercise stimulus with highly controlled parameters, these modalities are often more stressful for the animals. On the other hand, as the name suggests, voluntary wheel running is completely reliant on the behavioural patterns of the subject, which can increase variability, but also allows animals to run according to their own environmental and behavioural patterns (45). This model can be especially useful when studying vulnerable mouse populations that may not be able to sustain more stressful protocols. Widely used in many studies, rodents often readily run on running wheels, which allows their distance to be quantified and used as a measure of moderate endurance training (20, 46, 47).

Throughout literature, the concept of “exercise as medicine” is well established due to the numerous benefits on skeletal muscle and the mitochondrial pool. However, the degree of adaptation is highly dependent on different exercise parameters such as duration, intensity, and modality. Acute exercise has been shown to induce transient metabolic disturbances, promoting

the activation of various upstream kinases such as p38 MAPK, CAMK, and AMPK, which positively regulate the transcription and nuclear translocation of key mitochondrial proteins such as PGC-1α (20, 48–51). These changes in gene expression can be further mediated by changes in the methylation of the promoter region of numerous genes such as PGC-1α and PPAR, which impact its transcriptional activity (52). Acute exercise has also been implicated in the active remodelling of skeletal muscle mitochondria through increasing the physical interactions at the mitochondrial membrane, which can improve mitochondrial efficiency through the sharing of resources and dilution of dysfunctional molecules (53). However, while acute exercise can promote transient changes in cellular signaling, repeated exercise bouts are often required to induce long-term adaptations in the skeletal muscle phenotype. Chronic endurance training is a well-established exercise modality that has been investigated using voluntary models such as wheel running, or involuntary protocols such as treadmill training or CCA. In 1967, Holloszy demonstrated a fundamental relationship between endurance training and mitochondrial content as shown through increases in mitochondrial protein content and the activity of important mitochondrial enzymes such as cytochrome C oxidase and succinate dehydrogenase (54). This work has been further characterized by numerous studies highlighting an increased mitochondrial volume post-training, within both the SS and IMF mitochondrial subpopulations (55, 56). These changes in mitochondrial content can be partially attributed to an exercise-induced drive towards mitochondrial biogenesis which is apparent through increases in PGC-1α transcription and mRNA content (57). This ultimately leads to the increased expression of NuGEMPs including ETC proteins to support aerobic respiration, and TFAM to promote mtDNA replication and transcription (58). The increase in protein expression works in conjunction with exercise-induced increases in mitochondrial protein import promoting the generation of new mitochondria (59, 60).

While PGC-1α plays an important role in the transcription of NuGEMPs, it is important to note that exercise-induced adaptations within skeletal muscle can occur independently of PGC-1α, suggesting redundancy within the signaling towards mitochondrial biogenesis (61). While the generation of new mitochondria is beneficial to increasing overall mitochondrial volume, mitochondrial functioning is highly dependent on the turnover of the mitochondrial reticulum. Through increases in the fusion: fission ratio, exercise training can promote an elongated mitochondrial phenotype by increasing the expression of pro-fusion proteins, Mfn1/2 and OPA1, while downregulating the expression of proteins involved in mitochondrial fission such as DRP1 and FIS1 (62–64). In addition, the activity of these proteins can be further augmented through post-translational modifications. Fealy et al. demonstrated that within insulin-resistant skeletal muscle, 12 weeks of endurance exercise was able to markedly reduce the activation of DRP1 through a reduction in its phosphorylation at Ser616 (65). At the terminal end of the mitochondrial life cycle, the turnover of dysfunctional mitochondria relies on the complex interplay between mitophagy initiation and the quality of the terminal lysosomes. Chronic endurance exercise stimulates a larger capacity for mitophagy in conjunction with an increased drive towards lysosomal biogenesis, which is evident through increases in the expression of Parkin and the transcription factor, TFEB, which is closely linked to lysosomal biogenesis (46, 66). Following 4 weeks of voluntary wheel running, basal autophagy flux is enhanced alongside BNIP3 protein expression, possibly suggesting enhancements in receptor-mediated mitophagy, however, this response was only seen in oxidative fiber types (67). These adaptations ultimately lead to increased mitochondrial efficiency and a more oxidative phenotype within trained skeletal muscle, which serves to improve functional parameters such as fatiguability and VO_2 max (56). Due to the increased quality of the mitochondrial pool, there is a decreased drive for mitochondrial-mediated

apoptosis following endurance exercise training. At both basal levels and in response to a cellular stressor, chronic endurance training attenuates the release of pro-apoptotic factors such as AIF and Cytochrome C from the mitochondria, decreasing mitochondrial-mediated apoptosis (11, 68). In addition, exercise training can also increase the expression of other stress response proteins such as the 70-kDa heat shock protein (HSP70) within the mitochondria, which has been shown to directly inhibit the formation of the apoptosome complex and initiator caspase activation (11, 69).

3.2. Muscle Disuse

Due to the adaptive nature of mitochondria, physiological changes that occur over extended periods of muscle disuse can have notable effects on the mitochondrial pool and skeletal muscle health. Within the body of literature, there have been a variety of well-established models that are used to induce muscle disuse which range in their degree of severity. To induce potent changes in a controlled manner, several models are commonly used to limit movement or activity within the hindlimb muscles including sciatic nerve transection, hindlimb immobilization, and hindlimb suspension (70). While these models are well-suited for studying large responses in a relatively short time frame, it is also valuable to investigate more realistic progressions of skeletal muscle disuse, such as those observed with aging.

3.2.1. Skeletal Muscle Denervation

As mentioned previously, skeletal muscle denervation is a well-validated experimental model for studying muscle disuse due to the potent response and presence of an internal control to minimize variability. The sciatic nerve originates from the spine and branches out into the distal tibial and peroneal nerves within the lower hindlimbs, innervating a variety of muscles including the gastrocnemius, soleus, tibialis anterior, extensor digitorum longus, and plantaris. As the largest nerve in the body, the sciatic nerve can be isolated and transected to block neural input to the

hindlimb muscles and has been commonly used to investigate skeletal muscle adaptions to disuse (71–73). Several groups have demonstrated that skeletal muscle denervation disrupts the balance between protein synthesis and protein degradation, favoring a pro-catabolism phenotype characterized by reductions in fiber size. As early as 24 hours post-denervation, protein breakdown is upregulated, contributing to the observed decreases in muscle mass (73). Further contributing to this imbalance, several catabolic pathways are activated such as the FoxO signaling pathway, which promotes the upregulation of atrophy-related genes termed "atrogenes" including Gadd45α and E3 ubiquitin ligases, Murf1, and Atrogin-1. These atrogenes promote protein degradation via several mechanisms including the inhibition of protein synthesis in conjunction with the activation of proteosome-mediated protein degradation (74–77). As a central component of skeletal muscle health, mitochondria also undergo maladaptive changes in response to periods of disuse, partly attributed to impairments in various quality control mechanisms. Prior research from our lab has demonstrated that 7 days of hindlimb denervation is sufficient to reduce the nuclear expression of PGC-1α alongside reductions in TFAM, which reduces the drive toward mitochondrial biogenesis (78, 79). A study by Sandri and colleagues showed that the disuse-induced decrease in PGC-1α protein can also further enhance protein breakdown, as PGC-1α is also implicated in the suppression of FoxO-mediated protein degradation (80). As a result, denervation is often characterized by reductions in mitochondrial content as early as 5-7 days, which can be attributed to the decreased expression of essential mitochondrial proteins and import machinery, which impedes the generation of new mitochondria (71, 72, 81). Interestingly, it has been shown that inducing beneficial mitochondrial adaptations with chronic contractile activity prior to denervation can prevent these reductions in mitochondrial content and preserve muscle oxidative capacity (82). Within the remaining mitochondrial pool, mitochondria also exhibit increased signs of dysfunction

and abnormal morphology. Following denervation, the mitochondrial pool becomes increasingly fragmented due to imbalances in mitochondrial dynamics. The balance favours mitochondrial fission, seen through increases in the expression of fission proteins, FIS1 and DRP1, and associated reductions in the expression of fusion proteins Mfn1, Mfn2, and OPA1 (64, 83). As seen through transmission electron microscopy, mitochondria display abnormal structural morphology that is characterized by a rounded, smaller shape with increased cristae disorganization (84). Consequently, these fragmented mitochondria exhibit declines in their functional capacity through reductions in oxygen consumption and increased ROS emission that precedes muscle atrophy (85–87). The accumulation of ROS has been shown to activate a variety of catabolic systems including the ubiquitin-proteosome system mentioned previously, as well as calpains and autophagy pathways. To try and degrade these dysfunctional organelles, this process is upregulated in denervated muscle seen through an increased expression of several mitophagy and lysosomal markers such as TFEB, PINK1, Parkin, and p62 (79, 83, 88). However, while mitophagy machinery is upregulated, the active degradation of dysfunctional mitochondria which can be measured via mitophagy flux, is downregulated (71, 78). Altogether, these findings demonstrate that while signaling towards mitophagy is activated following periods of denervation, due to impaired degradation, skeletal muscle accumulates dysfunctional mitochondria which further propagates catabolic processes. When mitophagy cannot sufficiently degrade poorly functioning mitochondria, the increased oxidative stress can promote cellular damage, leading to the initiation of apoptosis and mPTP opening (89, 90). Mitochondrial-mediated apoptosis has been implicated as a significant contributor to muscle wasting by investigating knockout models of apoptosis effector, caspase-3, and pro-apoptotic proteins Bax and Bak, which protects against denervated-induced muscle atrophy (91, 92). Overall, a large body of literature has established that skeletal

muscle denervation impairs mitochondrial quality control mechanisms and promotes the accumulation of dysfunctional, fragmented mitochondria leading to deleterious effects on skeletal muscle mass and function.

3.2.2. The Aging Phenotype

As mentioned previously, while sciatic nerve transections produce robust changes in a relatively short time frame, they are not reflective of the natural progression of skeletal muscle dysfunction which can be observed with aging. While the degree of muscle atrophy may be more variable, aging investigations provide insight into the whole-body adaptations and inter-tissue crosstalk that can impact skeletal muscle health and quality of life (93). Several studies have shown that beginning as early as the age of 50, aging populations lose 1-2% of muscle mass per year which contributes to reduced endurance capacity, strength, and increased frailty that can interfere with one's ability to perform daily living activities (94–96). As a result, this progressive loss of muscle mass with age, termed sarcopenia, has become a prominent area of research to better understand the cellular changes associated with its progression. As critical metabolic and signaling hubs within skeletal muscle, alterations in the mitochondrial reticulum with age have been largely implicated in the progression of sarcopenia. Similar to the changes seen following muscle denervation, aged muscle often exhibits decreased mitochondrial content that promotes a more glycolytic phenotype (97). This reduction in content is associated with a progressive decline in mitochondrial function that is characterized by altered structural morphology, impaired respiration capacity, and increased oxidative stress (97–99). Consequently, the mitochondrial reticulum demonstrates a pro-fission phenotype with increased fragmentation in both SS and IMF populations, which stimulates a larger drive towards mitophagy and mitochondrial-mediated apoptosis, further leading to reductions in mitochondrial volume (64, 98, 100). However, while

aged muscle demonstrates basal increases in autophagy-lysosomal protein expression such as p62, Parkin, and LC3-II in comparison to young counterparts, aged muscle exhibits an impaired ability to initiate autophagy in response to metabolic stressors (101). This balance in mitochondrial quality is further altered through a reduced drive towards mitochondrial biogenesis, evident through decreases in PGC-1α at both the transcriptional and protein level, which can be improved with both acute and chronic bouts of exercise (102, 103). This upregulation in PGC-1α is critical, as Leick and colleagues demonstrated that exercise-induced improvements in mitochondrial content and anti-oxidant capacity within aged mice are abolished in the absence of PGC-1α (104). Due to its many benefits, chronic exercise has been universally highlighted as an effective strategy to preserve skeletal muscle mass and functional performance with age, in part by improving the health of the mitochondrial pool (105–107).

As a whole-body phenomenon, it is also important to recognize the wide variety of cellular changes in alternative tissue types that can directly impact skeletal muscle function with age. Skeletal muscle and mitochondria are reliant on the transportation of nutrients and oxygenated blood through the vasculature to support metabolic tissue function, which is impaired with age through reduced skeletal muscle capillary density (108, 109). Furthermore, at the neural level, aging has been associated with several neurochemical and structural abnormalities including motor cortex cortical atrophy, reduced motor neuron activation, and impaired neuromuscular transmission, leading to functional deficits in force production (110). Skeletal muscle also undergoes compositional changes that contribute to the loss of muscle strength, including increased intramuscular fat infiltration within aging muscle (111). Skeletal muscle regeneration and growth also rely on the interactions between skeletal muscle anabolic signaling and muscle satellite cell activation. Several works have characterized declines in muscle satellite cell

activation and regeneration in aged animals compared to their young counterparts, which can exacerbate reductions in muscle mass and the development of sarcopenia (112). Moreover, an emerging role of inflammation is being increasingly explored in the context of aging, which has been coined “Inflammaging”. This refers to the systemic low-grade chronic inflammation and senescence-associated secretory phenotype often observed with age that can contribute towards muscle wasting (113). Evident from these studies, the aging phenotype is closely associated with maladaptive changes in many tissue types that can converge on reduced skeletal muscle quality and functioning.

4. Innate Immune Signaling

4.1. The First Line of Defense

All cellular organisms require the ability to defend themselves against foreign invaders and perturbations including external pathogens or endogenous damage brought about by injury or disease. The immune system, comprised of both the innate immune system and adaptive immune system, works to recognize abnormal entities and swiftly launch effector responses to eliminate the source and maintain homeostatic conditions. The innate immune system is often termed “the first line of defense” and provides non-specific and rapid responses against foreign substances or damaged molecules. Innate defenses are comprised of both structural components such as skin barriers and mucous membranes, as well as several immune cells called leukocytes including monocytes, neutrophils, and natural killer cells that rapidly act upon the presence of foreign material within the cellular environment. In contrast, the adaptive immune system consists of specialized leukocytes, known as B-cells and T-cells, which are responsible for the specific recognition and targeting of foreign antigens, as well as immunological memory of pathogens (114). All leukocytes or “white blood cells” are derived from hematopoietic stem cells within the

bone marrow that eventually develop into specialized immune cells that can either remain within the bone marrow or migrate to other compartments such as peripheral tissues, circulation, or lymphatic vessels (114). Although the adaptive and innate immune system possess distinct features, the ability to induce immune responses and effectively respond to threats is heavily reliant on the complex interplay between the two systems. The innate immune system plays a critical role in activating adaptive effector mechanisms via antigen-presenting dendritic cells, and also serves as a critical initiator of inflammation that provides sufficient time for an adaptive response to be mounted (115). Additionally, in contrast to the original notion, several works have begun to demonstrate that the innate immune system is capable of "trained immunity" in preventing reinfection within invertebrates, which lack an adaptive immune system (116). This could implicate the innate immune system as a potential contributor to immunological memory in addition to the adaptive immune system.

4.2. Pattern Recognition Receptors (PRRs)

To better understand the role of the innate immune system in responding to foreign stimuli, it is critical to investigate the precise mechanism through which recognition occurs. One of the initial theories of recognition was proposed by Dr. Charles Janeway in 1989, who proposed "non-self" driven activation. This theory suggested that innate immune cells use germ-line encoded receptors, termed pattern recognition receptors (PRRs), to recognize pathogen-derived compounds not expressed through the host organism called pathogen-associated molecular patterns (PAMPS) (117). However, in contrast to this concept, another theory later emerged by Dr. Polly Matzinger in 1994 termed the "danger model", which suggested that these PRRs are activated by danger signals produced from damaged host cells termed damage-associated molecular patterns (DAMPs) (118). Throughout the literature, many have accepted that it is a combination of these theories that

drive the recognition of exogenous pathogens and endogenous damage molecules by PRRs to launch innate immune responses. PRRs can be separated into four major classes each possessing unique structural characteristics and cellular localization including Toll-like receptors (TLRs), NOD-like receptors (NLRs), Rig-I-like receptors (RLRs), and C-type lectin receptors (CLRs), and are responsible for recognizing a fixed range of molecular patterns. To ensure that signals are not going undetected, PRRs are strategically located in various compartments including cellular membranes and the cytosol. In brief, PRRs bind to structures through their ligand recognition domains, which recruit various adaptor proteins to launch downstream signaling cascades to exert effects on effector molecules (119). While PRRs have been predominantly studied within the context of immune cells, they are also expressed in other cell types including endothelial cells and muscle cells, which highlights opportunities for cellular crosstalk that can contribute to whole-body inflammation. Within this literature review, we will be focusing specifically on the contribution of TLRs and NLRs and their capacity to respond to a variety of PAMPS and DAMPS.

4.2.1. Toll-like receptors (TLRs) & NOD-like receptors (NLRs)

Toll-like receptors (TLRs) are transmembrane receptors initially named due to their resemblance to the protein encoded by the Toll gene in *Drosophila*. In foundational work by Janeway, the deletion of the Toll gene resulted in an inability to combat fungal infections, which highlighted an important link between TLRs and the induction of immune responses (120). To date, there are currently ten variations of TLRs that have been identified in humans, and twelve variations in mice, which differ based on their cellular location and ligand recognition (121). For example, TLR4 is expressed within the plasma membrane of immune and non-immune cells and is primarily responsive to lipopolysaccharides found within gram-negative bacteria. On the other hand, TLR9 is located within endosomal membranes and primarily recognizes unmethylated CpG

DNA motifs characteristic of bacterial DNA and mitochondrial DNA (122). Despite these differences, TLRs share common pathways of activation to initiate immune responses. The stimulation of TLRs by their respective ligands prompts the activation of intracellular signaling pathways mediated by adaptor proteins such as MyD88, which converge upon the activation of transcription factors such as NF-κB and IRF7. This transcriptionally upregulates the production of pro-inflammatory proteins such as cytokines and inflammasome components to facilitate immune signaling.

In addition to TLRs, NLRs are an additional class of PRRs that serve a similar function as critical components of innate immune signaling. However, while both receptors lead to the upregulation of similar signaling pathways (ex. NF-κB and IRFs), they possess several distinct features. While TLRs are localized to cellular membranes, NLRs are located within the cytoplasm, which influences the variety of PAMPS and DAMPS that are recognized. In addition to various PAMPS, due to its central location within the cell, NLRs are primed to recognize various internal danger signals that occur with cellular stress including extracellular ATP, foreign DNA, ROS, and changes in ion levels (123). From a protective stance, the presence of PRRs in various cellular compartments provides an additional layer of security for any PAMPS or DAMPS that bypass membrane-bound PRRs. To date, NLRs can be further classified into smaller protein groups including the NODs, NLRPs, and NLRCs that differ based on their structural components and ligand-sensing capabilities (123). Within the literature, several NLRs have also demonstrated the ability to assemble into multi-protein complexes termed inflammasomes, including NLRP1, NLRP2, NLRP3, and NLRC4 (124). Due to its unique ability to respond to a wide variety of PAMPS and DAMPS, this study will focus on the NLRP3 protein along with its mechanism of action, which will be further explored throughout *Section 5. The NLRP3 Inflammasome*.

4.2.2. cGAS-STING Pathway

Beyond TLRs and NLRs, another mechanism involved in innate immune pattern recognition is the cyclic GMP-AMP synthase (cGAS)-stimulator of interferon genes (STING) DNA sensing pathway. cGAS is an intracellular PRR found within the cytoplasm, which initially seemed to bear a resemblance to the NLR protein family. However, this signaling pathway is highly specific to recognizing double-stranded DNA (dsDNA) leading to its classification as a cytosolic DNA sensor. dsDNA can be released into the cytosol from various sources including foreign pathogenic sources such as viral or bacterial invaders and/or self-deriving sources of dsDNA that can be released from damaged cells (125). Various studies have demonstrated that mitochondrial DNA can be a potent activator of this immune response and mediate inflammasome activation, senescence-associated phenotypes, and chronic inflammation (126, 127). In brief, the allosteric binding of dsDNA to cGAS activates its enzymatic activity and promotes the synthesis of cyclic GMP-AMP (cGAMP). This potent second messenger can translocate to the endoplasmic reticulum and bind to the sensor STING protein, which induces its trafficking from the endoplasmic reticulum to the Golgi apparatus via various transport machinery including coatomer protein complex II (COPII) vesicles. This translocation leads to the recruitment of the tank-binding kinase 1 (TBK1) which can phosphorylate the transcription factor IRF3 to promote their nuclear translocation and transcription of various type I interferons (128). However, it is important to note that activated STING has also been implicated in other signaling cascades. For instance, the activation of STING and TBK1 can additionally recruit and activate the IKK complexes via phosphorylation, allowing the release and nuclear translocation of the transcription factor NF-κB from its negative regulator IκB (128). Furthermore, beyond its effects on gene transcription, the activation of this pathway is now being increasingly explored in the context of autophagy and cell

death processes, which highlights other potential functions that have not yet been fully elucidated (125).

4.3. Inflammation and Skeletal Muscle Function

As discussed in earlier sections, skeletal muscle displays impressive adaptive capabilities that can be influenced by the multi-system crosstalk to impact its functioning. While skeletal muscle health is highly discussed in relation to the cardiovascular, respiratory and nervous system, the role of inflammation and specifically, the innate immune system, is often not as appreciated. Due to the strenuous role of skeletal muscle in mediating muscle contraction and physical movement, it becomes vulnerable to stress-related damages and requires constant repair to maintain proper health. Muscle damage, while often most associated with traumatic injuries or disease, can also be seen following acute exercise bouts and is generally resolved by the organized coordination between immune cells, muscle stem cells, and satellite cells (129). Following muscle damage induced by acute injury, various circulating immune cells such as neutrophils and monocytes, as well as tissue-resident macrophages are recruited to the site of injury by the release of damage molecules including ROS and extracellular matrix components (130, 131). Specifically, monocytes play an important role in muscle regeneration due to their heterogeneous nature, enabling them to take on a different phenotype depending on the stage of the immune response. Upon early time points of injury, these macrophages primarily take on a pro-inflammatory or "M1" state to release a variety of cytokines and chemokines including TNF-α, IL-1β, and the myokine IL-6, which have been implicated in supporting satellite cell proliferation. Following this initial phase, skeletal muscle regeneration is reliant on the switch to "M2" or anti-inflammatory macrophages to aid in resolving inflammation and promoting muscle differentiation and growth (132, 133). Furthermore, acute exercise is associated with the increased nuclear translocation of

NF-κB in response to transient oxidative stress during increased energetic demands. While this signaling pathway is implicated in a broad range of cellular processes, it has been suggested to upregulate both the inflammatory and antioxidant response during muscle recovery (134). In contrast, while acute exercise is considered transiently pro-inflammatory, exercise adaptations over time are often associated with an attenuated inflammatory response. For instance, chronic endurance training by voluntary wheel running and treadmill training, on healthy mice and obese mice respectively, has been shown to decrease skeletal muscle macrophage content as well as promote an increased proportion of M2 to M1 macrophages compared to sedentary controls (135, 136). Consequently, this is associated with reductions in circulating pro-inflammatory cytokines including TNF-α and IL-6, and increases in classic anti-inflammatory cytokines such as IL-10 (136, 137). However, some studies have shown opposing results suggesting that chronic high-intensity endurance training was associated with increases in skeletal muscle cytokines including IL-1β, IL-12, and anti-inflammatory IL-1ra, possibly suggesting an impact of exercise intensity on immune adaptations (138).

While the adaptive capability of the immune system is highly beneficial in response to damage or infection, dysregulated inflammatory responses can be detrimental to skeletal muscle health and functioning. Many conditions are associated with chronic inflammation and detriments to mitochondrial and skeletal muscle health including aging (139), type 2 diabetes (140), muscular dystrophies (141), and myositis (142), which emphasizes the need for investigating potential therapeutics to alleviate excess inflammation within muscle.

5. The NLRP3 Inflammasome Complex

The term “inflammasome” was first coined in 2002 by Dr. Jürg Tschopp and his colleagues, upon the discovery of what is currently known as the NLRP1 inflammasome complex. Prior to

this, NLRs were thought to contribute towards leukocyte apoptosis due to their notable structure which was reminiscent of apoptosis effectors and apoptosome formation. However, this work characterized the role of NLRs in mediating innate immune response by assembling into multi-protein complexes that promote the activation of inflammatory caspase-1/5 and pro-inflammatory cytokine IL-1β in response to lipopolysaccharide (LPS) treatment (143). In 2004, these researchers later found a similar pattern of activation for NLRP3, which eventually emerged as the most well-characterized inflammasome due to its ability to respond to a variety of DAMPs and PAMPs, further establishing its involvement in both pathogenic and sterile inflammation (144, 145).

5.1. NLRP3 Structural Characteristics

NLRP3, also known as cryopyrin, is a tripartite protein comprised of 3 domains: the amino (N)-terminal pyrin domain (PYD), the central nucleotide-binding and oligomerization domain (NACHT), and the carboxy (C)-terminal leucine-rich repeat (LRR) domain (146). The PYD domain has been implicated in mediating protein-protein interactions, which is required for inflammasome activation. Due to the lack of a caspase activation and recruitment domain (CARD) internally within NLRP3, the assembly of the NLRP3 inflammasome complex is reliant on its interactions with the apoptosis-associated speck-like protein containing CARD (ASC). ASC contains an N-terminal PYD domain and a C-terminal CARD domain, making it an essential link between NLRP3 and the recruited procaspase-1 by aiding in the formation caspase-1 activation sites via CARD-CARD interactions (147, 148). The PYD domains in both ASC and NLRP3 undergo homotypic protein interactions driven by their hydrophobic cores and charged amino acid residues that promote their association (149). Furthermore, the NACHT domain exhibits ATPase activity that allows the binding and hydrolysis of ATP, which aids in the oligomerization of NLRP3 monomers to promote inflammasome formation (150). Additionally, recent works have

begun to implicate the NACHT region as an autoinhibitory feature of NLRP3 inflammasome activation which contributes to its tight regulation (151). Lastly, the LRR domain has been most investigated for its role in ligand detection and mediating protein-protein interactions with other constituents such as the protein kinase NEK7 to facilitate proper assembly. In addition, this region has been implicated as a site for several post-translational modifications to modulate NLRP3 activation including phosphorylation and ubiquitination. However, the importance of this region in inflammasome activation is still up for debate. For instance, while some works have shown that the deletion of the LRR domain inhibits NLRP3 inflammasome activation in macrophages, other groups have demonstrated that it is not required for adequate inflammation activity (152, 153).

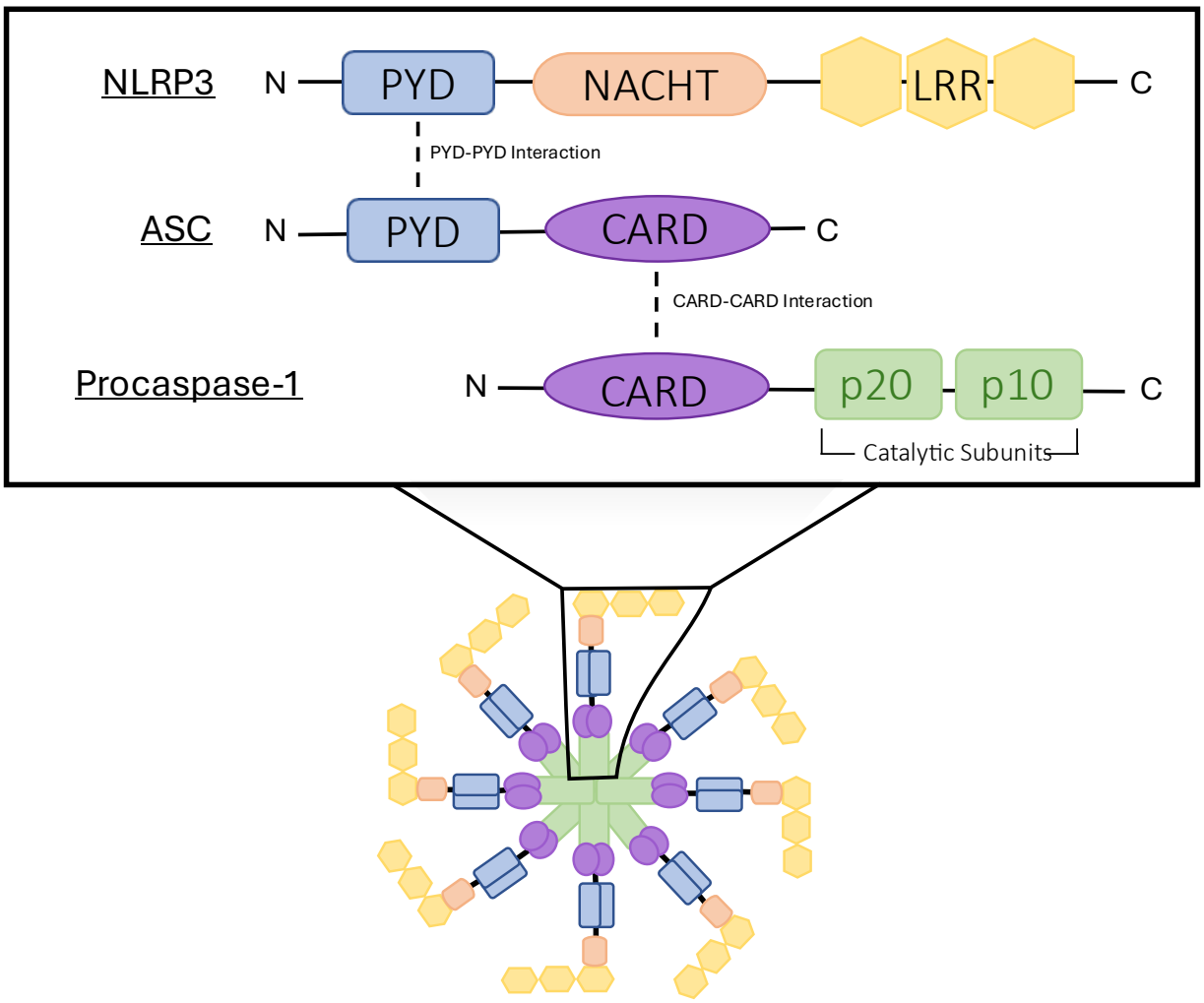

Figure 2. Structure of the NLRP3 Inflammasome Complex. The NLRP3 Inflammasome is a multiprotein complex that is comprised of 3 proteins including NLRP3, adaptor ASC, and procaspase-1. The sensor protein NLRP3 is comprised of 1033 amino acids [*mus musculus*] and can be further divided into three domains. The C-terminal LRR domain has been primarily implicated in ligand detection and stabilizing the inflammasome structure. The central NACHT domain is critical in the hydrolysis of ATP that promotes inflammasome oligomerization and assembly. Lastly, the N-terminal PYD domain mediates homotypic protein-protein interactions with the PYD domain located on the 193-amino acid adaptor protein, ASC. As NLRP3 itself lacks a CARD domain, this interaction is critical in promoting procaspase-1 recruitment through the formation of ASC filaments and subsequent CARD-CARD protein interaction. The effector protein of the inflammasome complex, procaspase-1, is a 402 amino acid protein that is comprised by an N-terminal CARD domain, as well as two primary catalytic subunits termed the p10 and p20 subunits. Through the CARD-CARD interactions, the procaspase-1 proteins form a filament structure which allows for the proximity-induced autocatalytic cleavage between the p20 and p10 subunits to obtain the enzymatically active caspase-1 protein.

5.2. NLPR3 Inflammasome: Canonical Mechanism of Action

Due to its role in innate immune activation, the NLRP3 inflammasome must be closely regulated to avoid overactivation and detrimental health effects. As a result, canonical activation of the NLPR3 inflammasome generally require a two-step activation pattern that consists of the priming stage, followed by subsequent assembly and activation. The priming stage is initiated at the level of PRRs including TLRs following the recognition of various PAMPs such as foreign DNA and pathogenic molecules. This leads to the activation of downstream signaling cascades that promote the nuclear translocation of NF-κB which can interact with NF-κB binding sites within the promotor region of various pro-inflammatory proteins including NLRP3, pro-IL-1β, and pro-IL-18 (124). Under basal conditions, these proteins are not abundantly expressed and therefore need to be transcriptionally "primed" before inflammasome assembly. Following the initial priming step, the second step of activation requires an additional stress signal which includes the presence of various PAMPs and DAMPs such as extracellular ATP, ROS, viral RNA, β-amyloid, potassium efflux, monosodium urate crystals, and various other damage molecules (124, 154). Following this signal, activated NLRP3 monomers can oligomerize into the classic inflammasome structure, allowing the interaction with ASC and recruitment of procaspase-1. This interaction leaves to the autocatalytic cleavage of procaspase-1 into its active form at aspartic acid residues, Asp296 and Asp315 in mice, to yield a p20 and p10 catalytic subunit. As an effector caspase, this activation has two main downstream effects that contribute towards a pro-inflammatory environment. The first effect is the caspase-1 mediated cleavage of pro-inflammatory cytokines, pro-IL-1β (Asp116) and pro-IL-18 (Asp36) into their mature and active forms. As members of the interleukin family, both cytokines are heavily implicated in the innate immune response through mediating different pathways. IL-1β is critical in the initiation of the

immune response by controlling fever, the stimulation of other cytokines, and the recruitment of additional immune cells through vasodilation, which has been demonstrated by the lack of acute inflammation in IL-1β KO mice when faced with various pathogens (155). In contrast, IL-18 is closely linked to the adaptive immune response through the production of IFNγ (156). Additionally, activation of the NLRP3 inflammasome contributes towards a pro-inflammatory form of lytic cell death termed "pyroptosis" through cleavage of the Gasdermin-D (GSDMD) molecule at Asp 276, releasing its active N-terminal fragment (GSDMD-N) that promotes pore-formation, cell death and the subsequent release of IL-1β and IL-18 (157, 158).

While this is the most well-understood pathway, it is important to recognize that other redundant signaling pathways can also converge upon NLRP3 inflammasome activation in the absence of microbial infections. For example, while the priming step is often linked to the presence of PAMPS or toxins, such as the commonly used LPS, other stimuli such as TNF-α mediated signaling or additional damage molecules can also contribute towards sterile inflammatory responses (159, 160).

5.3. Mitochondria and NLRP3 Inflammasome Activation

While mitochondria are traditionally known as powerful metabolic hubs, an emerging role of mitochondria as prominent contributors to the innate immune response has started to gain more attention. Due to the endosymbiotic origins of mitochondria, it is thought that they contribute to pro-inflammatory responses due to their structural similarities to bacterial organisms and ability to release endogenous damage molecules. For instance, several mitochondrial components have been implicated as mitochondrial DAMPS (mtDAMPS) that can be released under stressful conditions including ATP (161), cardiolipin (162), N-formyl peptides (163), ROS (164), and mtDNA (165). Specifically, many of these mtDAMPS have been linked to immune signaling,

immune cell infiltration and the direct activation of the NLRP3 inflammasome complex. In addition, several works have implicated mitochondria as scaffolding platforms for NLRP3 assembly. Several works have shown that in the presence of various PAMPs and DAMPs, there is increased co-localization between the NLRP3 inflammasome and mitochondria as well as several mitochondrial proteins that can facilitate physical interactions with NLRP3 such as Mfn2 and mitochondrial antiviral proteins (164, 166, 167).

5.3.1. mtDNA as a mtDAMP

In early works, Collins and colleagues highlighted that mtDNA could elicit inflammatory responses due to its susceptibility to oxidative damage and unmethylated CpG motifs. This was demonstrated following injections of oxidized mtDNA into the synovial joints of mice which resulted in an arthritic pro-inflammatory phenotype through the upregulation of NF-κB signaling, which was not seen with the addition of nuclear DNA (168). Later works by Shimada et al., further expanded the role of mtDNA as a specific activator of the NLRP3 inflammasome complex in bone-marrow derived macrophages (BMDMs). Through a diverse range of experiments, they demonstrated that oxidized mtDNA, identified by the marker of DNA oxidation 8-OHdG, can directly bind to the NLRP3 protein to promote inflammasome activation (169). This is further supported by several studies that have shown mtDNA release and a subsequent pro-inflammatory response following mitochondrial outer membrane permeabilization mediated by the Bak/Bax pore and VDAC oligomerization. This response was also blunted by the overexpression of the anti-apoptotic Bcl-2 protein, implicating mitochondrial permeabilization in augmenting inflammatory processes (24, 170). Following its release, mtDNA can then interact with various PRRs including NLRs, cGAS, and TLRs to initiate inflammatory signaling via primarily NF-κB signaling and the type I interferon response.

Several studies have investigated the role of mitochondrial quality control mechanisms in mitigating mitochondrial dysfunction and subsequent mtDNA release to elucidate the importance of mitochondrial health in inflammation. Irazoki and colleagues demonstrated that excessive mitochondrial fragmentation via the knockdown of fusion protein Mfn1 led to increased VDAC-mediated mtDNA release and the upregulation of endosomal TLR9 signaling and NLRP3 inflammasome components. This pro-inflammatory phenotype subsequently had detrimental effects of skeletal muscle performance, which was mitigated upon the inhibition of NF-κB signaling (171). Furthermore, autophagy plays an essential role in the degradation of potential DAMPs and impeding their ability to evoke inflammatory responses. Several groups have demonstrated that impairments in autophagy processes stimulated by the absence of BNIP3 and beclin-1 have also been linked to an accumulation of mtDNA and ROS, which drives TLR9 inflammatory signaling (165, 172). The protective role of mitophagy can further be demonstrated through the use of mitophagy inducers such as the nutraceutical Urolithin A, which has been shown to attenuate the release of mtDNA and downstream inflammatory responses (126).

5.3.2. mtROS

In addition to mtDNA, another well-established mtDAMP is mitochondrial reactive oxygen species (mtROS). As discussed earlier, due to their role in energy production and the presence of the electron transport chain, mitochondria can produce large amounts of mtROS in cases of dysfunction or metabolic disturbances. In 2010, Zhou et al., established a link between the mitochondria, mtROS, and NLRP3 inflammasome activation in BMDMs. They demonstrated that the inhibition of Complex III in the electron transport chain led to a pronounced upregulation of mtROS and NLRP3 inflammasome activation, which was attenuated with NLRP3 and caspase-1 knockout (164). While the specific site of mtROS and NLRP3 inflammasome activation has not

been fully identified, the crystal structure of NLRP3 demonstrates disulfide bonds between cysteine residues that could be potentially regulated through oxidative stress (149). Through investigating possible mechanisms of ROS-mediated inflammasome activation, several works have identified a role for Thioredoxin-interacting protein (TXNIP), which as the name suggests, usually remains bound to the antioxidant Thioredoxin and inhibits its activity. However, in a ROS-dependent manner, this interaction is disrupted and TXNIP can bind to the NLRP3 protein at its LRR region to induce NLRP3 inflammasome activation in BMDMs (173). Within skeletal muscle, the upregulation of this ROS-TXNIP-NLRP3 axis has been associated with chronic inflammasome activation and impairments in glucose uptake following high-fat feeding, indicating the broader impacts of NLRP3 inflammasome overactivation (174, 175).

However, while it has been made clear that there is a strong relationship between mitochondria and NLRP3 inflammasome, there is some conflicting evidence as to whether mitochondrial dysfunction is a cause or consequence of NLRP3 inflammasome activation. For instance, Park and colleagues found that the knockdown of the mitochondrial fission GTPase, DRP1, was associated with increased activation of the NLRP3 inflammasome, mtROS, and mtDNA release in response to ATP treatment. However, similar to findings from Nakahira et al., the inhibition of caspase-1 prevented mitochondrial fragmentation and the release of mtDNA, which suggests that mitochondrial damage can be a consequence of inflammasome activation (165, 176). Furthermore, the treatment of C2C12 myotubes with LPS was also associated with mtROS production, however, this was blunted in the presence of NLRP3 inhibitor, MCC950 (177). In contrast to this, other studies have demonstrated that mtROS production and the binding of released mtDNA to NLRP3 occurs independent of caspase-1 activity, suggesting the upstream involvement of mitochondrial damage prior to inflammasome activation (165, 169).

Overall, these studies underscore the role of mitochondria in mediating NLRP3 inflammasome activation in various cell types. While NLRP3 inflammasome activation can be beneficial in host protection and the propagation of innate immune responses, chronic activation become dysregulated and have deleterious effects on health. This can be seen through the spectrum of conditions including cryopyrin-associated periodic syndromes, muscular dystrophy, insulin resistance and cancer. By further elucidating the mechanisms surrounding mitochondrial-mediated DAMP release, it can introduce several sites of potential intervention to regulate the NLRP3 inflammasome complex and maintain cellular homeostasis.

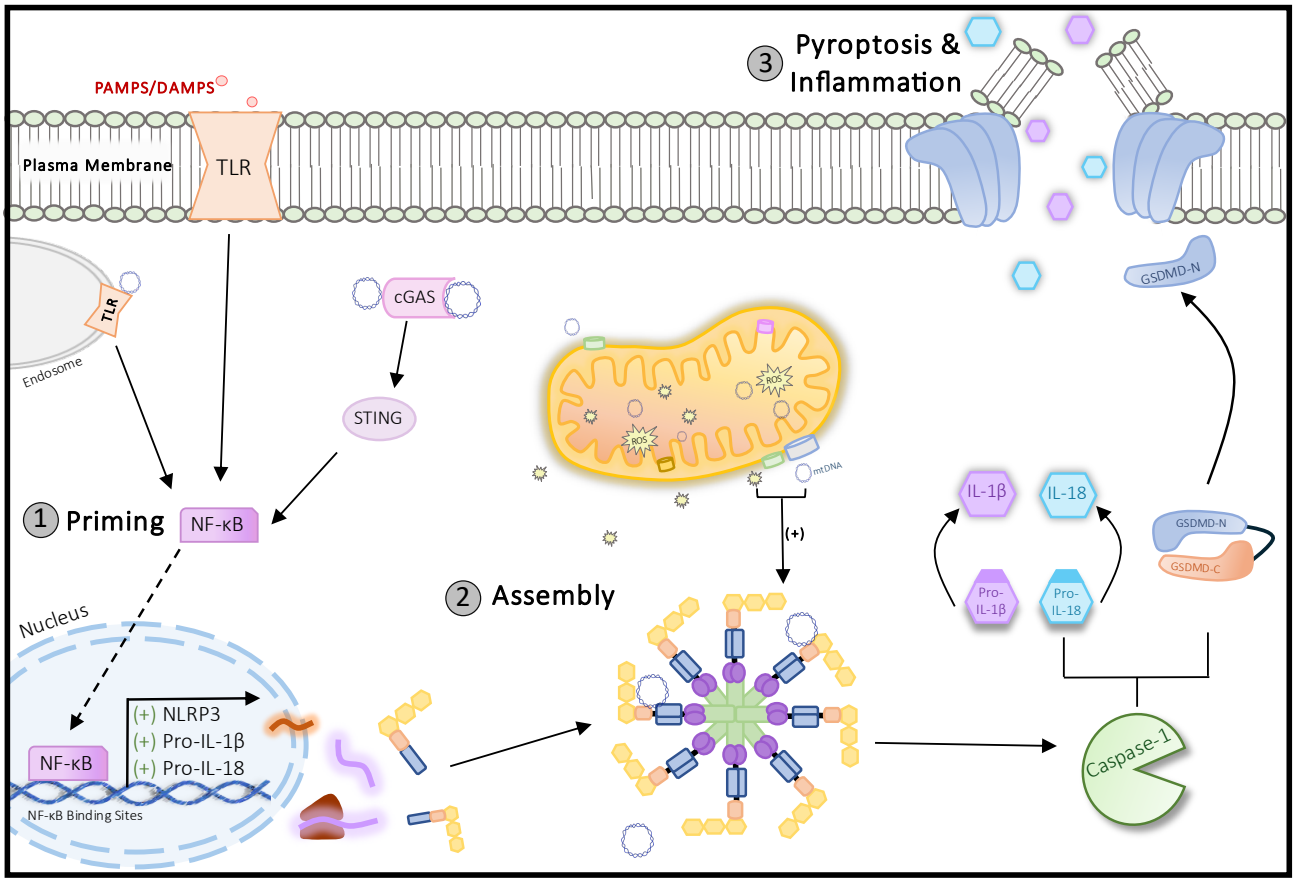

Figure 3. Canonical mechanism of NLRP3 Inflammasome Activation. To maintain tight regulation of its activity, the NLRP3 inflammasome complex is generally activated by a two-step activation mechanism of priming and subsequent assembly. The priming stage is mediated by the recognition of various extracellular and intracellular DAMPs/PAMPs. This promotes the nuclear translocation of NF-κB, where it can bind to NF-κB binding sites located within the promoter regions of various pro-inflammatory genes involved in the NLRP3 inflammasome pathway. Following the priming stage, inflammasome assembly requires an additional signal which can be mediated by the accumulation of various DAMPs such as mtDNA and mtROS. These damage molecules can be released from poorly functioning mitochondria via various mitochondrial pores. The recognition of this stimuli promotes the assembly of NLRP3, ASC and procaspase-1 into the active NLRP3 inflammasome complex and leads to the subsequent cleavage of procaspase-1. The enzymatically active caspase-1 leads to the cleavage of GSDMD and pro-inflammatory cytokines, pro-IL-1β and pro-IL-18, which releases GSDMD-N and the mature IL-1β and IL-18. GSDMD-N contains the ability to form pores within the plasma membrane to induce pyroptosis by disrupting osmotic pressure and promoting cellular swelling. Pyroptosis enables the release of DAMPs, PAMPs and pro-inflammatory cytokines to amplify to induce a larger local inflammatory response.

5.4. NLRP3 Adaptations to Skeletal Muscle Disuse

5.4.1. Muscle Denervation

As outlined in Section 3, muscle denervation is an severe model of muscle disuse that is often characterized by reductions in muscle strength, increased atrophy, and impairments in mitochondrial health (71). Due to the adaptable nature of the mitochondrial reticulum, prolonged periods of muscle disuse can contribute to increased fragmentation, impaired energy production, and an accumulation of mtDAMPs that can amplify immune responses. Following muscle disuse by peripheral nerve injury, skeletal muscle transitions towards a pro-inflammatory environment that involves immune cell infiltration and the production of cytokines such as IL-6 and TNF-α, which can further propagate signaling toward muscle atrophy (178). In addition, other studies have demonstrated an active role for NLRP3 inflammasome activation in response to various inducers of muscle atrophy including IL-1β and angiotensin-II treatment, which can be attenuated by NLRP3 KO or the upregulation of anti-inflammatory signaling (179, 180). However, while the role of the NLRP3 inflammasome has been explored in the context of skeletal muscle atrophy, there is still a lack of information surrounding its involvement in skeletal muscle denervation. A study by You et al., demonstrated that 14-28 days of skeletal muscle denervation was sufficient to induce NLRP3 inflammasome activation and downstream components including caspase-1, GSDMD-N, IL-1β and IL-18. Furthermore, this was associated with an upregulation of atrogenes, Murf-1 and Atrogin-1, which can upregulate protein degradation through the ubiquitin-proteosome system to stimulate muscle atrophy. However, the absence of NLRP3 blunts these responses suggesting that the NLRP3 inflammasome activation can contribute to denervation-induced skeletal muscle atrophy (181). While this study implicates the NLRP3 inflammasome in mediating

skeletal muscle adaptations to denervation, more work needs to be done to understand the relationship between mitochondrial health and this pro-inflammatory environment.

5.4.2. NLRP3 Inflammasome in the Aging Phenotype

In 2000, Franceschi and colleagues coined the term "inflammaging" which has since expanded to describe the pro-inflammatory environment observed with the progression of age. Generally, this is characterized by chronic systemic inflammation that is mediated by an increased processing of pro-inflammatory receptors and cytokines, as well as reductions in anti-inflammatory signaling (113, 182). Basally with age, several immune factors are upregulated including the expressions of various TLRs, MyD88, and NF-κB components, which suggest an increased drive towards pro-inflammatory signaling in skeletal muscle (183). Furthermore, as previously mentioned, aged muscle often suffers from increases in protein catabolism and deficits in mitochondrial function leading to reductions in skeletal muscle mass. Due to its involvement in activating caspases and inflammatory cell death, several studies have aimed to characterize the potential role of NLRP3 inflammasome activation in age-related sarcopenia. Work done by Mcbride et al., and Antuña et al., have demonstrated basal increases in several proteins associated with NLRP3 inflammasome signaling including caspase-1 and IL-1β, which was associated with reductions in myofiber size and the increased circulation of DAMPs including extracellular ATP (184, 185). However, in the absence of NLRP3, 24-month old mice were protected from age-related losses in muscle mass in specifically type II fibers, which was also associated with improvements in physical performance (184). Furthermore, several deficits in mitochondrial quality control processes have also been implicated in the observed inflammation with age. For instance, a reduced drive towards mitophagy with age is associated with an accumulation of dysfunctional mitochondria and subsequent activation of TLR9-NLRP3 and cGAS-STING mediated signaling. Interestingly, this

can be attenuated by enhancing the drive towards mitophagy through external agents or overexpressing mitophagy receptors such as BNIP3 (126, 172). Overall, the current literature provides some evidence of age-related increases in NLRP3 signaling within skeletal muscle, however, the connection between inflammasome activation and mtDAMPs, as well as the potential mitigation through exercise has yet to be investigated.

5.4.3. NLRP3 Inflammasome Adaptations to Endurance Training

Exercise is generally considered to be "mitochondrial medicine" due to its ability to enhance the quality of the mitochondrial reticulum and skeletal muscle health. Seen consistently within literature, chronic endurance training has been associated with enhanced mitochondrial quality control mechanisms and reduced oxidative stress, ultimately contributing to an oxidative muscle phenotype (3, 56, 65). In relation to mtDAMPs, chronic training has been associated with reductions in mtROS production due to increased mitochondrial efficiency and an improved clearance of dysfunctional organelles. However, there is little evidence surrounding the impact of endurance training on mtDAMP release in skeletal muscle and the subsequent innate immune activation. In regards to the general inflammation, chronic endurance training has also been praised for its role in shifting the inflammatory environment through the upregulation of anti-inflammatory cytokines and suppression of pro-inflammatory cytokines (136). In addition, endurance exercise has been shown to induce PGC-1α expression, which has been linked to the repression of pro-inflammatory NF-κB signaling in skeletal muscle, as well as the inhibition of NLRP3 inflammasome activation by improving mitochondrial health in renal tubular epithelial cells (186, 187). While there is little to no evidence surrounding the effects of endurance training on the NLRP3 inflammasome activation within skeletal muscle, a few studies have demonstrating promising findings in other tissue types. For instance, in cardiomyocytes, 8 weeks of moderate

endurance training has been associated with reductions in mitochondrial stress as well as NLRP3 inflammasome activation and IL-1β release in a model of cardiac overload hypertrophy (188). Furthermore, in a model of high-fat diet induced obesity, 14 weeks of voluntary wheel running was capable of attenuating NLRP3 inflammasome signaling and oxidative stress originating from NADPH oxidases (189). A similar reduction in inflammasome signaling can be observed in neuronal cells from a mouse model of Parkinson's disease and adipose tissue from obese mouse models, following 10 and 6 weeks of treadmill training, respectively (190, 191). Considering the highly adaptive nature of skeletal muscle mitochondria along with the effects of exercise training on the NLRP3 inflammasome complex in other tissue types, there is a strong foundation for further exploring this relationship within future studies.

RESEARCH OBJECTIVES

Considering the current body of literature, the main research objectives of this thesis were to:

- Assess changes in the mitochondrial reticulum following 7 days of muscle denervation using an *in vivo* mouse model;
- Characterize NLRP3 inflammasome activation in denervated skeletal muscle to assess the innate inflammatory response;
- Investigate changes in potential DAMPS within skeletal muscle following muscle disuse;
- Assess basal effects of age *in vivo* on mitochondrial health and adaptations to endurance training;
- Elucidate basal NLRP3 inflammasome activation in young and aged skeletal muscle, and investigate whether 6 weeks of endurance training can alter the inflammatory profile;
- Characterize changes in DAMPS with age, as well as in response to chronic endurance training;

HYPOTHESES

We hypothesized that:

- Mitochondrial content and function will decrease following 7 days of skeletal muscle disuse;
- The NLRP3 inflammasome will be responsive to muscle disuse through changes in protein expression;
- Muscle denervation will augment mitochondrial dysfunction leading to an increased production of DAMPS;
- Aging muscle will demonstrate reductions in mitochondrial health basally, which will be improved in young and aged muscle following 6 weeks of endurance training;

- Basally, aging muscle will exhibit increased NLRP3 inflammasome activation at the protein level. The expression of NLRP3 inflammasome components will be attenuated in both young and aged muscle following the exercise training period;
- Endurance training will reduce the production of DAMPS within skeletal muscle, which will contribute towards a reduced inflammatory profile in both age groups;

REFERENCES

1. Frontera WR, Ochala J. Skeletal Muscle: A Brief Review of Structure and Function. *Calcif Tissue Int* 96: 183–195, 2015. doi: 10.1007/s00223-014-9915-y.
2. Scott W, Stevens J, Binder–Macleod SA. Human Skeletal Muscle Fiber Type Classifications. *Phys Ther* 81: 1810–1816, 2001. doi: 10.1093/ptj/81.11.1810.
3. Luden N, Hayes E, Minchev K, Louis E, Raue U, Conley T, Trappe S. Skeletal muscle plasticity with marathon training in novice runners. *Scand J Med Sci Sports* 22: 662–670, 2012. doi: 10.1111/j.1600-0838.2011.01305.x.
4. Lee W-S, Cheung W-H, Qin L, Tang N, Leung K-S. Age-associated Decrease of Type IIA/B Human Skeletal Muscle Fibers: *Clin Orthop* 450: 231–237, 2006. doi: 10.1097/01.blo.0000218757.97063.21.
5. Frontera WR, Suh D, Krivickas LS, Hughes VA, Goldstein R, Roubenoff R. Skeletal muscle fiber quality in older men and women. *Am J Physiol-Cell Physiol* 279: C611–C618, 2000. doi: 10.1152/ajpcell.2000.279.3.C611.
6. Hood DA, Memme JM, Oliveira AN, Triolo M. Maintenance of Skeletal Muscle Mitochondria in Health, Exercise, and Aging. *Annu Rev Physiol* 81: 19–41, 2019. doi: 10.1146/annurev-physiol-020518-114310.
7. Protasoni M, Zeviani M. Mitochondrial Structure and Bioenergetics in Normal and Disease Conditions. *Int J Mol Sci* 22: 586, 2021. doi: 10.3390/ijms22020586.
8. Hood DA, Joseph A-M. Mitochondrial assembly: protein import. *Proc Nutr Soc* 63: 293–300, 2004. doi: 10.1079/PNS2004342.
9. Lowell BB, Spiegelman BM. Towards a molecular understanding of adaptive thermogenesis. *Nature* 404: 652–660, 2000. doi: 10.1038/35007527.
10. Kirkwood SP, Munn EA, Brooks GA. Mitochondrial reticulum in limb skeletal muscle. *Am J Physiol* 251: C395-402, 1986. doi: 10.1152/ajpcell.1986.251.3.C395.
11. Adhihetty PJ, Ljubicic V, Hood DA. Effect of chronic contractile activity on SS and IMF mitochondrial apoptotic susceptibility in skeletal muscle. *Am J Physiol-Endocrinol Metab* 292: E748–E755, 2007. doi: 10.1152/ajpendo.00311.2006.
12. Vincent A, White K, Phillips J, Ogden T, Lawless C, Warren C, Hall M, Ng YS, Falkous G, Deehan D, Turnbull D, Picard M. Quantitative 3D Mapping of the Human Skeletal Muscle Mitochondrial Network. *Cell Rep* 26, 2019. doi: 10.1016/j.celrep.2019.01.010.
13. Bayr H. Reactive oxygen species: *Crit Care Med* 33: S498–S501, 2005. doi: 10.1097/01.CCM.0000186787.64500.12.
14. Powers SK, Jackson MJ. Exercise-Induced Oxidative Stress: Cellular Mechanisms and Impact on Muscle Force Production. *Physiol Rev* 88: 1243–1276, 2008. doi: 10.1152/physrev.00031.2007.
15. Sies H, De Groot H. Role of reactive oxygen species in cell toxicity. *Toxicol Lett* 64–65: 547–551, 1992. doi: 10.1016/0378-4274(92)90230-H.
16. Davies KJA, Quintanilha AT, Brooks GA, Packer L. Free radicals and tissue damage produced by exercise. *Biochem Biophys Res Commun* 107: 1198–1205, 1982. doi: 10.1016/S0006-291X(82)80124-1.
17. Barja G. Mitochondrial Oxygen Radical Generation and Leak: Sites of Production in States 4 and 3, Organ Specificity, and Relation to Aging and Longevity. *J Bioenerg Biomembr* 31: 347–366, 1999. doi: 10.1023/A:1005427919188.
18. Chance B, Sies H, Boveris A. Hydroperoxide metabolism in mammalian organs. *Physiol Rev* 59: 527–605, 1979. doi: 10.1152/physrev.1979.59.3.527.
19. Kabe Y, Ando K, Hirao S, Yoshida M, Handa H. Redox Regulation of NF-κB Activation: Distinct Redox Regulation Between the Cytoplasm and the Nucleus. *Antioxid Redox Signal* 7: 395–403, 2005. doi: 10.1089/ars.2005.7.395.
20. Akimoto T, Pohnert SC, Li P, Zhang M, Gumbs C, Rosenberg PB, Williams RS, Yan Z. Exercise stimulates Pgc-1alpha transcription in skeletal muscle through activation of the p38 MAPK pathway. *J Biol Chem* 280: 19587–19593, 2005. doi: 10.1074/jbc.M408862200.

21. Negre-Salvayre A, Coatrieux C, Ingueneau C, Salvayre R. Advanced lipid peroxidation end products in oxidative damage to proteins. Potential role in diseases and therapeutic prospects for the inhibitors. *Br J Pharmacol* 153: 6–20, 2008. doi: 10.1038/sj.bjp.0707395.
22. Pillon NJ, Croze ML, Vella RE, Soulère L, Lagarde M, Soulage CO. The Lipid Peroxidation By-Product 4-Hydroxy-2-Nonenal (4-HNE) Induces Insulin Resistance in Skeletal Muscle through Both Carbonyl and Oxidative Stress. *Endocrinology* 153: 2099–2111, 2012. doi: 10.1210/en.2011-1957.
23. Huang Z, Chen Y, Zhang Y. Mitochondrial reactive oxygen species cause major oxidative mitochondrial DNA damages and repair pathways. *J Biosci* 45: 84, 2020. doi: 10.1007/s12038-020-00055-0.
24. Xian H, Watari K, Sanchez-Lopez E, Offenberger J, Onyuru J, Sampath H, Ying W, Hoffman HM, Shadel GS, Karin M. Oxidized DNA fragments exit mitochondria via mPTP- and VDAC-dependent channels to activate NLRP3 inflammasome and interferon signaling. *Immunity* 55: 1370-1385.e8, 2022. doi: 10.1016/j.immuni.2022.06.007.
25. Nass MMK, Nass S. Intramitochondrial Fibers with DNA Characteristics. *J Cell Biol* 19: 593–611, 1963. doi: 10.1083/jcb.19.3.593.
26. Sagan L. On the origin of mitosing cells. *J Theor Biol* 14: 225-IN6, 1967. doi: 10.1016/0022-5193(67)90079-3.
27. Bibb MJ, Van Etten RA, Wright CT, Walberg MW, Clayton DA. Sequence and gene organization of mouse mitochondrial DNA. *Cell* 26: 167–180, 1981. doi: 10.1016/0092-8674(81)90300-7.
28. Kukat C, Wurm CA, Spåhr H, Falkenberg M, Larsson N-G, Jakobs S. Super-resolution microscopy reveals that mammalian mitochondrial nucleoids have a uniform size and frequently contain a single copy of mtDNA. *Proc Natl Acad Sci* 108: 13534–13539, 2011. doi: 10.1073/pnas.1109263108.
29. Lee SR, Han J. Mitochondrial Nucleoid: Shield and Switch of the Mitochondrial Genome. *Oxid Med Cell Longev* 2017: 1–15, 2017. doi: 10.1155/2017/8060949.
30. Ekstrand MI. Mitochondrial transcription factor A regulates mtDNA copy number in mammals. *Hum Mol Genet* 13: 935–944, 2004. doi: 10.1093/hmg/ddh109.
31. Larsson N-G, Wang J, Wilhelmsson H, Oldfors A, Rustin P, Lewandoski M, Barsh GS, Clayton DA. Mitochondrial transcription factor A is necessary for mtDNA maintance and embryogenesis in mice. *Nat Genet* 18: 231–236, 1998. doi: 10.1038/ng0398-231.
32. Tyynismaa H, Sembongi H, Bokori-Brown M, Granycome C, Ashley N, Poulton J, Jalanko A, Spelbrink JN, Holt IJ, Suomalainen A. Twinkle helicase is essential for mtDNA maintenance and regulates mtDNA copy number. *Hum Mol Genet* 13: 3219–3227, 2004. doi: 10.1093/hmg/ddh342.
33. Hillen HS, Morozov YI, Sarfallah A, Temiakov D, Cramer P. Structural Basis of Mitochondrial Transcription Initiation. *Cell* 171: 1072-1081.e10, 2017. doi: 10.1016/j.cell.2017.10.036.
34. Saleem A, Hood DA. Acute exercise induces tumour suppressor protein p53 translocation to the mitochondria and promotes a p53-Tfam-mitochondrial DNA complex in skeletal muscle. *J Physiol* 591: 3625–3636, 2013. doi: 10.1113/jphysiol.2013.252791.
35. Hood DA, Adhihetty PJ, Colavecchia M, Gordon JW, Irrcher I, Joseph A-M, Lowe ST, Rungi AA. Mitochondrial biogenesis and the role of the protein import pathway. *Med Sci Sports Exerc* 35: 86–94, 2003. doi: 10.1097/00005768-200301000-00015.
36. Hood DA. The role of mitochondrial fusion and fission in skeletal muscle function and dysfunction. *Front Biosci* 20: 157–172, 2015. doi: 10.2741/4303.
37. Djalalvandi A, Scorrano L. Mitochondrial dynamics: roles in exercise physiology and muscle mass regulation. *Curr Opin Physiol* 27: 100550, 2022. doi: 10.1016/j.cophys.2022.100550.
38. Youle RJ, Narendra DP. Mechanisms of mitophagy. *Nat Rev Mol Cell Biol* 12: 9–14, 2011. doi: 10.1038/nrm3028.
39. Chatzinikita E, Maridaki M, Palikaras K, Koutsilieris M, Philippou A. The Role of Mitophagy in Skeletal Muscle Damage and Regeneration. *Cells* 12: 716, 2023. doi: 10.3390/cells12050716.
40. Elmore S. Apoptosis: A Review of Programmed Cell Death. *Toxicol Pathol* 35: 495–516, 2007. doi: 10.1080/01926230701320337.

41. Liu X, Kim CN, Yang J, Jemmerson R, Wang X. Induction of Apoptotic Program in Cell-Free Extracts: Requirement for dATP and Cytochrome c. *Cell* 86: 147–157, 1996. doi: 10.1016/S0092-8674(00)80085-9.
42. Wang C, Youle RJ. The Role of Mitochondria in Apoptosis. *Annu Rev Genet* 43: 95–118, 2009. doi: 10.1146/annurev-genet-102108-134850.
43. Crompton M, Virji S, Ward JM. Cyclophilin-D binds strongly to complexes of the voltage-dependent anion channel and the adenine nucleotide translocase to form the permeability transition pore. *Eur J Biochem* 258: 729–735, 1998. doi: 10.1046/j.1432-1327.1998.2580729.x.
44. Adhihetty PJ, O'Leary MFN, Hood DA. Mitochondria in skeletal muscle: adaptable rheostats of apoptotic susceptibility. *Exerc Sport Sci Rev* 36: 116–121, 2008. doi: 10.1097/JES.0b013e31817be7b7.
45. Manzanares G, Brito-da-Silva G, Gandra PG. Voluntary wheel running: patterns and physiological effects in mice. *Braz J Med Biol Res* 52: e7830, 2019. doi: 10.1590/1414-431x20187830.
46. Chen CCW, Erlich AT, Hood DA. Role of Parkin and endurance training on mitochondrial turnover in skeletal muscle. *Skelet Muscle* 8: 10, 2018. doi: 10.1186/s13395-018-0157-y.
47. Wong JC, Oliveira AN, Khemraj P, Hood DA. The role of TFE3 in mediating skeletal muscle mitochondrial adaptations to exercise training. *J Appl Physiol* 136: 262–273, 2024. doi: 10.1152/japplphysiol.00484.2023.
48. Little JP, Safdar A, Cermak N, Tarnopolsky MA, Gibala MJ. Acute endurance exercise increases the nuclear abundance of PGC-1alpha in trained human skeletal muscle. *Am J Physiol Regul Integr Comp Physiol* 298: R912-917, 2010. doi: 10.1152/ajpregu.00409.2009.
49. Wu H, Kanatous SB, Thurmond FA, Gallardo T, Isotani E, Bassel-Duby R, Williams RS. Regulation of mitochondrial biogenesis in skeletal muscle by CaMK. *Science* 296: 349–352, 2002. doi: 10.1126/science.1071163.
50. Irrcher I, Ljubicic V, Kirwan AF, Hood DA. AMP-activated protein kinase-regulated activation of the PGC-1alpha promoter in skeletal muscle cells. *PloS One* 3: e3614, 2008. doi: 10.1371/journal.pone.0003614.
51. Puigserver P, Wu Z, Park CW, Graves R, Wright M, Spiegelman BM. A cold-inducible coactivator of nuclear receptors linked to adaptive thermogenesis. *Cell* 92: 829–839, 1998. doi: 10.1016/s0092-8674(00)81410-5.
52. Barrès R, Yan J, Egan B, Treebak JT, Rasmussen M, Fritz T, Caidahl K, Krook A, O'Gorman DJ, Zierath JR. Acute Exercise Remodels Promoter Methylation in Human Skeletal Muscle. *Cell Metab* 15: 405–411, 2012. doi: 10.1016/j.cmet.2012.01.001.
53. Picard M, Gentil BJ, McManus MJ, White K, St. Louis K, Gartside SE, Wallace DC, Turnbull DM. Acute exercise remodels mitochondrial membrane interactions in mouse skeletal muscle. *J Appl Physiol* 115: 1562–1571, 2013. doi: 10.1152/japplphysiol.00819.2013.
54. Holloszy JO. Biochemical Adaptations in Muscle. *J Biol Chem* 242: 2278–2282, 1967. doi: 10.1016/S0021-9258(18)96046-1.
55. Jacobs RA, Lundby C. Mitochondria express enhanced quality as well as quantity in association with aerobic fitness across recreationally active individuals up to elite athletes. *J Appl Physiol* 114: 344–350, 2013. doi: 10.1152/japplphysiol.01081.2012.
56. Suter E, Hoppeler H, Claassen H, Billeter R, Aebi U, Horber F, Jaeger P, Marti B. Ultrastructural Modification of Human Skeletal Muscle Tissue with 6-Month Moderate-Intensity Exercise Training. *Int J Sports Med* 16: 160–166, 1995. doi: 10.1055/s-2007-972985.
57. Pilegaard H, Saltin B, Neufer PD. Exercise induces transient transcriptional activation of the PGC-1alpha gene in human skeletal muscle. *J Physiol* 546: 851–858, 2003. doi: 10.1113/jphysiol.2002.034850.
58. Gordon JW, Rungi AA, Inagaki H, Hood DA. Effects of contractile activity on mitochondrial transcription factor A expression in skeletal muscle. *J Appl Physiol Bethesda Md 1985* 90: 389–396, 2001. doi: 10.1152/jappl.2001.90.1.389.

59. Joseph A-M, Hood DA. Plasticity of TOM complex assembly in skeletal muscle mitochondria in response to chronic contractile activity. *Mitochondrion* 12: 305–312, 2012. doi: 10.1016/j.mito.2011.11.005.
60. Takahashi M, Hood DA. Protein Import into Subsarcolemmal and Intermyofibrillar Skeletal Muscle Mitochondria. *J Biol Chem* 271: 27285–27291, 1996. doi: 10.1074/jbc.271.44.27285.
61. Adhihetty PJ, Uguccioni G, Leick L, Hidalgo J, Pilegaard H, Hood DA. The role of PGC-1alpha on mitochondrial function and apoptotic susceptibility in muscle. *Am J Physiol Cell Physiol* 297: C217-225, 2009. doi: 10.1152/ajpcell.00070.2009.
62. Jiang H-K, Wang Y-H, Sun L, He X, Zhao M, Feng Z-H, Yu X-J, Zang W-J. Aerobic Interval Training Attenuates Mitochondrial Dysfunction in Rats Post-Myocardial Infarction: Roles of Mitochondrial Network Dynamics. *Int J Mol Sci* 15: 5304–5322, 2014. doi: 10.3390/ijms15045304.
63. Axelrod CL, Fealy CE, Mulya A, Kirwan JP. Exercise training remodels human skeletal muscle mitochondrial fission and fusion machinery towards a pro-elongation phenotype. *Acta Physiol* 225: e13216, 2019. doi: 10.1111/apha.13216.
64. Iqbal S, Ostojic O, Singh K, Joseph A-M, Hood DA. Expression of mitochondrial fission and fusion regulatory proteins in skeletal muscle during chronic use and disuse. *Muscle Nerve* 48: 963–970, 2013. doi: 10.1002/mus.23838.
65. Fealy CE, Mulya A, Lai N, Kirwan JP. Exercise training decreases activation of the mitochondrial fission protein dynamin-related protein-1 in insulin-resistant human skeletal muscle. *J Appl Physiol* 117: 239–245, 2014. doi: 10.1152/japplphysiol.01064.2013.
66. Erlich AT, Brownlee DM, Beyfuss K, Hood DA. Exercise induces TFEB expression and activity in skeletal muscle in a PGC-1α-dependent manner. *Am J Physiol Cell Physiol* 314: C62–C72, 2018. doi: 10.1152/ajpcell.00162.2017.
67. Lira VA, Okutsu M, Zhang M, Greene NP, Laker RC, Breen DS, Hoehn KL, Yan Z. Autophagy is required for exercise training-induced skeletal muscle adaptation and improvement of physical performance. *FASEB J Off Publ Fed Am Soc Exp Biol* 27: 4184–4193, 2013. doi: 10.1096/fj.13-228486.
68. Heo J-W, Yoo S-Z, No M-H, Park D-H, Kang J-H, Kim T-W, Kim C-J, Seo D-Y, Han J, Yoon J-H, Jung S-J, Kwak H-B. Exercise Training Attenuates Obesity-Induced Skeletal Muscle Remodeling and Mitochondria-Mediated Apoptosis in the Skeletal Muscle. *Int J Environ Res Public Health* 15: 2301, 2018. doi: 10.3390/ijerph15102301.
69. Beere HM, Wolf BB, Cain K, Mosser DD, Mahboubi A, Kuwana T, Tailor P, Morimoto RI, Cohen GM, Green DR. Heat-shock protein 70 inhibits apoptosis by preventing recruitment of procaspase-9 to the Apaf-1 apoptosome. *Nat Cell Biol* 2: 469–475, 2000. doi: 10.1038/35019501.
70. Cho SH, Kim JH, Song W. *In Vivo* Rodent Models of Skeletal Muscle Adaptation to Decreased Use. *Endocrinol Metab* 31: 31, 2016. doi: 10.3803/EnM.2016.31.1.31.
71. Triolo M, Slavin M, Moradi N, Hood DA. Time-dependent changes in autophagy, mitophagy and lysosomes in skeletal muscle during denervation-induced disuse. *J Physiol* 600: 1683–1701, 2022. doi: 10.1113/JP282173.
72. Tryon LD, Crilly MJ, Hood DA. Effect of denervation on the regulation of mitochondrial transcription factor A expression in skeletal muscle. *Am J Physiol-Cell Physiol* 309: C228–C238, 2015. doi: 10.1152/ajpcell.00266.2014.
73. Goldspink DF. The effects of denervation on protein turnover of rat skeletal muscle. *Biochem J* 156: 71–80, 1976. doi: 10.1042/bj1560071.
74. Tang H, Inoki K, Lee M, Wright E, Khuong A, Khuong A, Sugiarto S, Garner M, Paik J, DePinho RA, Goldman D, Guan K-L, Shrager JB. mTORC1 Promotes Denervation-Induced Muscle Atrophy Through a Mechanism Involving the Activation of FoxO and E3 Ubiquitin Ligases. *Sci Signal* 7, 2014. doi: 10.1126/scisignal.2004809.
75. Ebert SM, Dyle MC, Kunkel SD, Bullard SA, Bongers KS, Fox DK, Dierdorff JM, Foster ED, Adams CM. Stress-induced Skeletal Muscle Gadd45a Expression Reprograms Myonuclei and Causes Muscle Atrophy. *J Biol Chem* 287: 27290–27301, 2012. doi: 10.1074/jbc.M112.374777.

76. Bongers KS, Fox DK, Ebert SM, Kunkel SD, Dyle MC, Bullard SA, Dierdorff JM, Adams CM. Skeletal muscle denervation causes skeletal muscle atrophy through a pathway that involves both Gadd45a and HDAC4. *Am J Physiol-Endocrinol Metab* 305: E907–E915, 2013. doi: 10.1152/ajpendo.00380.2013.
77. Sacheck JM, Hyatt JK, Raffaello A, Thomas Jagoe R, Roy RR, Reggie Edgerton V, Lecker SH, Goldberg AL. Rapid disuse and denervation atrophy involve transcriptional changes similar to those of muscle wasting during systemic diseases. *FASEB J* 21: 140–155, 2007. doi: 10.1096/fj.06-6604com.
78. Memme JM, Oliveira AN, Hood DA. p53 regulates skeletal muscle mitophagy and mitochondrial quality control following denervation-induced muscle disuse. *J Biol Chem* 298: 101540, 2022. doi: 10.1016/j.jbc.2021.101540.
79. Triolo M, Bhattacharya D, Hood DA. Denervation induces mitochondrial decline and exacerbates lysosome dysfunction in middle-aged mice. *Aging* 14: 8900–8913, 2022. doi: 10.18632/aging.204365.
80. Sandri M, Lin J, Handschin C, Yang W, Arany ZP, Lecker SH, Goldberg AL, Spiegelman BM. PGC-1α protects skeletal muscle from atrophy by suppressing FoxO3 action and atrophy-specific gene transcription. *Proc Natl Acad Sci* 103: 16260–16265, 2006. doi: 10.1073/pnas.0607795103.
81. Singh K, Hood DA. Effect of denervation-induced muscle disuse on mitochondrial protein import. *Am J Physiol-Cell Physiol* 300: C138–C145, 2011. doi: 10.1152/ajpcell.00181.2010.
82. O'Leary MFN, Hood DA. Effect of prior chronic contractile activity on mitochondrial function and apoptotic protein expression in denervated muscle. *J Appl Physiol* 105: 114–120, 2008. doi: 10.1152/japplphysiol.00724.2007.
83. Graham ZA, Harlow L, Bauman WA, Cardozo CP. Alterations in mitochondrial fission, fusion, and mitophagic protein expression in the gastrocnemius of mice after a sciatic nerve transection: Mitophagy after Paralysis. *Muscle Nerve* 58: 592–599, 2018. doi: 10.1002/mus.26197.
84. Lu D-X, Huang S-K, Carlson BM. Electron microscopic study of long-term denervated rat skeletal muscle. *Anat Rec* 248: 355–365, 1997. doi: 10.1002/(SICI)1097-0185(199707)248:3<355::AID-AR8>3.0.CO;2-O.
85. Muller FL, Song W, Jang YC, Liu Y, Sabia M, Richardson A, Van Remmen H. Denervation-induced skeletal muscle atrophy is associated with increased mitochondrial ROS production. *Am J Physiol-Regul Integr Comp Physiol* 293: R1159–R1168, 2007. doi: 10.1152/ajpregu.00767.2006.
86. Powers SK, Wiggs MP, Duarte JA, Zergeroglu AM, Demirel HA. Mitochondrial signaling contributes to disuse muscle atrophy. *Am J Physiol-Endocrinol Metab* 303: E31–E39, 2012. doi: 10.1152/ajpendo.00609.2011.
87. Min K, Smuder AJ, Kwon O, Kavazis AN, Szeto HH, Powers SK. Mitochondrial-targeted antioxidants protect skeletal muscle against immobilization-induced muscle atrophy. *J Appl Physiol* 111: 1459–1466, 2011. doi: 10.1152/japplphysiol.00591.2011.
88. Oliveira AN, Memme JM, Wong J, Hood DA. Dimorphic effect of TFE3 in determining mitochondrial and lysosomal content in muscle following denervation. *Skelet Muscle* 14: 7, 2024. doi: 10.1186/s13395-024-00339-1.
89. Adhihetty PJ, O'Leary MFN, Chabi B, Wicks KL, Hood DA. Effect of denervation on mitochondrially mediated apoptosis in skeletal muscle. *J Appl Physiol* 102: 1143–1151, 2007. doi: 10.1152/japplphysiol.00768.2006.
90. Siu PM, Alway SE. Mitochondria-associated apoptotic signalling in denervated rat skeletal muscle. *J Physiol* 565: 309–323, 2005. doi: 10.1113/jphysiol.2004.081083.
91. O′Leary MFN, Vainshtein A, Carter HN, Zhang Y, Hood DA. Denervation-induced mitochondrial dysfunction and autophagy in skeletal muscle of apoptosis-deficient animals. *Am J Physiol-Cell Physiol* 303: C447–C454, 2012. doi: 10.1152/ajpcell.00451.2011.
92. Plant PJ, Bain JR, Correa JE, Woo M, Batt J. Absence of caspase-3 protects against denervation-induced skeletal muscle atrophy. *J Appl Physiol* 107: 224–234, 2009. doi: 10.1152/japplphysiol.90932.2008.
93. López-Otín C, Blasco MA, Partridge L, Serrano M, Kroemer G. The Hallmarks of Aging. *Cell* 153: 1194–1217, 2013. doi: 10.1016/j.cell.2013.05.039.

94. Jackson AS, Sui X, Hébert JR, Church TS, Blair SN. Role of Lifestyle and Aging on the Longitudinal Change in Cardiorespiratory Fitness. *Arch Intern Med* 169, 2009. doi: 10.1001/archinternmed.2009.312.
95. Cheng S-J, Yang Y-R, Cheng F-Y, Chen I-H, Wang R-Y. The Changes of Muscle Strength and Functional Activities During Aging in Male and Female Populations. *Int J Gerontol* 8: 197–202, 2014. doi: 10.1016/j.ijge.2013.08.014.
96. Goldspink G. Age-Related Loss of Muscle Mass and Strength. *J Aging Res* 2012: 1–11, 2012. doi: 10.1155/2012/158279.
97. Crane JD, Devries MC, Safdar A, Hamadeh MJ, Tarnopolsky MA. The Effect of Aging on Human Skeletal Muscle Mitochondrial and Intramyocellular Lipid Ultrastructure. *J Gerontol A Biol Sci Med Sci* 65A: 119–128, 2010. doi: 10.1093/gerona/glp179.
98. Triolo M, Oliveira AN, Kumari R, Hood DA. The influence of age, sex, and exercise on autophagy, mitophagy, and lysosome biogenesis in skeletal muscle. *Skelet Muscle* 12: 13, 2022. doi: 10.1186/s13395-022-00296-7.
99. Chabi B, Ljubicic V, Menzies KJ, Huang JH, Saleem A, Hood DA. Mitochondrial function and apoptotic susceptibility in aging skeletal muscle. *Aging Cell* 7: 2–12, 2008. doi: 10.1111/j.1474-9726.2007.00347.x.
100. Dethlefsen MM, Halling JF, Møller HD, Plomgaard P, Regenberg B, Ringholm S, Pilegaard H. Regulation of apoptosis and autophagy in mouse and human skeletal muscle with aging and lifelong exercise training. *Exp Gerontol* 111: 141–153, 2018. doi: 10.1016/j.exger.2018.07.011.
101. O'Leary MF, Vainshtein A, Iqbal S, Ostojic O, Hood DA. Adaptive plasticity of autophagic proteins to denervation in aging skeletal muscle. *Am J Physiol-Cell Physiol* 304: C422–C430, 2013. doi: 10.1152/ajpcell.00240.2012.
102. Carter HN, Pauly M, Tryon LD, Hood DA. Effect of contractile activity on PGC-1α transcription in young and aged skeletal muscle. *J Appl Physiol Bethesda Md 1985* 124: 1605–1615, 2018. doi: 10.1152/japplphysiol.01110.2017.
103. Cobley JN, Bartlett JD, Kayani A, Murray SW, Louhelainen J, Donovan T, Waldron S, Gregson W, Burniston JG, Morton JP, Close GL. PGC-1α transcriptional response and mitochondrial adaptation to acute exercise is maintained in skeletal muscle of sedentary elderly males. *Biogerontology* 13: 621–631, 2012. doi: 10.1007/s10522-012-9408-1.
104. Leick L, Lyngby SS, Wojtasewski JF, Pilegaard H. PGC-1α is required for training-induced prevention of age-associated decline in mitochondrial enzymes in mouse skeletal muscle. *Exp Gerontol* 45: 336–342, 2010. doi: 10.1016/j.exger.2010.01.011.
105. Zampieri S, Mammucari C, Romanello V, Barberi L, Pietrangelo L, Fusella A, Mosole S, Gherardi G, Höfer C, Löfler S, Sarabon N, Cvecka J, Krenn M, Carraro U, Kern H, Protasi F, Musarò A, Sandri M, Rizzuto R. Physical exercise in aging human skeletal muscle increases mitochondrial calcium uniporter expression levels and affects mitochondria dynamics. *Physiol Rep* 4: e13005, 2016. doi: 10.14814/phy2.13005.
106. Yoo S-Z, No M-H, Heo J-W, Park D-H, Kang J-H, Kim SH, Kwak H-B. Role of exercise in age-related sarcopenia. *J Exerc Rehabil* 14: 551–558, 2018. doi: 10.12965/jer.1836268.134.
107. Ziaaldini MM, Koltai E, Csende Z, Goto S, Boldogh I, Taylor AW, Radak Z. Exercise training increases anabolic and attenuates catabolic and apoptotic processes in aged skeletal muscle of male rats. *Exp Gerontol* 67: 9–14, 2015. doi: 10.1016/j.exger.2015.04.008.
108. Landers-Ramos RQ, Prior SJ. The Microvasculature and Skeletal Muscle Health in Aging. *Exerc Sport Sci Rev* 46: 172–179, 2018. doi: 10.1249/JES.0000000000000151.
109. Ryan NA, Zwetsloot KA, Westerkamp LM, Hickner RC, Pofahl WE, Gavin TP. Lower skeletal muscle capillarization and VEGF expression in aged vs. young men. *J Appl Physiol* 100: 178–185, 2006. doi: 10.1152/japplphysiol.00827.2005.
110. Hunter SK, Pereira HM, Keenan KG. The aging neuromuscular system and motor performance. *J Appl Physiol* 121: 982–995, 2016. doi: 10.1152/japplphysiol.00475.2016.

111. Delmonico MJ, Harris TB, Visser M, Park SW, Conroy MB, Velasquez-Mieyer P, Boudreau R, Manini TM, Nevitt M, Newman AB, Goodpaster BH. Longitudinal study of muscle strength, quality, and adipose tissue infiltration. *Am J Clin Nutr* 90: 1579–1585, 2009. doi: 10.3945/ajcn.2009.28047.
112. Henze H, Jung MJ, Ahrens HE, Steiner S, Von Maltzahn J. Skeletal muscle aging – Stem cells in the spotlight. *Mech Ageing Dev* 189: 111283, 2020. doi: 10.1016/j.mad.2020.111283.
113. Franceschi C, Bonafè M, Valensin S, Olivieri F, De Luca M, Ottaviani E, De Benedictis G. Inflamm-aging: An Evolutionary Perspective on Immunosenescence. *Ann N Y Acad Sci* 908: 244–254, 2000. doi: 10.1111/j.1749-6632.2000.tb06651.x.
114. Delves PJ, Roitt IM. The Immune System. *N Engl J Med* 343: 37–49, 2000. doi: 10.1056/NEJM200007063430107.
115. Clark R, Kupper T. Old Meets New: The Interaction Between Innate and Adaptive Immunity. *J Invest Dermatol* 125: 629–637, 2005. doi: 10.1111/j.0022-202X.2005.23856.x.
116. Netea MG, Quintin J, van der Meer JWM. Trained Immunity: A Memory for Innate Host Defense. *Cell Host Microbe* 9: 355–361, 2011. doi: 10.1016/j.chom.2011.04.006.
117. Janeway CA. Approaching the Asymptote? Evolution and Revolution in Immunology. *Cold Spring Harb Symp Quant Biol* 54: 1–13, 1989. doi: 10.1101/SQB.1989.054.01.003.
118. Matzinger P. Tolerance, Danger, and the Extended Family. *Annu Rev Immunol* 12: 991–1045, 1994. doi: 10.1146/annurev.iy.12.040194.005015.
119. Li D, Wu M. Pattern recognition receptors in health and diseases. *Signal Transduct Target Ther* 6: 291, 2021. doi: 10.1038/s41392-021-00687-0.
120. Medzhitov R, Preston-Hurlburt P, Janeway CA. A human homologue of the Drosophila Toll protein signals activation of adaptive immunity. *Nature* 388: 394–397, 1997. doi: 10.1038/41131.
121. Duan T, Du Y, Xing C, Wang HY, Wang R-F. Toll-Like Receptor Signaling and Its Role in Cell-Mediated Immunity. *Front Immunol* 13: 812774, 2022. doi: 10.3389/fimmu.2022.812774.
122. Fukata M, Vamadevan AS, Abreu MT. Toll-like receptors (TLRs) and Nod-like receptors (NLRs) in inflammatory disorders. *Semin Immunol* 21: 242–253, 2009. doi: 10.1016/j.smim.2009.06.005.
123. Almeida-da-Silva CLC, Savio LEB, Coutinho-Silva R, Ojcius DM. The role of NOD-like receptors in innate immunity. *Front Immunol* 14: 1122586, 2023. doi: 10.3389/fimmu.2023.1122586.
124. Guo H, Callaway JB, Ting JP-Y. Inflammasomes: mechanism of action, role in disease, and therapeutics. *Nat Med* 21: 677–687, 2015. doi: 10.1038/nm.3893.
125. Decout A, Katz JD, Venkatraman S, Ablasser A. The cGAS–STING pathway as a therapeutic target in inflammatory diseases. *Nat Rev Immunol* 21: 548–569, 2021. doi: 10.1038/s41577-021-00524-z.
126. Jiménez-Loygorri JI, Villarejo-Zori B, Viedma-Poyatos Á, Zapata-Muñoz J, Benítez-Fernández R, Frutos-Lisón MD, Tomás-Barberán FA, Espín JC, Area-Gómez E, Gomez-Duran A, Boya P. Mitophagy curtails cytosolic mtDNA-dependent activation of cGAS/STING inflammation during aging. *Nat Commun* 15: 830, 2024. doi: 10.1038/s41467-024-45044-1.
127. Li Y, Cui J, Liu L, Hambright WS, Gan Y, Zhang Y, Ren S, Yue X, Shao L, Cui Y, Huard J, Mu Y, Yao Q, Mu X. mtDNA release promotes cGAS-STING activation and accelerated aging of postmitotic muscle cells. *Cell Death Dis* 15: 523, 2024. doi: 10.1038/s41419-024-06863-8.
128. Chen Q, Sun L, Chen ZJ. Regulation and function of the cGAS–STING pathway of cytosolic DNA sensing. *Nat Immunol* 17: 1142–1149, 2016. doi: 10.1038/ni.3558.
129. Chazaud B. Inflammation during skeletal muscle regeneration and tissue remodeling: application to exercise-induced muscle damage management. *Immunol Cell Biol* 94: 140–145, 2016. doi: 10.1038/icb.2015.97.
130. Nunes-Silva A, Bernardes PTT, Rezende BM, Lopes F, Gomes EC, Marques PE, Lima PMA, Coimbra CC, Menezes GB, Teixeira MM, Pinho V. Treadmill Exercise Induces Neutrophil Recruitment into Muscle Tissue in a Reactive Oxygen Species-Dependent Manner. An Intravital Microscopy Study. *PLoS ONE* 9: e96464, 2014. doi: 10.1371/journal.pone.0096464.
131. McLoughlin TJ, Mylona E, Hornberger TA, Esser KA, Pizza FX. Inflammatory cells in rat skeletal muscle are elevated after electrically stimulated contractions. *J Appl Physiol* 94: 876–882, 2003. doi: 10.1152/japplphysiol.00766.2002.

132. Wang H, Melton DW, Porter L, Sarwar ZU, McManus LM, Shireman PK. Altered Macrophage Phenotype Transition Impairs Skeletal Muscle Regeneration. *Am J Pathol* 184: 1167–1184, 2014. doi: 10.1016/j.ajpath.2013.12.020.
133. Arnold L, Henry A, Poron F, Baba-Amer Y, van Rooijen N, Plonquet A, Gherardi RK, Chazaud B. Inflammatory monocytes recruited after skeletal muscle injury switch into antiinflammatory macrophages to support myogenesis. *J Exp Med* 204: 1057–1069, 2007. doi: 10.1084/jem.20070075.
134. Ji LL, Gomezcabrera M, Steinhafel N, Vina J. Acute exercise activates nuclear factor (NF)-KB signaling pathway in rat skeletal muscle. *FASEB J* 18: 1499–1506, 2004. doi: 10.1096/fj.04-1846com.
135. Leung A, Gregory NS, Allen L-AH, Sluka KA. Regular physical activity prevents chronic pain by altering resident muscle macrophage phenotype and increasing interleukin-10 in mice. *Pain* 157: 70–79, 2016. doi: 10.1097/j.pain.0000000000000312.
136. Samaan MC, Marcinko K, Sikkema S, Fullerton MD, Ziafazeli T, Khan MI, Steinberg GR. Endurance interval training in obese mice reduces muscle inflammation and macrophage content independently of weight loss. *Physiol Rep* 2: e12012, 2014. doi: 10.14814/phy2.12012.
137. Lira FS, Koyama CH, Yamashita AS, Rosa JC, Zanchi NE, Batista ML, Seelaender MC. Chronic exercise decreases cytokine production in healthy rat skeletal muscle. *Cell Biochem Funct* 27: 458–461, 2009. doi: 10.1002/cbf.1594.
138. Gomez-Merino D, Drogou C, Guezennec CY, Chennaoui M. Effects of chronic exercise on cytokine production in white adipose tissue and skeletal muscle of rats. *Cytokine* 40: 23–29, 2007. doi: 10.1016/j.cyto.2007.07.188.
139. Jo E, Lee S-R, Park B-S, Kim J-S. Potential mechanisms underlying the role of chronic inflammation in age-related muscle wasting. *Aging Clin Exp Res* 24: 412–422, 2012. doi: 10.1007/BF03654825.
140. Perry BD, Caldow MK, Brennan-Speranza TC, Sbaraglia M, Jerums G, Garnham A, Wong C, Levinger P, Asrar Ul Haq M, Hare DL, Price SR, Levinger I. Muscle atrophy in patients with Type 2 Diabetes Mellitus: roles of inflammatory pathways, physical activity and exercise. *Exerc Immunol Rev* 22: 94–109, 2016.
141. De Paepe B, De Bleecker JL. Cytokines and Chemokines as Regulators of Skeletal Muscle Inflammation: Presenting the Case of Duchenne Muscular Dystrophy. *Mediators Inflamm* 2013: 1–10, 2013. doi: 10.1155/2013/540370.
142. Loell I, Lundberg IE. Can muscle regeneration fail in chronic inflammation: a weakness in inflammatory myopathies?: Review: Muscle weakness in myositis. *J Intern Med* 269: 243–257, 2011. doi: 10.1111/j.1365-2796.2010.02334.x.
143. Martinon F, Burns K, Tschopp J. The Inflammasome. *Mol Cell* 10: 417–426, 2002. doi: 10.1016/S1097-2765(02)00599-3.
144. Agostini L, Martinon F, Burns K, McDermott MF, Hawkins PN, Tschopp J. NALP3 Forms an IL-1β-Processing Inflammasome with Increased Activity in Muckle-Wells Autoinflammatory Disorder. *Immunity* 20: 319–325, 2004. doi: 10.1016/S1074-7613(04)00046-9.
145. Martinon F, Pétrilli V, Mayor A, Tardivel A, Tschopp J. Gout-associated uric acid crystals activate the NALP3 inflammasome. *Nature* 440: 237–241, 2006. doi: 10.1038/nature04516.
146. Fu J, Wu H. Structural Mechanisms of NLRP3 Inflammasome Assembly and Activation. *Annu Rev Immunol* 41: 301–316, 2023. doi: 10.1146/annurev-immunol-081022-021207.
147. Mariathasan S, Newton K, Monack DM, Vucic D, French DM, Lee WP, Roose-Girma M, Erickson S, Dixit VM. Differential activation of the inflammasome by caspase-1 adaptors ASC and Ipaf. *Nature* 430: 213–218, 2004. doi: 10.1038/nature02664.
148. Dick MS, Sborgi L, Rühl S, Hiller S, Broz P. ASC filament formation serves as a signal amplification mechanism for inflammasomes. *Nat Commun* 7: 11929, 2016. doi: 10.1038/ncomms11929.
149. Bae JY, Park HH. Crystal Structure of NALP3 Protein Pyrin Domain (PYD) and Its Implications in Inflammasome Assembly. *J Biol Chem* 286: 39528–39536, 2011. doi: 10.1074/jbc.M111.278812.

150. Duncan JA, Bergstralh DT, Wang Y, Willingham SB, Ye Z, Zimmermann AG, Ting JP-Y. Cryopyrin/NALP3 binds ATP/dATP, is an ATPase, and requires ATP binding to mediate inflammatory signaling. *Proc Natl Acad Sci* 104: 8041–8046, 2007. doi: 10.1073/pnas.0611496104.
151. Dekker C, Mattes H, Wright M, Boettcher A, Hinniger A, Hughes N, Kapps-Fouthier S, Eder J, Erbel P, Stiefl N, Mackay A, Farady CJ. Crystal Structure of NLRP3 NACHT Domain With an Inhibitor Defines Mechanism of Inflammasome Inhibition. *J Mol Biol* 433: 167309, 2021. doi: 10.1016/j.jmb.2021.167309.
152. Duan Y, Wang J, Cai J, Kelley N, He Y. The leucine-rich repeat (LRR) domain of NLRP3 is required for NLRP3 inflammasome activation in macrophages. *J Biol Chem* 298: 102717, 2022. doi: 10.1016/j.jbc.2022.102717.
153. Hafner-Bratkovič I, Sušjan P, Lainšček D, Tapia-Abellán A, Cerović K, Kadunc L, Angosto-Bazarra D, Pelegrin P, Jerala R. NLRP3 lacking the leucine-rich repeat domain can be fully activated via the canonical inflammasome pathway. *Nat Commun* 9: 5182, 2018. doi: 10.1038/s41467-018-07573-4.
154. Kelley N, Jeltema D, Duan Y, He Y. The NLRP3 Inflammasome: An Overview of Mechanisms of Activation and Regulation. *Int J Mol Sci* 20: E3328, 2019. doi: 10.3390/ijms20133328.
155. Zheng H, Fletcher D, Kozak W, Jiang M, Hofmann KJ, Corn CA, Soszynski D, Grabiec C, Trumbauer ME, Shaw A, Kostura MJ, Stevens K, Rosen H, North RJ, Chen HY, Tocci MJ, Kluger MJ, Van Der Ploeg LHT. Resistance to fever induction and impaired acute-phase response in interleukin-1β-deficient mice. *Immunity* 3: 9–19, 1995. doi: 10.1016/1074-7613(95)90154-X.
156. Dinarello CA. Immunological and Inflammatory Functions of the Interleukin-1 Family. *Annu Rev Immunol* 27: 519–550, 2009. doi: 10.1146/annurev.immunol.021908.132612.
157. Shi J, Zhao Y, Wang K, Shi X, Wang Y, Huang H, Zhuang Y, Cai T, Wang F, Shao F. Cleavage of GSDMD by inflammatory caspases determines pyroptotic cell death. *Nature* 526: 660–665, 2015. doi: 10.1038/nature15514.
158. Cookson BT, Brennan MA. Pro-inflammatory programmed cell death. *Trends Microbiol* 9: 113–114, 2001. doi: 10.1016/S0966-842X(00)01936-3.
159. Gross O, Thomas CJ, Guarda G, Tschopp J. The inflammasome: an integrated view. *Immunol Rev* 243: 136–151, 2011. doi: 10.1111/j.1600-065X.2011.01046.x.
160. Franchi L, Eigenbrod T, Núñez G. Cutting Edge: TNF-α Mediates Sensitization to ATP and Silica via the NLRP3 Inflammasome in the Absence of Microbial Stimulation. *J Immunol* 183: 792–796, 2009. doi: 10.4049/jimmunol.0900173.
161. Sadatomi D, Nakashioya K, Mamiya S, Honda S, Kameyama Y, Yamamura Y, Tanimura S, Takeda K. Mitochondrial function is required for extracellular ATP-induced NLRP3 inflammasome activation.
162. Iyer SS, He Q, Janczy JR, Elliott EI, Zhong Z, Olivier AK, Sadler JJ, Knepper-Adrian V, Han R, Qiao L, Eisenbarth SC, Nauseef WM, Cassel SL, Sutterwala FS. Mitochondrial cardiolipin is required for Nlrp3 inflammasome activation. *Immunity* 39: 311–323, 2013. doi: 10.1016/j.immuni.2013.08.001.
163. Hazeldine J, Hampson P, Opoku FA, Foster M, Lord JM. N-Formyl peptides drive mitochondrial damage associated molecular pattern induced neutrophil activation through ERK1/2 and P38 MAP kinase signalling pathways. *Injury* 46: 975–984, 2015. doi: 10.1016/j.injury.2015.03.028.
164. Zhou R, Yazdi AS, Menu P, Tschopp J. A role for mitochondria in NLRP3 inflammasome activation. *Nature* 469: 221–225, 2011. doi: 10.1038/nature09663.
165. Nakahira K, Haspel JA, Rathinam VAK, Lee S-J, Dolinay T, Lam HC, Englert JA, Rabinovitch M, Cernadas M, Kim HP, Fitzgerald KA, Ryter SW, Choi AMK. Autophagy proteins regulate innate immune responses by inhibiting the release of mitochondrial DNA mediated by the NALP3 inflammasome. *Nat Immunol* 12: 222–230, 2011. doi: 10.1038/ni.1980.
166. Ichinohe T, Yamazaki T, Koshiba T, Yanagi Y. Mitochondrial protein mitofusin 2 is required for NLRP3 inflammasome activation after RNA virus infection. *Proc Natl Acad Sci U S A* 110: 17963–17968, 2013. doi: 10.1073/pnas.1312571110.

167. Subramanian N, Natarajan K, Clatworthy MR, Wang Z, Germain RN. The adaptor MAVS promotes NLRP3 mitochondrial localization and inflammasome activation. *Cell* 153: 348–361, 2013. doi: 10.1016/j.cell.2013.02.054.
168. Collins LV, Hajizadeh S, Holme E, Jonsson I-M, Tarkowski A. Endogenously oxidized mitochondrial DNA induces in vivo and in vitro inflammatory responses. *J Leukoc Biol* 75: 995–1000, 2004. doi: 10.1189/jlb.0703328.
169. Shimada K, Crother TR, Karlin J, Dagvadorj J, Chiba N, Chen S, Ramanujan VK, Wolf AJ, Vergnes L, Ojcius DM, Rentsendorj A, Vargas M, Guerrero C, Wang Y, Fitzgerald KA, Underhill DM, Town T, Arditi M. Oxidized mitochondrial DNA activates the NLRP3 inflammasome during apoptosis. *Immunity* 36: 401–414, 2012. doi: 10.1016/j.immuni.2012.01.009.
170. Yamazaki T, Galluzzi L. BAX and BAK dynamics control mitochondrial DNA release during apoptosis. *Cell Death Differ* 29: 1296–1298, 2022. doi: 10.1038/s41418-022-00985-2.
171. Irazoki A, Gordaliza-Alaguero I, Frank E, Giakoumakis NN, Seco J, Palacín M, Gumà A, Sylow L, Sebastián D, Zorzano A. Disruption of mitochondrial dynamics triggers muscle inflammation through interorganellar contacts and mitochondrial DNA mislocation. *Nat Commun* 14: 108, 2023. doi: 10.1038/s41467-022-35732-1.
172. Irazoki A, Martinez-Vicente M, Aparicio P, Aris C, Alibakhshi E, Rubio-Valera M, Castellanos J, Lores L, Palacín M, Gumà A, Zorzano A, Sebastián D. Coordination of mitochondrial and lysosomal homeostasis mitigates inflammation and muscle atrophy during aging. *Aging Cell* 21: e13583, 2022. doi: 10.1111/acel.13583.
173. Zhou R, Tardivel A, Thorens B, Choi I, Tschopp J. Thioredoxin-interacting protein links oxidative stress to inflammasome activation. *Nat Immunol* 11: 136–140, 2010. doi: 10.1038/ni.1831.
174. Américo-Da-Silva L, Aguilera J, Quinteros-Waltemath O, Sánchez-Aguilera P, Russell J, Cadagan C, Meneses-Valdés R, Sánchez G, Estrada M, Jorquera G, Barrientos G, Llanos P. Activation of the NLRP3 Inflammasome Increases the IL-1β Level and Decreases GLUT4 Translocation in Skeletal Muscle during Insulin Resistance. *Int J Mol Sci* 22: 10212, 2021. doi: 10.3390/ijms221910212.
175. Russell-Guzmán J, Américo-Da Silva L, Cadagan C, Maturana M, Palomero J, Estrada M, Barrientos G, Buvinic S, Hidalgo C, Llanos P. Activation of the ROS/TXNIP/NLRP3 pathway disrupts insulin-dependent glucose uptake in skeletal muscle of insulin-resistant obese mice. *Free Radic Biol Med* 222: 187–198, 2024. doi: 10.1016/j.freeradbiomed.2024.06.011.
176. Park S, Won J-H, Hwang I, Hong S, Lee HK, Yu J-W. Defective mitochondrial fission augments NLRP3 inflammasome activation. *Sci Rep* 5: 15489, 2015. doi: 10.1038/srep15489.
177. Eggelbusch M, Shi A, Broeksma BC, Vázquez-Cruz M, Soares MN, de Wit GMJ, Everts B, Jaspers RT, Wüst RCI. The NLRP3 inflammasome contributes to inflammation-induced morphological and metabolic alterations in skeletal muscle. *J Cachexia Sarcopenia Muscle* n/a, 2022. doi: 10.1002/jcsm.13062.
178. Xiang Y, Dai J, Xu L, Li X, Jiang J, Xu J. Research progress in immune microenvironment regulation of muscle atrophy induced by peripheral nerve injury. *Life Sci* 287: 120117, 2021. doi: 10.1016/j.lfs.2021.120117.
179. Huang N, Kny M, Riediger F, Busch K, Schmidt S, Luft FC, Slevogt H, Fielitz J. Deletion of Nlrp3 protects from inflammation-induced skeletal muscle atrophy. *Intensive Care Med Exp* 5: 3, 2017. doi: 10.1186/s40635-016-0115-0.
180. Liu Y, Bi X, Zhang Y, Wang Y, Ding W. Mitochondrial dysfunction/NLRP3 inflammasome axis contributes to angiotensin II-induced skeletal muscle wasting via PPAR-γ. *Lab Invest* 100: 712–726, 2020. doi: 10.1038/s41374-019-0355-1.
181. You Z, Huang X, Xiang Y, Dai J, Xu L, Jiang J, Xu J. Ablation of NLRP3 inflammasome attenuates muscle atrophy via inhibiting pyroptosis, proteolysis and apoptosis following denervation. *Theranostics* 13: 374–390, 2023. doi: 10.7150/thno.74831.
182. Franceschi C, Garagnani P, Parini P, Giuliani C, Santoro A. Inflammaging: a new immune–metabolic viewpoint for age-related diseases. *Nat Rev Endocrinol* 14: 576–590, 2018. doi: 10.1038/s41574-018-0059-4.

183. Perkins RK, Lavin KM, Raue U, Jemiolo B, Trappe SW, Trappe TA. Effects of aging and lifelong aerobic exercise on expression of innate immune components in human skeletal muscle. J Appl Physiol (1985) 129: 1483–1492, 2020. doi: 10.1152/japplphysiol.00615.2020.
184. McBride MJ, Foley KP, D'Souza DM, Li YE, Lau TC, Hawke TJ, Schertzer JD. The NLRP3 inflammasome contributes to sarcopenia and lower muscle glycolytic potential in old mice. *Am J Physiol Endocrinol Metab* 313: E222–E232, 2017. doi: 10.1152/ajpendo.00060.2017.
185. Antuña E, Potes Y, Baena-Huerta FJ, Cachán-Vega C, Menéndez-Coto N, Álvarez Darriba E, Fernández-Fernández M, Burgos Bencosme N, Bermúdez M, López Álvarez EM, Gutiérrez-Rodríguez J, Boga JA, Caballero B, Vega-Naredo I, Coto-Montes A, Garcia-Gonzalez C. NLRP3 Contributes to Sarcopenia Associated to Dependency Recapitulating Inflammatory-Associated Muscle Degeneration. *Int J Mol Sci* 25: 1439, 2024. doi: 10.3390/ijms25031439.
186. Nam BY, Jhee JH, Park J, Kim S, Kim G, Park JT, Yoo T-H, Kang S-W, Yu J-W, Han SH. PGC-1α inhibits the NLRP3 inflammasome via preserving mitochondrial viability to protect kidney fibrosis. *Cell Death Dis* 13: 31, 2022. doi: 10.1038/s41419-021-04480-3.
187. Eisele PS, Salatino S, Sobek J, Hottiger MO, Handschin C. The Peroxisome Proliferator-activated Receptor γ Coactivator 1α/β (PGC-1) Coactivators Repress the Transcriptional Activity of NF-κB in Skeletal Muscle Cells. *J Biol Chem* 288: 2246–2260, 2013. doi: 10.1074/jbc.M112.375253.
188. Ma M, Chen W, Hua Y, Jia H, Song Y, Wang Y. Aerobic exercise ameliorates cardiac hypertrophy by regulating mitochondrial quality control and endoplasmic reticulum stress through M2 AChR. *J Cell Physiol* 236: 6581–6596, 2021. doi: 10.1002/jcp.30342.
189. Lee J, Lee Y, LaVoy EC, Umetani M, Hong J, Park Y. Physical activity protects NLRP3 inflammasome-associated coronary vascular dysfunction in obese mice. *Physiol Rep* 6: e13738, 2018. doi: 10.14814/phy2.13738.
190. Wang W, Lv Z, Gao J, Liu M, Wang Y, Tang C, Xiang J. Treadmill exercise alleviates neuronal damage by suppressing NLRP3 inflammasome and microglial activation in the MPTP mouse model of Parkinson's disease. *Brain Res Bull* 174: 349–358, 2021. doi: 10.1016/j.brainresbull.2021.06.024.
191. Mardare C, Krüger K, Liebisch G, Seimetz M, Couturier A, Ringseis R, Wilhelm J, Weissmann N, Eder K, Mooren F-C. Endurance and Resistance Training Affect High Fat Diet-Induced Increase of Ceramides, Inflammasome Expression, and Systemic Inflammation in Mice. *J Diabetes Res* 2016: 4536470, 2016. doi: 10.1155/2016/4536470.

CHAPTER 2: MANUSCRIPT

MANUSCRIPT AUTHOR CONTRIBUTIONS

Priyanka Khemraj: Performed denervation surgeries and tissue collection for all animals; collected data for chronic and acute training protocols; conducted experimental testing and data analysis for DNA extractions, subcellular isolations, qPCR, ELISA, respiration, ROS analysis and western blotting; wrote the manuscript.

Anastasiya Kuznyetsova: Aided in performing mitochondrial fractionations.

Dr. David A. Hood: Supervisor of the project and is the Principal Investigator.

INVESTIGATING THE EFFECT OF AGING, ENDURANCE TRAINING AND MUSCLE DENERVATION ON INNATE IMMUNE SIGNALING WITHIN SKELETAL MUSCLE

Priyanka Khemraj, Anastasiya Kuznyetsova and David A. Hood

Muscle Health Research Centre, School of Kinesiology and Health Science, York University, Toronto, Ontario, M3J 1P3, Canada

To whom correspondence should be addressed: David A. Hood, PhD. (dhood@yorku.ca)
Muscle Health Research Centre
School of Kinesiology and Health Science
York University, Toronto, ON, M3J 1P3,
Canada

ABSTRACT

Skeletal muscle function heavily relies on the intricate mitochondrial reticulum that contributes towards its unique plasticity. As a component of the innate immune system, the NLRP3 inflammasome complex has been recognized in its ability to respond to various mitochondrial damage-associated molecular patterns, however, its relation to mitochondrial dysfunction within skeletal muscle still requires further exploration. The purpose of this study was to characterize innate immune signaling and mitochondrial function in response to skeletal muscle disuse and use. To study a severe form of muscle disuse, we utilized a sciatic nerve transection, which was associated with decreases in hindlimb muscle mass, mitochondrial content, and impaired respiration. In conjunction, western blotting and ELISA revealed increases in NF-κB p65 subunit, and downstream inflammasome components including NLRP3, procaspase-1, caspase-1, GSDMD, GSDMD-N, and pro-inflammatory cytokine IL-1β. Other pathways that could further stimulate innate immune activation such as STING protein expression and pro-apoptotic BAX and AIF protein were also upregulated. When assessing potential DAMPS, denervation was associated with increased ROS production, but no changes in cytosolic mtDNA levels. Since we suspected that inflammasome activation would be increased with age, we studied young (6-7 months) and aged (21-22 months) mice and subjected them to a 6-week voluntary wheel running protocol. Training adaptations were apparent, especially within the aged animals, through the preservation of hindlimb muscle mass and improvements in oxygen consumption and endurance performance. Furthermore, we observed an effect of training on attenuating age-related increases in NLRP3, procaspase-1, caspase-1, and GSDMD protein expression, which was similarly observed with both STING and BAX protein expression. However, no changes in ROS and cytosolic mtDNA were detected. However, this work demonstrated that aged muscle displays increased innate immune

adaptability despite reduced exercise capacity. By demonstrating that the NLRP3 inflammasome complex is responsive to skeletal muscle activity, this work could implicate endurance training as a promising therapeutic for combatting age-related inflammation and skeletal muscle dysfunction.

Keywords: mitochondria, aging, denervation, endurance training, NLRP3 Inflammasome

INTRODUCTION

Skeletal muscle is a dynamic organ that plays a critical role in whole-body metabolism, locomotion, and structural stability (1). As an essential component of skeletal muscle health, the mitochondrial reticulum has been increasingly recognized for its remarkable plasticity, allowing skeletal muscle to adapt to changing metabolic needs (1). The innate immune system is another highly reactive network that aids in the recognition and response towards harmful stimuli, ultimately promoting cellular homeostasis and survival (2). While often underappreciated, the immune system is heavily involved in maintaining skeletal muscle health by mediating muscle regeneration, pathogenic invasion, and acute muscle damage (3, 4). However, while this response is beneficial for short-term recovery, chronic inflammation has been linked to detrimental impacts on skeletal muscle function and mass, and the development of various conditions (5, 6). As a primary component of the innate immune system, the NLRP3 inflammasome complex has been gaining increased attention for its role in recognizing and responding to a variety of pathogen-associated molecular patterns (PAMPs) and endogenous damage-associated molecular patterns (DAMPs) including viral RNA, ROS, bacterial antigens and ion fluctuations (7). To carefully regulate its activation, the NLRP3 inflammasome complex generally uses a two-step activation process including priming and subsequent assembly. The priming stage is initiated by the recognition of DAMPs and PAMPs by pattern recognition receptors (PRRs) such as Toll-like receptors and the cGAS-STING pathway (8, 9). This promotes the nuclear translocation of NF-κB, which aids in the transcriptional upregulation of NLRP3, pro-IL-1β and pro-IL-18. Following this step, a second signal initiates the assembly of the multi-protein complex comprised of NLRP3, apoptosis speck-like protein (ASC), and the cysteine protease procaspase-1. The formation of the NLRP3 inflammasome complex ultimately leads to the maturation of IL-1β, IL-18, and pyroptosis

initiator Gasdermin-D to aid in the destruction of dysfunctional cells and promote the secretion of pro-inflammatory factors to mount a local immune response (7, 10).

Due to the dynamic nature of skeletal muscle mitochondria, there has been an increased focus on investigating how mitochondrial adaptations can influence NLRP3 inflammasome activation and skeletal muscle health. Specifically, due to their roles as vital signaling hubs, skeletal muscle mitochondria have been implicated in the release of several DAMPS (mtDAMPS) including ROS, mitochondrial DNA (mtDNA) and cardiolipin, that can stimulate an innate immune response (11). Chronic skeletal muscle disuse, which is often observed in conditions such as paralysis and aging, is associated with increased mitochondrial dysfunction and poor muscle function (12). Due to a fragmented mitochondrial reticulum and the accumulation of mtDAMPs such as mtROS and mtDNA, prior literature has observed a pro-inflammatory profile and skeletal muscle wasting following periods of chronic disuse that is augmented by increased NLRP3 inflammasome activity (13, 14). In addition, the natural progression of aging is also associated with similar adaptations including impairments in several mitochondrial quality control processes, leading to a chronic state of low-grade inflammation which has been coined “Inflammaging” (15). The NLRP3 inflammasome complex has been implicated in contributing to this pro-inflammatory environment within skeletal muscle as the overactivation of caspase-1 increased muscle atrophy alongside reductions in force and endurance, which was rescued upon NLRP3 KO (16). In contrast, chronic exercise has been widely considered one of the best interventions for skeletal muscle by promoting an interconnected mitochondrial reticulum that is characterized by improved mitochondrial functioning and the reduced production of damage molecules such as ROS (17). In other tissue types, long-term aerobic training has been associated with a reduced inflammatory environment and a decreased drive toward NLRP3 inflammasome activation (18, 19). However, the relationship

between chronic exercise, skeletal muscle health, and NLRP3 inflammasome activation has yet to be explored.

These findings have prompted us to further investigate the relationship between mitochondrial adaptations and NLRP3 inflammasome activation *in vivo* using mouse models of chronic muscle disuse and chronic use to elucidate the impact of these opposing stimuli. In this study, we induced muscle disuse through a hindlimb denervation procedure performed on young wild-type (WT) mice and analyzed various parameters of mitochondrial function and NLRP3 inflammasome activation. In addition, recognizing that hindlimb denervation is an extreme model of muscle disuse, we also investigated aging as a more realistic condition associated with skeletal muscle dysfunction and immune dysregulation by using 21-22 month aged mice to establish the basal influence of age on innate immune signaling. Furthermore, as chronic exercise has been shown to possess anti-inflammatory effects, we decided to superimpose a 6-week voluntary wheel running protocol with our aging model to investigate whether exercise influenced NLRP3 inflammasome activation within skeletal muscle. Briefly, our findings indicate a positive relationship between skeletal muscle disuse, maladaptive mitochondrial adaptations, and activation of the NLRP3 inflammasome complex within skeletal muscle. In contrast, chronic exercise leads to improvements in skeletal muscle function and an attenuation of innate immune signaling in particularly the aged mice, despite a reduced exercise capacity compared to their young counterparts. Thus, these findings highlight a promising relationship between skeletal muscle metabolic conditions, mitochondrial health and innate immune signaling that can be further explored.

METHODS

Animals. All mice were obtained from Jackson Laboratories and housed in the York University vivarium with a 12:12h light-dark cycle and open access to food and water. Approval for all experiments was obtained from the York University Animal Care Committee. For the denervation study, male FVB mice were 3-6 months at the time of tissue collection. For the voluntary wheel running study, young mice were 6-7 months, and aged mice were 21-22 months at the time of tissue collection.

Sciatic Transection Surgery. At 3-6 months of age, male wild-type FVB mice were subjected to a sciatic nerve transection to induce hindlimb muscle denervation. Briefly, mice were anesthetized using isoflurane, and a small incision was made to reveal the sciatic nerve. In the denervated limb, a 2-3 mm section of the nerve was transected, and the incision was subsequently closed. The contralateral limb was sham-operated and used as an internal control. For post-surgery pain management, mice were given subcutaneous injections of Metacam for two days post-surgery (Day 1: 2µg/g body weight; Day 2: 1µg/g body weight). Additionally, all mice were also provided Baytril (25mg/100mL) within their water to reduce the risk of infection for the denervation period. After 7 days following denervation, the hindlimb muscles were collected and flash-frozen in liquid nitrogen for subsequent analysis.

Voluntary Wheel Running. Male young (4-5 months) and old (19-20 months) C57BL6/J mice were randomly assigned to either a sedentary control group or a training group, so that they were approximately 6-7 months and 21-22 months at the time of tissue collection. Mice assigned to the training group had their cages fixed with a freely rotating running wheel for the remainder of the training intervention. Animals were given a one-week acclimatization period followed by a 6-week training period where revolutions were recorded by a magnetic counter. Distance in kilometres

was calculated by multiplying the circumference of the wheel by the number of revolutions (sample calculation listed in Appendix C). Any animals that did not engage with the running wheel during the acclimatization period were reassigned to the untrained group.

Acute Endurance Testing Protocol. An acute treadmill endurance test was performed for all animals before and after the intervention period. Mice were acclimatized to the treadmills for two consecutive days before testing (Day 1: 0 m/min for 5 minutes, 5 m/min for 5 mins, 10 m/min for 5 minutes; Day 2: 0 m/min for 5 minutes, 5 m/min for 5 minutes, and 10 m/min for 10 minutes). To avoid injury to the aged animals, the aged animals were tested with a less vigorous treadmill protocol compared to their young counterparts. Exhaustion was defined as the inability to remain on the treadmill despite prodding. Total distance and time ran were used to calculate percent changes as a measure of endurance improvement. The protocols used are listed in Table C1.

Muscle Protein Extraction. Protein extracts from the tibialis anterior were prepared from 25-30 grams of flash-frozen mouse muscle. The tissue was immersed in a Sakamoto Extraction Buffer (20mM HEPES, 2mM EGTA, 1% Triton X-100, 50% Glycerol, 50mM B-Glycerophosphate) containing protease and phosphatase inhibitors (Sigma) to prevent protein degradation. The tissue was then mechanically homogenized using a Tissue Lyser (Qiagen) at a frequency of 30Hz in one-minute intervals until a uniform homogenate was obtained. To isolate the protein extract, the homogenized tissue was centrifuged at 14000g for 10 minutes at 4ºC, and the resulting supernatant was stored at -80ºC until further analysis.

Mitochondrial and Cytosolic Fractionation. Immediately following collection, gastrocnemius muscle was immersed in a Mitochondrial Isolation Buffer (Appendix C). The muscle was minced on a glass plate over ice and subsequently homogenized using a Dounce homogenizer (Fisher Scientifics). The resulting homogenate was centrifuged at 1200g for 15 minutes, and the resulting

supernatant was collected and centrifuged at 21000g for 20 minutes to obtain a mitochondrial pellet and cytosolic fraction. The mitochondrial pellet was resuspended in 100µL of the mitochondrial isolation buffer and centrifuged at 21000g for 20 minutes. The supernatant was discarded, and the final pellet was resuspended in 20-40µL of buffer to obtain the final mitochondrial fraction. The cytosolic fraction was centrifuged twice at 21000g, where the supernatant was transferred to a new 1.5mL eppendorf tube following each spin to obtain the final cytosolic fraction. All centrifugation steps were performed at 4ºC. Both the mitochondrial and cytosolic fractions were stored at -80ºC until further analysis. Protein concentrations were assessed using a Bradford protein assay and purity was confirmed by western blotting using mitochondrial content markers COX-IV and VDAC, to ensure minimal mitochondrial contamination within the cytosolic fraction (Supplementary figure B3).

Western Blotting. Protein concentrations were determined using a Bradford protein concentration assay and a plate reader. For western blotting, 15-90µg of protein was loaded onto a 10-15% SDS-page gel and the proteins were separated by molecular weight using electrophoresis at 120 volts for approximately 90 minutes. The protein was then transferred to a nitrocellulose membrane and stained using Ponceau red to ensure proper transfer and for subsequent normalization. The membranes were then blocked with 5% skim milk in 1xTBS-T for an hour and incubated with the specific primary antibody overnight at 4ºC. The following day, the blots were washed with TBS-T (5 minutes x 3 washes) and incubated with the corresponding secondary antibody for 1 hour at room temperature. All antibodies used in this study are listed in Table 2. The blots were washed again (5x3) and imaged using enhanced chemiluminescence via the iBright CL1500 Imaging System. All samples were normalized to the corresponding ponceau to correct for protein loading.

Antibody List			
Antibody Target	**Manufacturer**	**Catalogue #**	**Molecular Weight (kDa)**
COX-IV	Abcam	ab14744	15
COX-I	Abcam	ab14705	39
VDAC	Abcam	ab14734	32
MURF-1	Santa Cruz	sc-398608	50
GADD-45α	Santa Cruz	sc-6850	22
NF-κB p65	Santa Cruz	sc-8008	65
NLRP3	Abcam	ab270449	~120
Procaspase-1/Caspase-1	Abcam	ab138483	Procaspase-1: 51 Caspase-1 p20: 25
GSDMD/GSDMD-N terminal fragment	Abcam	ab219800	Gasdermin-D: 53 Gasdermin-D N: ~32
STING	Cell Signaling	50494S	37
BAX	Santa Cruz	sc-7480	26
AIF	Santa Cruz	sc-13116	60
HRP-linked Anti-Mouse Secondary	Cell Signaling	7074S	-
HRP-linked Anti-Rabbit Secondary	Cell Signaling	7076S	-
Goat anti-Rabbit Secondary	Abcam	ab6721	-

Table 1: Antibodies used for western blotting.

ELISA. The Mouse IL-1β/IL-F2 Duoset ELISA kit (R&D Systems) was used to assess the protein levels of IL-1β. Using a 96-well plate, the IL-1β capture antibody was added to each well and incubated overnight. The following day, each well was washed and blocked with 1% BSA for 1 hour. Following this incubation, the plate was washed, and the corresponding skeletal muscle extracts and protein standard (15-1000 pg/mL) were incubated for 2 hours. Afterward, the IL-1β detection antibody was added and incubated for 2 hours. The Streptavidin-HRP conjugate was added to the wells and incubated, followed by the addition of a 1:1 hydrogen peroxide and tetramethyl benzadine substrate mixture for 20 minutes. Finally, the stop solution was combined, and the resulting absorbance was measured using a plate reader at 450nm and 570nm. To correct for optical inconsistencies and baseline absorbance, the 570nm values were subtracted from the 450nm measurements, and the blank solution absorbance was subtracted from the resulting values. To assess the concentration of IL-1β within the samples, the measured concentrations were compared to the standard curve and corrected for their respective dilution factor. All incubations took place at room temperature.

gDNA Extraction. Genomic DNA was isolated from gastrocnemius muscle and the corresponding cytosolic fraction for qPCR analysis using the DNeasy Blood and Tissue Kit (Qiagen) as per the manufacturer's instructions. For the whole muscle extraction, ~18-25 mg of frozen muscle was immersed in 180µL of Buffer ATL and 20µL of proteinase K and incubated at 56ºC for 1 hour and 20 minutes. Afterwards, 200µL of Buffer AL and 200µL of absolute ethanol were added, and the resulting mixture was added to the provided DNeasy spin column. The mixture was then centrifuged at 6000g for 1 minute, washed with 500µL of Buffer AW1, and spun again at 6000g for 1 minute. Following this spin, 500µL of Buffer AW2 was added and the mixture was centrifuged at 20000g for 3 minutes. To elute the DNA, 120µL of Buffer AE was added for 1

minute, and centrifuged for 6000g for 1 minute. The resulting gDNA was collected and stored at -20ºC. For the cytosolic gDNA extraction, 200µL of the cytosolic fraction was combined with 20µL of proteinase K and 200µL of buffer AL, before being incubated at 56ºC for 10 minutes. For the remaining steps, the same protocol was followed as for the gDNA extraction from whole tissue. Due to lower concentrations, the cytosolic gDNA was eluted in 70-100µL and stored at -20ºC. The resulting concentrations were measured using the NanoDrop 2000 and the cytosolic and gastrocnemius samples were diluted to equal concentrations, respectively.

Qualitative Polymerase Chain Reaction. To analyze the genes of interest, forward and reverse primers were created and optimized to the corresponding set of samples (Table 3). mRNA expression was measured using the StepOnePlus Real-time PCR system (Applied Biosystems) with the SYBR Green qPCR Master Mix (Sigma). Each well plate contains 25µL of reaction volume consisting of sterile water, the corresponding forward and reverse primers (20µM) and 2µL of gDNA. All samples are run in duplicates to increase reliability. The resulting gene expression is then normalized to the housekeeping gene GAPDH. Quantification is done by 1) Calculating the ΔCycle Threshold (CT) = mean CT of gene of interest – mean CT of housekeeping genes, 2) The resulting fold change is calculated by $2^{(-\Delta CT)}$. The obtained whole muscle fold changes were corrected to account for the increased dilution factor in the whole muscle samples compared to the cytosolic fractions.

List of Forward and Reverse Primers		
Gene of Interest	**Forward Sequence**	**Reverse Sequence**
16s rRNA	5'-AAC ACT GAG CAT CTC CCT CA-3'	5'-GTG GGT GCA GCG AAC TTT AT- 3'
GAPDH	5'-CTA GAA ACC CCG AAA CCA AA-3'	5'-CCA GCT ATC ACC AAG CTC GT- 3'

Table 2: qPCR primers used in the analysis of mitochondrial DNA.

High-resolution Respiratory and H_2O_2 Production. A small portion of the tibialis anterior muscle was collected and immediately stored in a cold BIOPS buffer (2.77mM CaK_2EGTA, 7.23mM K_2EGTA, 5.77mM Na_2ATP, 6.56mM $MgCl_2$ hexahydrate, 20mM Taurine, 15mM Na_2Phosphocreatine, 20mM Imidazole, 0.5mM Dithiothreitol, 50mM MES Hydrate). The muscle fibers were teased apart and permeabilized in a BIOPS buffer with 40µg/µL Saponin for 30 minutes at 4ºC on an orbital shaker with constant motion. The fiber bundles were then washed twice in Buffer Z (105mM K-MES, 30mM KCl, 10mM KH_2PO4, 5mM $MgCl_2$ hexahydrate, 1mM EGTA, 5mg/mL BSA). Following this preparation, the fibers were incubated in Buffer Z with 1µL Blebbistatin to avoid tetanic contractions (B592500, Toronto Research Chemicals), 10µM Amplex-Red (A36006, Thermofisher), 25 U/mL Cu/Zn SOD1 to convert any superoxide molecules to H_2O_2, and 2mM EGTA. For ROS measurements, 0.5U horseradish peroxidase and 0.1µM H_2O_2 were added to the chamber for calibration. To obtain measurements for various states of respiration, high-resolution respirometry was used (Power Oxygraph 2k-Fluorospirometer, Oroboros Instruments) and substrates were added in the following order: 1) Complex I inactive: pyruvate and malate, 2) Complex I active: ADP, and 3) Complex I+II active: succinate. All respiration and ROS emission measurements were corrected to the muscle fiber dry weight.

Statistical Analysis. All data was analyzed using GraphPad Prism 9.0, and values were expressed as mean ± standard deviation. The differences between the denervated and contralateral limb was assessed using a student's paired t-test. For the VWR study, all data was analyzed using a two-way ANOVA with a Tukey's post-hoc test to assess differences between groups. Statistical significance was considered as $p < 0.05$. All figures included in this manuscript were created using Microsoft PowerPoint and BioRender.com.

RESULTS

7 days of muscle denervation alters skeletal muscle and mitochondrial functioning. To induce muscle disuse, a sciatic nerve transection was performed (Figure 1A). Following 7 days of muscle denervation, there was a moderate reduction in total hindlimb muscle mass (Figure 1C, $p<0.0001$), but no reduction in total body weight (Figure 1B). This effect can be seen consistently across skeletal muscles of various fiber types including mixed muscles such as the tibialis anterior (Figure 1D, $p<0.0001$) and gastrocnemius (Figure 1F, $p<0.001$), as well as highly oxidative muscles like the soleus (Figure 1E, $p<0.0001$). To further confirm the presence of muscle atrophy, the protein expression of several muscle atrophy markers were assessed. Muscle denervation induced a drastic increase in the expression of the E3 ubiquitin ligase, MURF1 ($p<0.001$) and muscle atrophy inducer, GADD45α (Figure 1G, $p<0.05$) which indicates increased signaling towards muscle degradation.

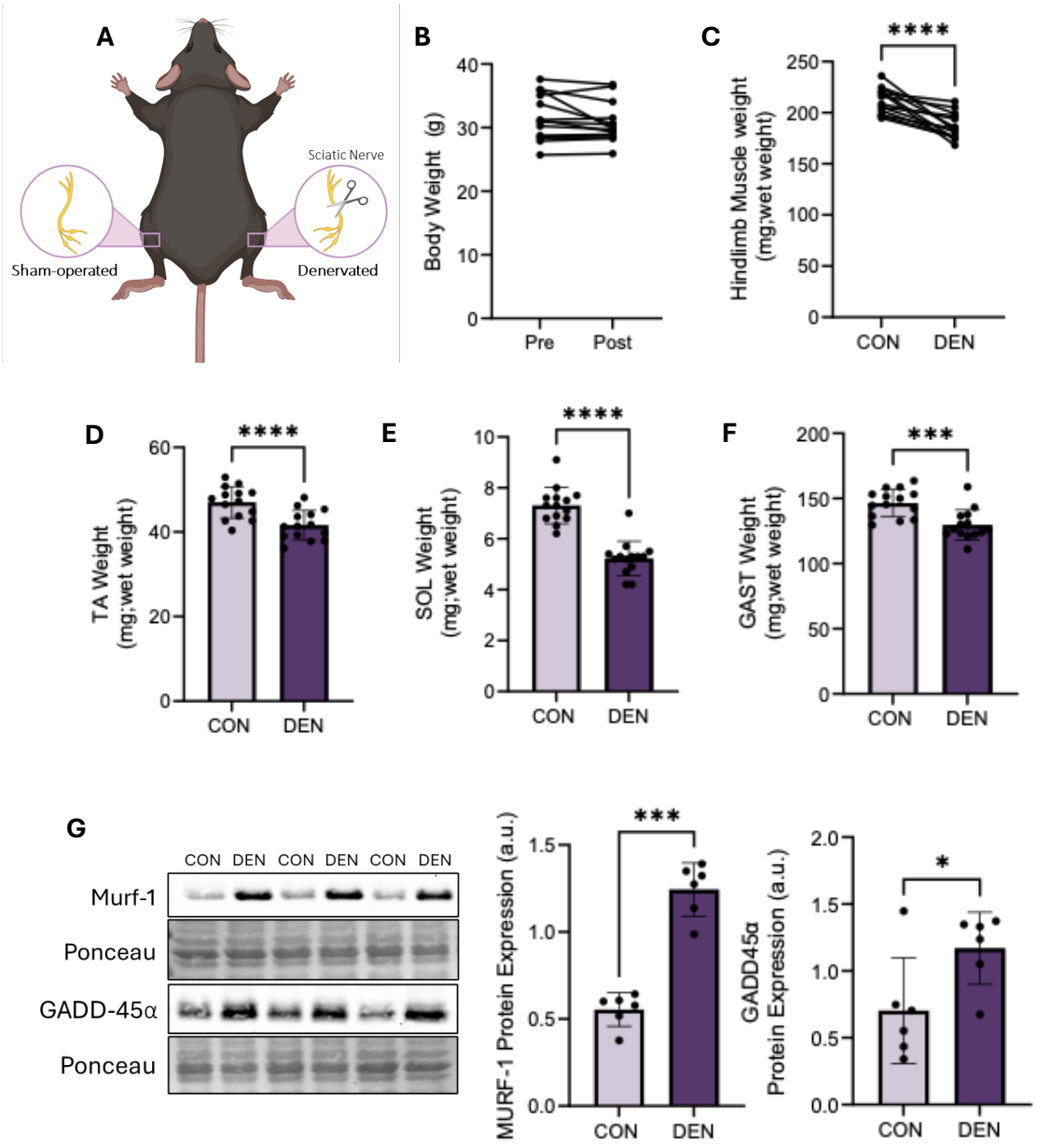

Figure 1: Skeletal muscle characteristics following 7 days of muscle denervation. Study design for the induction of skeletal muscle disuse using a sciatic nerve transection (A). Differences in body weight before and after denervation surgery (B) (n=14). Total hindlimb muscle mass (C) and individual muscle weights of TA (D), SOL (E), and (F) GAST compared to sham-operated control (n=14). Representative western blot of MURF-1 and GADD-45α protein expression alongside the corresponding quantifications (G) (n=6). All measurements underwent a paired student's t-test. *, $p<0.05$; ***, $p<0.001$; ****, $p<0.0001$). TA, tibialis anterior; SOL, soleus; GAST, gastrocnemius; CON, control; DEN, denervated. Values are expressed as mean ± SD. A portion of Figure 1A was created using BioRender.com.

Muscle denervation induces maladaptive changes within skeletal muscle mitochondria. To assess the impact of denervation on the mitochondrial reticulum, we evaluated several mitochondrial markers including the outer membrane protein VDAC, and a subunit of complex IV within the electron transport chain, COX-IV. Both content markers demonstrated reduced protein expression following the sciatic nerve transection indicating reduced mitochondrial content compared to the sham-operated control (Figure 2B, $p<0.05$; Figure 2C, $p<0.01$). Furthermore, to examine a functional parameter of the mitochondrial pool, respiration analysis was performed using O2k high-resolution respirometry. Muscle disuse led to impaired complex I inactive (Figure 2D, $p<0.05$) and active respiration (Figure 2E, $p=0.06$) when supplemented with pyruvate/malate and ADP respectively, indicating maladaptive mitochondrial functioning.

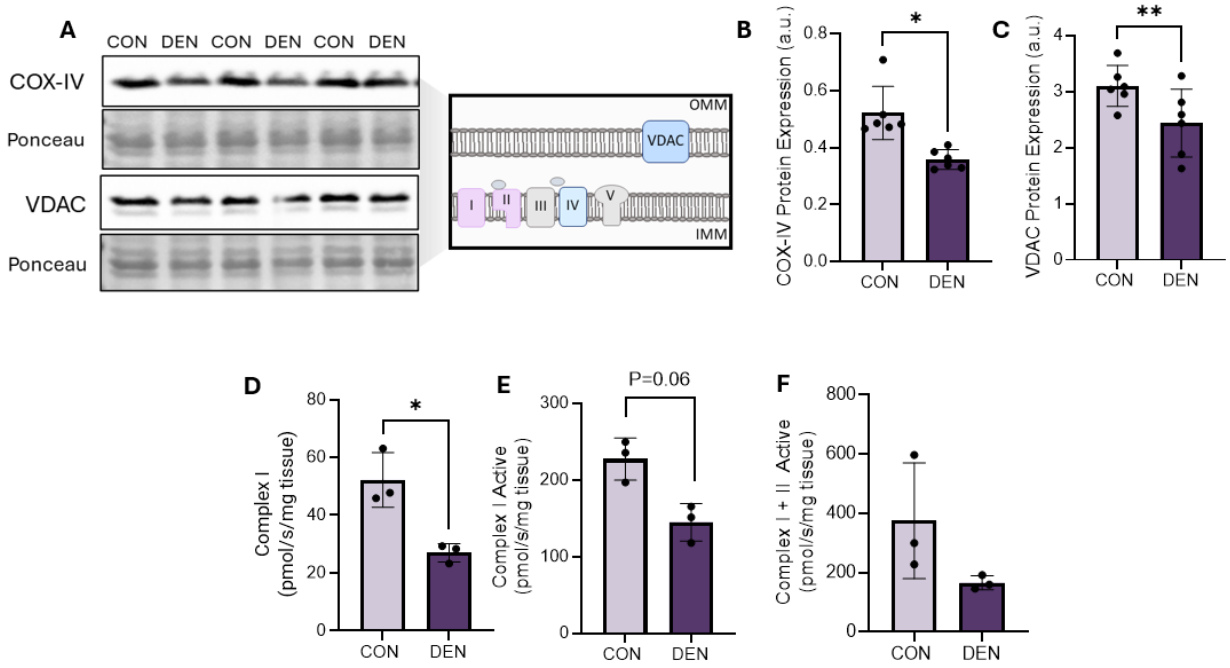

Figure 2: Skeletal muscle mitochondrial adaptations following 7 days of muscle denervation. Representative western blots of mitochondrial content markers, COX-IV and VDAC (A), alongside their corresponding quantifications (B, C) (n=6). Oxygen consumption rates during complex I (D), complex I active (E), and complex I+II active (F) states of respiration (n=3). Data was analyzed using a paired student's t-test. *, $p<0.05$; **, $p<0.01$. CON, control; DEN, denervated; OMM, outer mitochondrial membrane; IMM, inner mitochondrial membrane. Values are expressed as mean ± SD.

NLRP3 inflammasome activation is upregulated following 7 days of severe muscle disuse. To elucidate the effect of skeletal muscle disuse on NLRP3 inflammasome activation, the protein expression of various components of the signaling pathway were measured. Following denervation, there was a drastic increase in NF-κB subunit p65 expression, which partly drives the upstream transcriptional activation of the NLRP3 inflammasome complex (Figure 3A, 3B, $p<0.0001$). Next, to understand how the structural components of the NLRP3 inflammasome complex were affected, we measured the protein levels of NLRP3 and procaspase-1 protein. These results demonstrated a notable increase in NLRP3 (Figure 3C, $p<0.01$) and procaspase-1 protein expression (Figure 3E, $p<0.01$), demonstrating a larger capacity for inflammasome components. In addition, to characterize NLRP3 inflammasome activation within denervated skeletal muscle, downstream protein targets within the signaling pathway were measured. Muscle disuse led to an increased expression of caspase-1 p20 (Figure 3D, $p<0.05$), and its downstream targets GSDMD (Figure 3G, $p<0.001$) and its active N-terminal fragment, GSDMD-N (Figure 3F, $p<0.05$). Furthermore, disuse was also associated with increases in the pro-inflammatory cytokine IL-1β, suggesting an increased pro-inflammatory environment within the denervated hindlimb (Figure 3H, $p=0.05$).

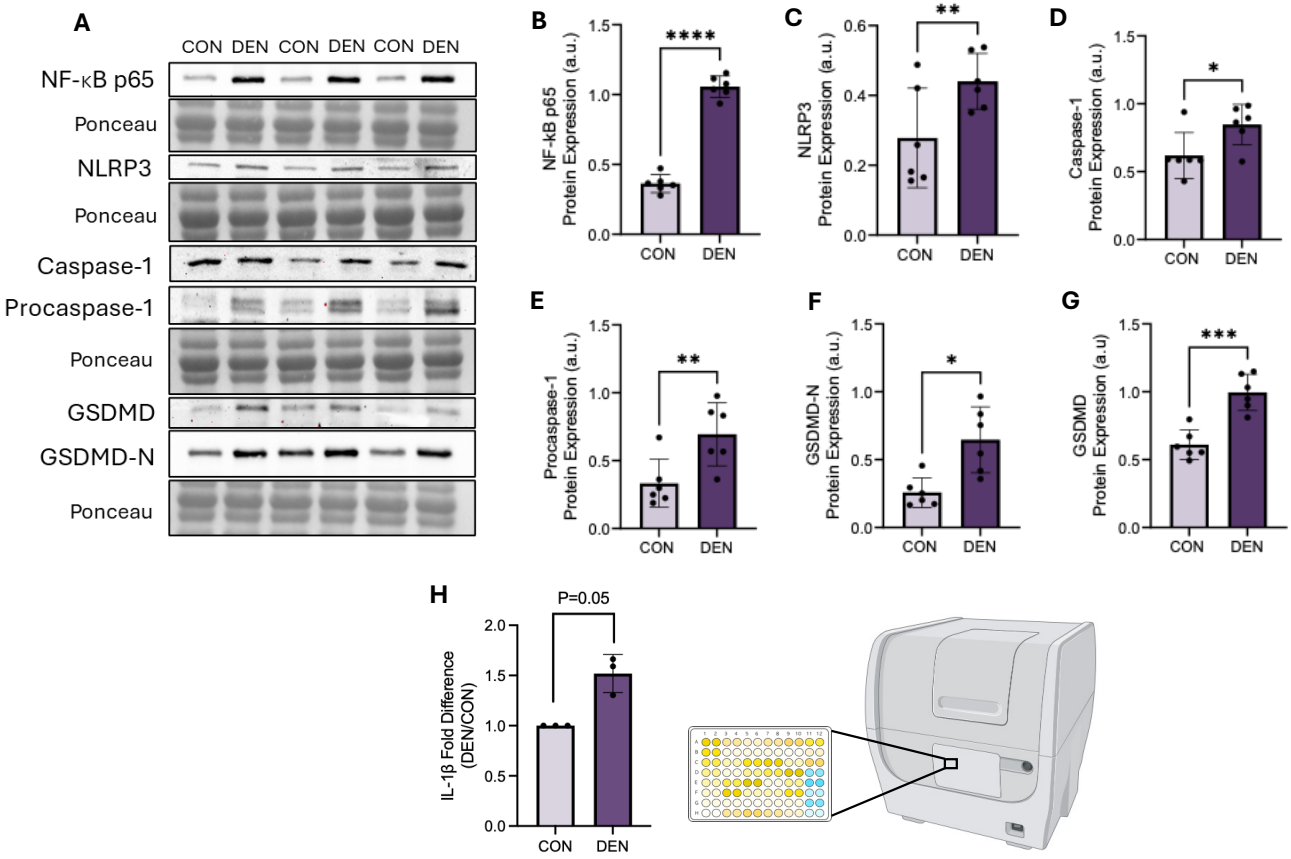

Figure 3: NLRP3 Inflammasome components following muscle denervation. Representative western blot of proteins involved in the NLRP3 Inflammasome signaling pathway (A), including NF-κB p65 (B), NLRP3 (C), Caspase-1 p20 (D), Procaspase-1 (E), GSDMD-N (F) and GSDMD (G) (n=6). Fold difference of IL-1β protein levels (DEN/CON) assessed by ELISA (H) (n=3). Data was analyzed using a paired student's t-test. *, $p<0.05$; **, $p<0.01$; ***, $p<0.001$; ****, $p<0.0001$. CON, control; DEN, denervated; GSDMD, Gasdermin-D; GSDMD-N, Gasdermin-D N-terminal fragment. All values are expressed as mean ± SD. A portion of Figure 3H was created using BioRender.com.

Muscle denervation is associated with alterations in DAMP release and proteins involved in mitochondrial permeabilization. After establishing increased NLRP3 inflammasome activation in atrophied muscle, we decided to investigate the presence of DAMPs that could mediate the pro-inflammatory environment. Using high-resolution respirometry, we assessed ROS emission by measuring H_2O_2 production. Denervation induced stark increases in ROS compared to the levels in the sham-operated control (Figure 4A, 4B, 4C, $p<0.05$). Another potent mtDAMP is the release of mtDNA from abnormally functioning mitochondria, which prompted us to measure the presence of mtDNA within the cytosolic and whole muscle fractions. As expected, the quantity of mtDNA within the gastrocnemius muscle significantly decreased following denervation (Figure 4D, $p<0.05$). However, the presence of mtDNA within the cytosolic fraction was also reduced in contrast to our original hypothesis (Figure 4E, $p<0.05$). As a result, the proportion of mtDNA within the cytosol corrected to whole muscle demonstrated no changes following the 7-day denervation period (Figure 4F). To investigate alternative pathways that have been previously implicated in NLRP3 inflammasome priming and activation, we decided to assess the cGAS-STING DNA-sensing pathway. Following the period of muscle disuse, there were apparent increases in both cGAS (Supplementary Figure B2, $p=0.05$) and STING protein expression which demonstrated approximately a 3-fold increase (Figure 4H, $p<0.0001$). This could suggest an increased drive towards innate immune signaling machinery and potential activation of cytosolic DNA sensing pathways within denervated muscle. Lastly, as mitochondrial permeabilization via mitochondrial pores has been previously implicated in augmenting the release of DAMPs, we measured several proteins that are involved in this process. As seen in Figure 4I and 4J, denervation was associated with increases in the pro-apoptotic BAX and AIF protein expression when

corrected to mitochondrial content ($p<0.01$, $p<0.05$, respectively), which could demonstrate the induction of mPTP pore opening and permeabilization.

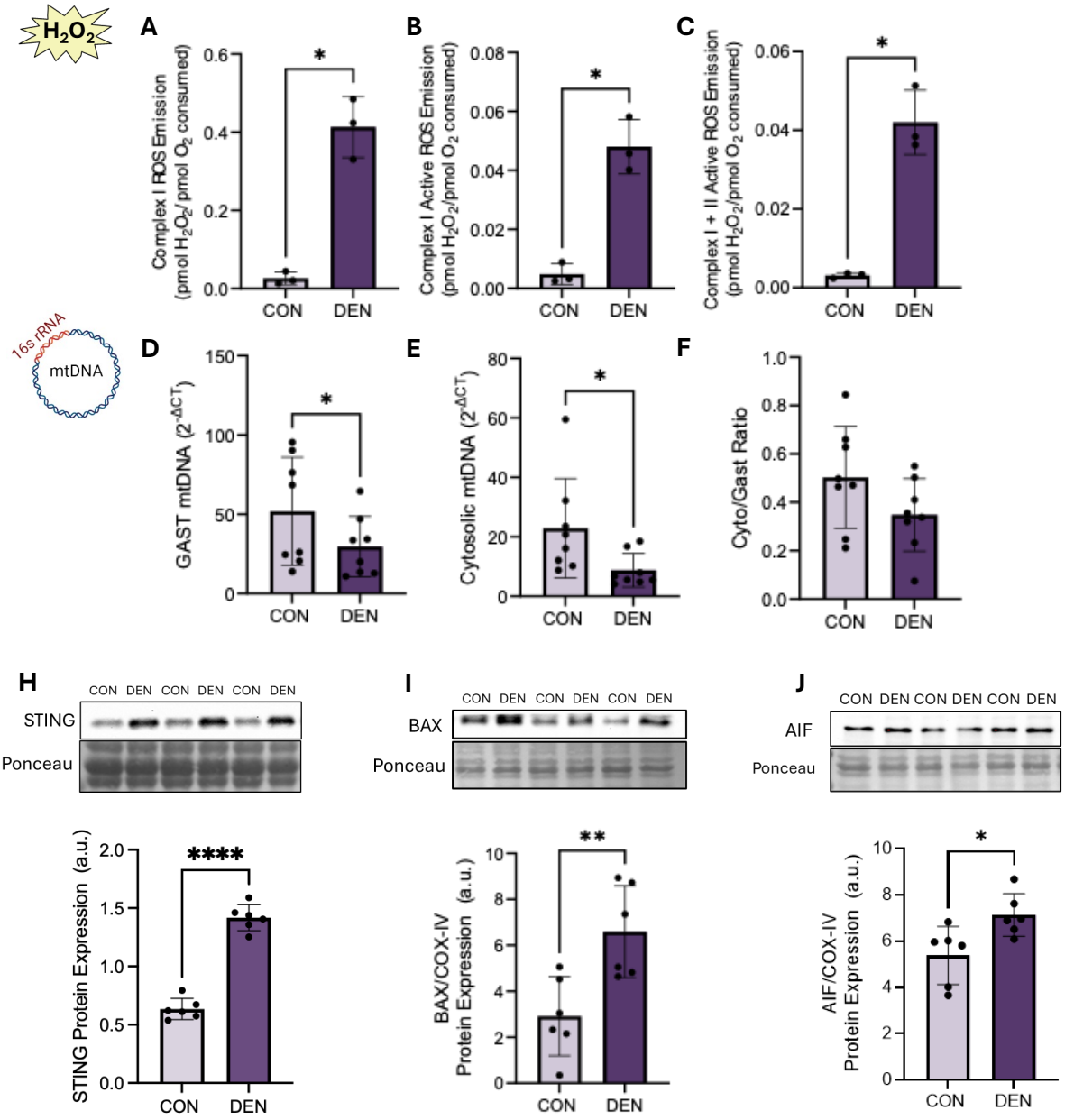

Figure 4: Assessment of potential DAMPs and alternative pathways following muscle denervation. ROS emission under complex I (A), complex I active (B), and complex I+II active (C) respiration states (n=3). qPCR analyses of the 16s rRNA mtDNA gene within whole muscle (D), cytosol (E), and the ratio of cytosolic/whole muscle mtDNA (F) (n=8). Representative western blots of STING (H), Bax (I), and AIF (J), alongside the corresponding graphical quantifications (n=6). Data was analyzed using a paired student's t-test. *, $p<0.05$; **, $p<0.01$; ****, $p<0.0001$. CON, control; DEN, denervated; Cyto, cytosolic; Gast, Gastrocnemius; All values are expressed as mean ± SD.

The aging phenotype exhibits decreased muscle mass which is recoverable with 6 weeks of voluntary wheel running. After obtaining promising results demonstrating NLRP3 inflammasome activation in denervated muscle, we decided to investigate the effects of aging and endurance training as shown in Figure 5A. Throughout the training period, the aged animals displayed a reduced capacity for endurance activity as shown by a lower total running distance compared to their young counterparts (Figure 3B, 3C, $p<0.0001$). To ensure that both cohorts demonstrated training adaptations, we assessed several physical characteristics of skeletal muscle. As shown in Figure 5D, the change in body weight taken before and after the intervention showed a main effect of age and training, with a significant effect of training within both groups ($p<0.05$). Furthermore, to gain an understanding of body composition we measured epididymal fat, which was markedly reduced within the young and aged trained mice compared to the untrained controls (Figure 5H, $p<0.05$). In addition, a main effect of training and age was also observed when measuring heart weight, which is a common measure of endurance training adaptations (Figure 5I, $p<0.05$). To assess a functional parameter of endurance, an acute treadmill test was performed before and after the 6-week training period. As shown in supplementary figure B6, the young and aged mice within the trained group showed significant improvements in their endurance capacity compared to the sedentary controls. To gain a better understanding of skeletal muscle characteristics, we also assessed the changes in muscle weight in the young and aged groups following training. Consistent across both mixed and oxidative fiber types including the tibialis anterior (Figure 5E), gastrocnemius (Figure 5F), and soleus (Figure 5G), there was a main effect of age and training indicating reductions in muscle mass basally with age and improvements in both age groups following training. As the aged mice demonstrated similar training adaptations despite a lower exercise quantity, we compared the extent of their adaptations normalized to the total distance run.

Interestingly, the aged mice tended to display a larger degree of adaptation in hindlimb muscle mass compared to their young counterparts (Supplementary Figure B4, $p=0.06$).

Aging exhibits altered mitochondrial quality, which is improved with exercise training. To assess changes in skeletal muscle mitochondria, we assessed changes in mitochondrial content markers COX-IV and COX-I, as subunits of complex IV in the electron transport chain. COX-I protein demonstrated a significant main effect of age (Figure 6C, $p<0.01$), with no changes in COX-IV protein expression (Figure 6B). Furthermore, as a functional measure of mitochondrial quality, we measured oxygen consumption within permeabilized muscle fibers. Consistent with the trend observed for muscle mass, there was an observed main effect of training in all respiration states (Figure 6D, 6E, 6F, $p<0.01$). Furthermore, the post-hoc test revealed a significant increase in oxygen consumption within the aged animals following training (Figure 6D, $p<0.05$; Figure 6E, $p<0.01$; Figure 6F, $p<0.01$.

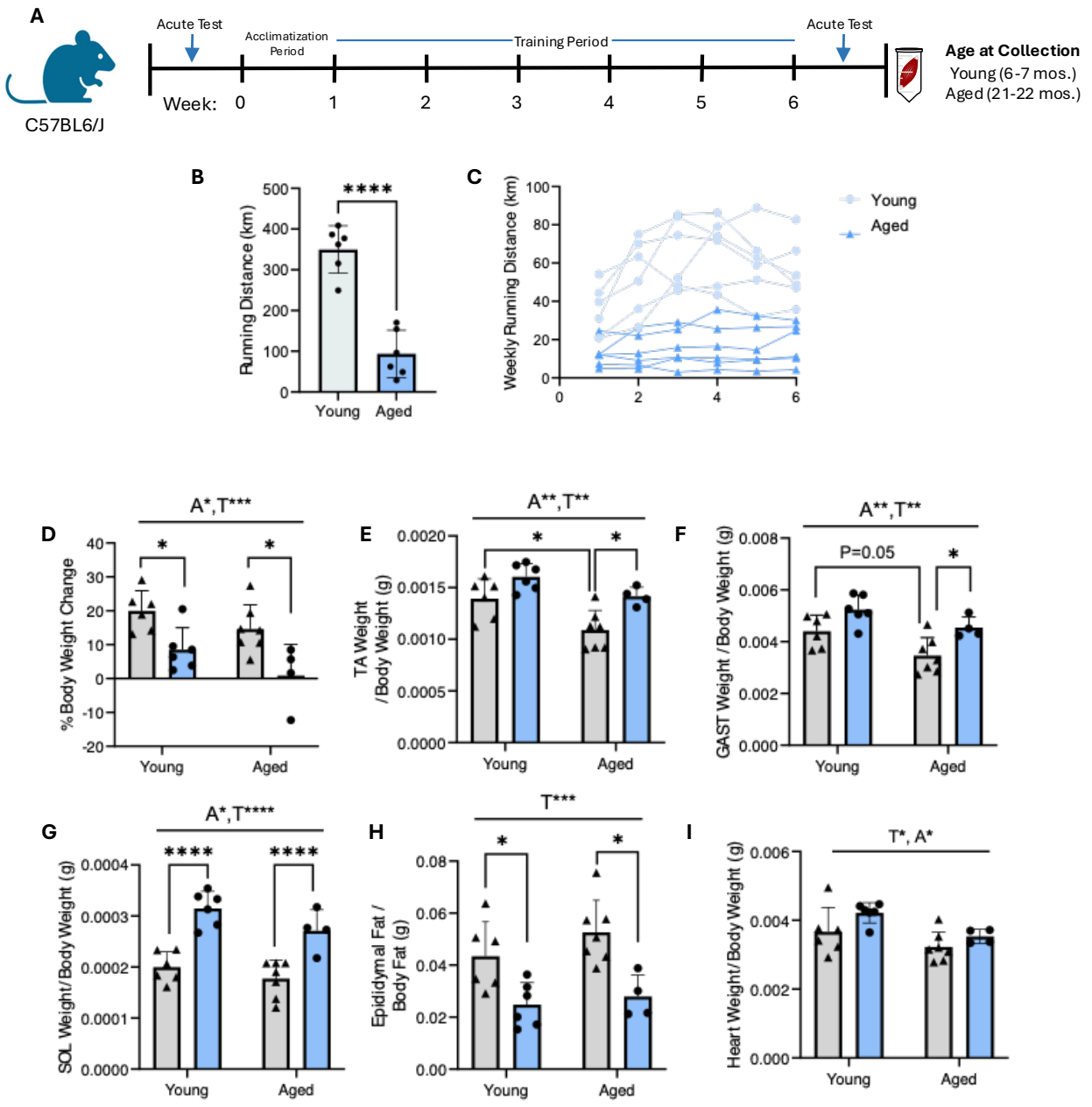

Figure 5: Physical characteristics in young and aged mice following 6 weeks of voluntary wheel running. Study design (A). Total distance ran over the 6-week training period for young and aged animals (km) (B) (n=6). Weekly running distance plotted per week (km) (C). % body weight change following the intervention in young and aged animals with and without training (D) (n=4-7). Individual muscle weights of TA (E), GAST (F) and SOL (G) corrected to body weight (n=4-7). Epididymal fat measurements compared across groups corrected to total body weight (H). Heart weight measurements between groups corrected to body weight (I) (n=4-6). Running differences were compared using an unpaired student's t-test. Body composition was compared using a two-way ANOVA. A, main effect of age; T, main effect of training. *, $p<0.05$; **, $p<0.01$; ***, $p<0.001$; ****, $p<0.0001$. TA, tibialis anterior; SOL, soleus; GAST, gastrocnemius. Values are expressed as mean ± SD. A portion of Figure 5A was created using BioRender.com.

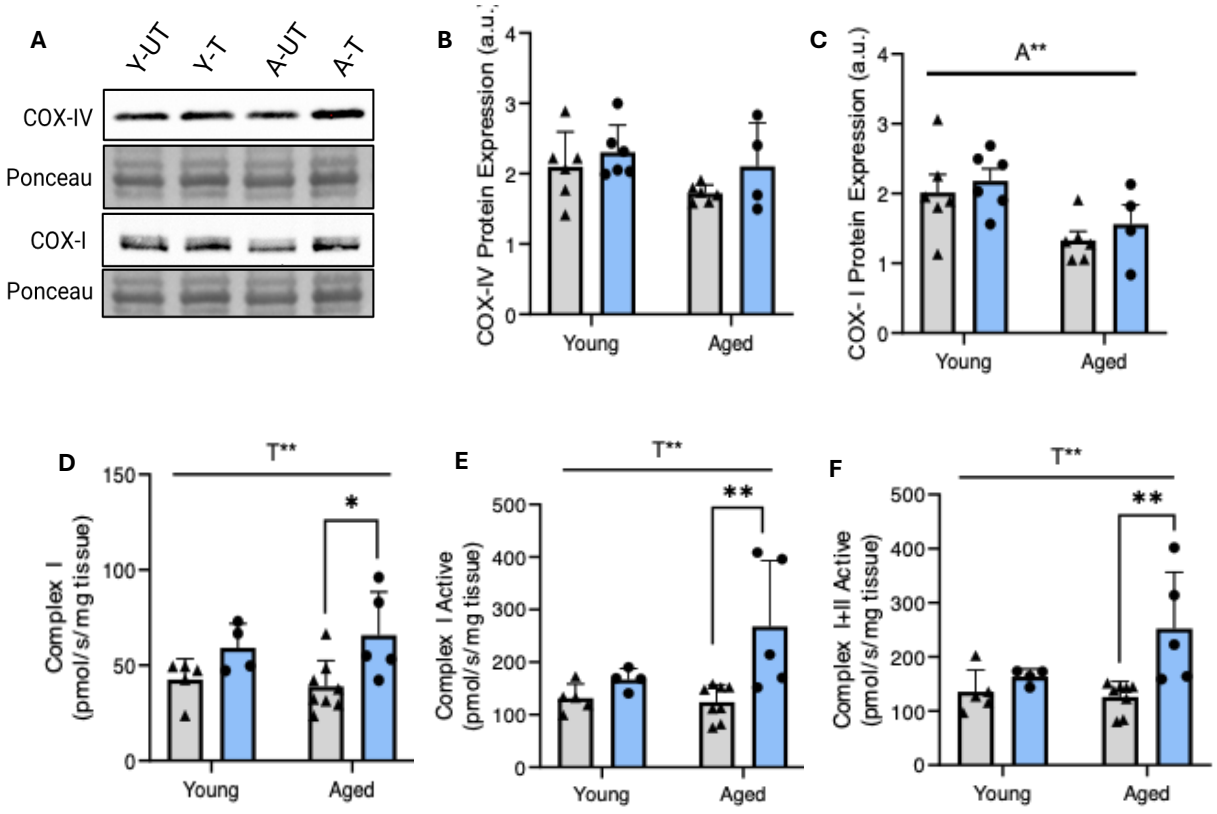

Figure 6: Mitochondrial adaptations in young and aged mice following the 6-week training period. Representative western blots of mitochondrial content markers COX-IV and COX-I (A), alongside the corresponding quantifications (B,C) (n=4-6). Oxygen consumption rates during complex I (D), complex I active (E), and complex I+II active (F) states of respiration (n=4-8). All values were analyzed using a two-way ANOVA. A, main effect of age; T, main effect of training. *, $p<0.05$; **, $p<0.01$. Values are expressed as mean ± SD.

Aged skeletal muscle demonstrates an increased pro-inflammatory environment, which is attenuated with exercise training. After confirming that the aged animals underwent mitochondrial and skeletal muscle adaptations following the exercise protocol, we assessed the innate inflammatory environment within skeletal muscle by measuring markers of NLRP3 inflammasome activation. As an upstream measure of transcriptional activation, we observed no significant differences in the protein expression of NF-κB subunit p65 across the groups (Figure 7B). However, when looking at the structural components of the NLRP3 inflammasome complex,

there was a main effect of age ($p<0.05$) and training ($p<0.01$) on NLRP3 protein expression, as well as a significant interaction between the two factors ($p<0.01$, Figure 7C). Similarly, procaspase-1 expression exhibited an interaction effect between age and training, indicating that inflammatory proteins within aged skeletal muscle respond differently to training compared to young (Figure 7E, $p<0.05$). Measuring several targets downstream of NLRP3 inflammasome activation, there was a basal increase in caspase-1 p20 protein expression with age ($p<0.001$), resulting in a significant main effect of age (Figure 7D). However, similar to NLRP3 protein expression, active caspase-1 protein expression exhibited a main effect of training following the 6-week intervention ($p<0.05$, Figure 7D). In addition, immature GSDMD and mature GSDMD-N showed a main effect of age ($p<0.05$ and $p=0.08$, respectively) indicating a greater accumulation of these pro-inflammatory markers (Figure 7F, 7G). However, while GSDMD protein expression decreased in aged muscle following training ($p=0.08$, Figure 7G), there was no clear change in GSDMD-N (Figure 7F). Lastly, when correcting the degree of training adaptations of NLPR3 inflammasome components (NLRP3, procaspase-1, and caspase-1) to the total distance ran, the aged animals remarkably displayed a greater attenuation of inflammatory markers compared to the young counterparts (Figure 7H, $p<0.001$).

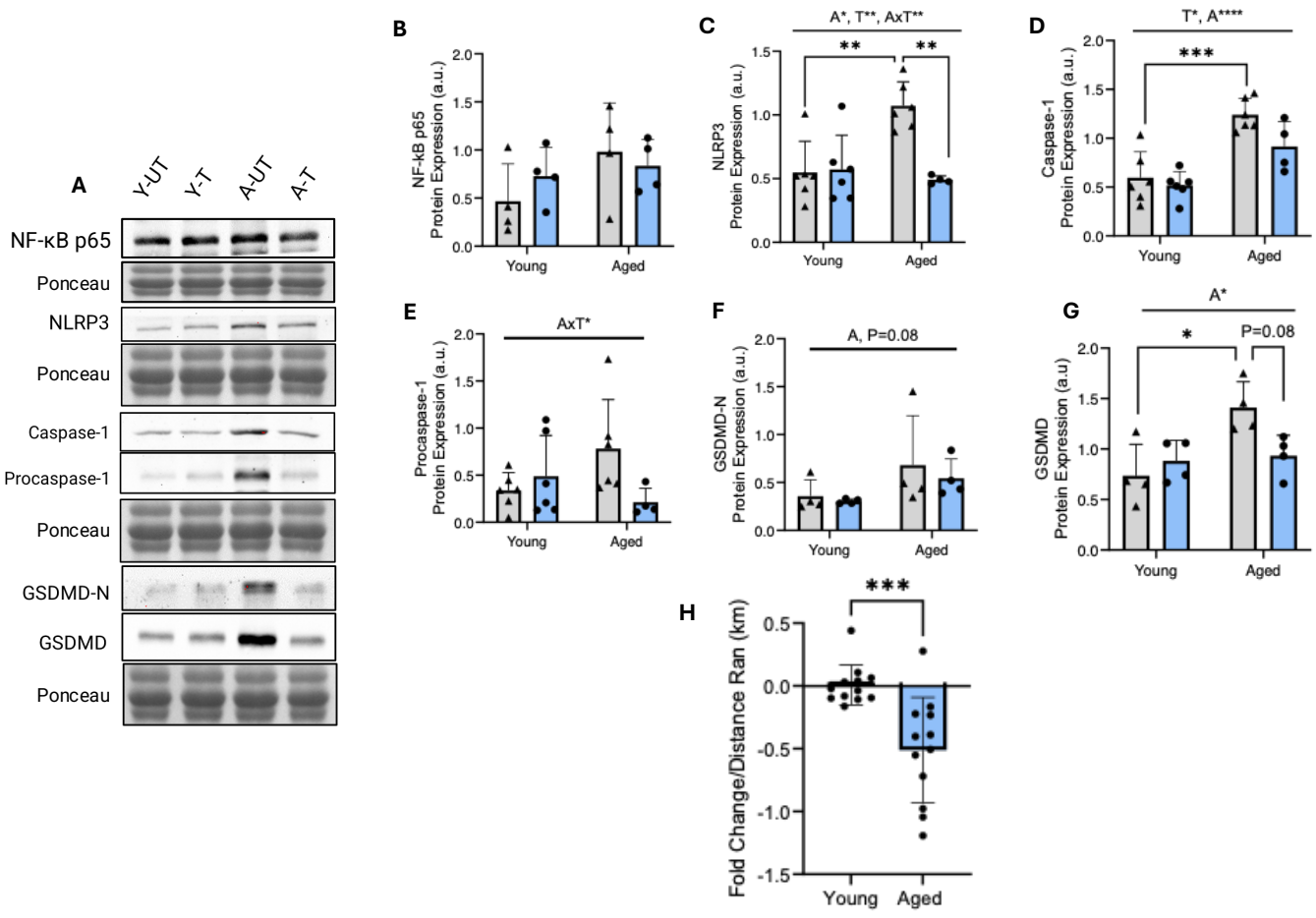

Figure 7: NLRP3 Inflammasome markers in young and aged animals following voluntary wheel running. Representative western blot of proteins involved in the NLRP3 Inflammasome signaling pathway (A), including NF-κB p65 (B), NLRP3 (C), Caspase-1 p20 (D), Procaspase-1 (E), GSDMD-N (F), GSDMD (G) (n=4-6). Fold change of protein components of the NLRP3 Inflammasome complex (NLRP3, Procaspase-1, Caspase-1) normalized to total distance ran in young and aged mice (H). Fold change was analyzed using an unpaired student's t-test, while protein expression underwent a two-way ANOVA. A, main effect of age; T, main effect of training; AxT, interaction between age and training. *, $p<0.05$; **, $p<0.01$; ***, $p<0.001$; ****, $p<0.0001$. All values are expressed as mean ± SD.

Age and training demonstrated no effect on ROS and mtDNA release but showed increased expression of innate immune markers and mPTP components. After observing the interesting effects of both age and training on NLRP3 inflammasome activation, we wanted to further characterize the presence of DAMPS within whole muscle and cytosolic fractions. With both age and training, there were no apparent changes in H_2O_2 production following complex I inactive (Figure 8A), complex I active (Figure 8B), and complex I+II active respiration (Figure 8C). When investigating the presence of mtDNA as a mtDAMP, there was a main effect of training in whole muscle mtDNA following the intervention (Figure 8D, $p<0.05$), but no changes in the release of mtDNA into the cytosolic fraction (Figure 8E). As a result, there was no change across the groups when assessing the ratio of cytosolic to whole muscle mtDNA. However, aged muscle appears to demonstrate a larger change in mtDNA release compared to young animals. Lastly, when assessing alternate pathways involved in innate immune signaling, we found that STING protein expression exhibited a trending main effect of training, which was also more apparent within the aged muscle (Figure 8G, $p=0.07$). Furthermore, in conjunction with improved mitochondrial function within the aged muscle, we found that BAX protein expression was upregulated basally within aging muscle ($p<0.01$) and dramatically attenuated with training ($p<0.01$) (Figure 8H), which was not observed in the young groups.

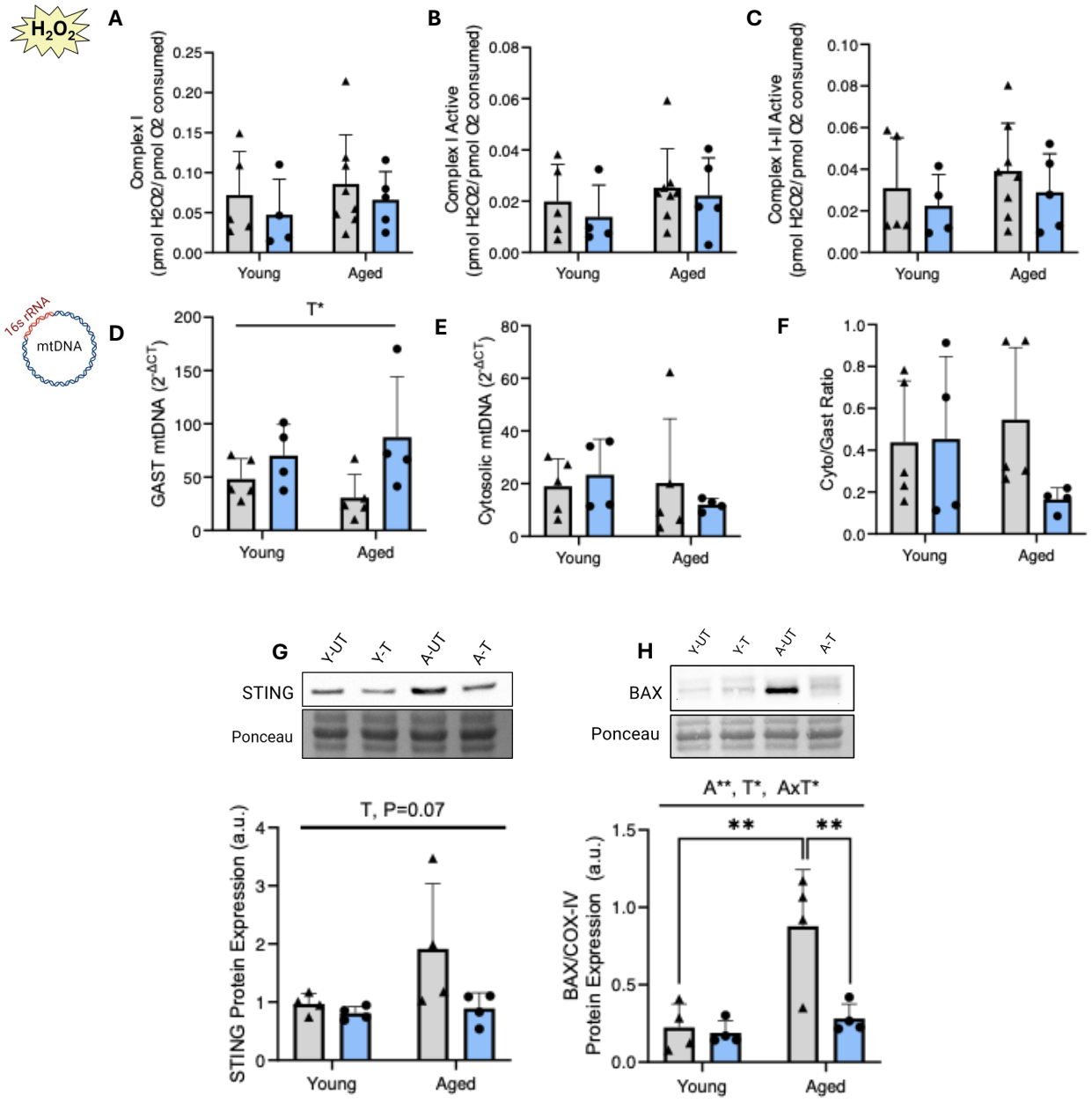

Figure 8: Analysis of potential DAMPS and associated pathways in young and aged animals following voluntary wheel running. ROS emission under complex I (A), complex I active (B), and complex I+II active (C) respiration states (n=4-8). qPCR analyses of the 16s rRNA mtDNA fragment within whole muscle (D), cytosol (E), and the ratio of cytosolic/whole muscle mtDNA (F) (n=4-5). Representative western blots of STING (G) and Bax (H) alongside the corresponding graphical quantifications (n=4). Data was analyzed using a two-way ANOVA. A, main effect of age; T, main effect of training; AxT, interaction between age and training; *, $p<0.05$; **, $p<0.01$; Cyto, cytosolic; Gast, Gastrocnemius; All values are expressed as mean ± SD.

DISCUSSION

The purpose of this study was to investigate *in vivo* innate immune signaling, specifically focused on the NLRP3 inflammasome complex in response to skeletal muscle use and disuse. Mitochondria are now being explored as critical signaling hubs that can mediate inflammatory processes, however, the relationship between mitochondrial health, skeletal muscle activity, and innate immune activation requires additional work. As a result, we utilized a potent model of muscle disuse through a sciatic nerve transection to assess the adaptive response of the NLRP3 inflammasome complex. Furthermore, aging has been established as a condition associated with skeletal muscle deterioration, inflammation, and functional impairments, prompting to investigate the downstream consequences and potential benefits of endurance training. By assessing various mitochondrial parameters and NLRP3 inflammasome activation, we aimed to better understand the inflammatory environment in relation to skeletal muscle mitochondrial adaptations.

Consistent with other findings, 7 days of muscle denervation upregulated catabolic signaling pathways as shown through an increased expression of the E3 ubiquitin ligase MURF1 and muscle atrophy marker GADD45-α which led to a decrease in muscle mass (12, 20). Furthermore, we observed consistent decreases in mitochondrial content and function, which has also been shown in other studies utilizing this model (12, 21). This suggests that 7 days of muscle denervation is sufficient to induce maladaptive changes within the mitochondrial pool, which encouraged us to investigate changes in NLRP3 inflammasome signaling. Previous work by You and colleagues demonstrated a relationship between muscle atrophy and the upregulation of proteins involved in the NLRP3 signaling cascade including NLRP3, caspase-1, GSDMD-N, and IL-1β following 14-28 days of denervation, which was attenuated by NLRP3 KO (13). This relationship was further demonstrated as LPS-induced NLRP3 inflammasome activation led to decreases in myotube

diameter that was rescued upon treatment with the NLRP3 inhibitor, MCC950 (14). Within our study, we demonstrated an upregulation in the protein expression of NF-κB p65, NLRP3, procaspase-1, caspase-1 p20, GSDMD, GSDMD-N, and IL-1β as early as 7 days following the sciatic nerve transection, confirming our initial hypothesis. This expands the current body of literature and suggests that NLRP3 inflammasome activation occurs at earlier time points of denervation-induced muscle disuse than previously described.

Furthermore, as several works have implicated the release of mtDAMPS as potent activators of the NLRP3 inflammasome (22, 23), we measured the production of ROS and mtDNA release to understand potential upstream activators. Consistent with other findings, 7 days of denervation induced dramatic increases in the production of ROS which has been implicated as a second signal for inflammasome activation and could be contributing to the observed protein changes (12, 22, 24). On the other hand, the release of mtDNA into the cytosol has been widely recognized as a pro-inflammatory molecule, which encouraged us to use a mtDNA-specific 16s rRNA primer to assess its localization. In contrast to our original hypothesis, the amount of mtDNA within the cytosolic fraction decreased alongside reductions in whole muscle mtDNA content, leading to no change in ratio of cytosolic mtDNA. This was surprising, as previous works have demonstrated that maladaptive changes to the mitochondrial reticulum such as impairments in autophagy (25) or mitochondrial dynamics (26) have been associated with the release of mtDNA and subsequent upregulation of NLRP3 inflammasome signaling. Furthermore, our data revealed an increased expression of cGAS and STING protein, which is involved in the recognition of double-stranded DNA within the cytosol. Other papers have demonstrated that cGAS-STING activation can promote the nuclear translocation of NF-κB, and converge on NLRP3 inflammasome activation, which is blunted in the absence of STING (8). This further highlights

that other innate immune responses that could possibly be mediating denervation-induced NLRP3 inflammasome signaling. Furthermore, several groups have implicated the formation of the mitochondrial permeability transition pore in augmenting the release of mtDAMPS and activation of innate immune responses, which is supported by the increased expression BAX and AIF protein following muscle denervation (27, 28). As our results demonstrated an increase in the expression of DNA-sensing pathways and mitochondrial permeabilization proteins, but no associated changes in cytosolic mtDNA, this could suggest several possibilities. As we observed increases in NLRP3 inflammasome activation as early as seven days, it could be valuable to assess earlier time points to identify the upstream signals involved. Furthermore, several studies have specifically implicated oxidized mtDNA in its ability to interact with and stimulate NLRP3 inflammasome assembly (23, 28). While we observed no changes in the quantity of cytosolic mtDNA relative to whole muscle, the elevated oxidative stress following denervation could contribute to a higher proportion of oxidized mtDNA, which is yet to be explored.

Similarly, the aging phenotype is associated with chronic low-grade inflammation and deteriorations in mitochondrial function, muscle mass, and functional performance, prompting us to investigate NLRP3 inflammasome expression and mitochondrial parameters (29). Given the universal aging process, potential interventions such as exercise are in high demand to address deteriorations in skeletal muscle associated with aging. While the aged animals displayed a reduced motivation towards running compared to their young counterparts throughout the 6-week voluntary wheel running protocol, they still exhibited a variety of training-induced adaptations including increases in heart mass and hindlimb muscle mass, consistent with other studies employing the same model (30, 31). Overall, the trained young and aged mice demonstrated improved body composition evident through a reduction of fat mass and reduced weight gain in

comparison to the untrained controls. Furthermore, when analyzing mitochondrial adaptations, aged animals displayed reduced mitochondrial content, which is also considered a consistent characteristic of aging skeletal muscle and could contribute towards an impaired running capacity (32). However, the training period was still able to increase oxygen consumption, particularly within the aged animals, demonstrating that the intervention was sufficient to enhance mitochondrial function despite different running quantities. These findings pushed us to further investigate the innate inflammatory profile within skeletal muscle to investigate if there was a similar relationship between mitochondrial function and NLRP3 inflammasome activation. Consistent across the protein expression of NLRP3, procaspase-1, caspase-1, GSDMD, and GSDMD-N, there was a basal increase in these inflammatory markers within aged skeletal muscle. Similarly, Mcbride and colleagues observed comparable findings in 24-month-old mice, which demonstrated increased muscle atrophy and caspase-1 activity that was blunted in the absence of NLRP3 (16). Furthermore, our findings suggest a novel beneficial role of endurance training in attenuating the age-related inflammatory profile in aged skeletal muscle, as the training intervention was able to reduce the protein expression of NLRP3, procaspase-1, caspase-1, and GSDMD. As NLRP3 inflammasome activity has been linked to muscle atrophy within muscle, this anti-inflammatory effect of exercise could be contributing towards the increase in muscle mass observed in the trained animals. This aligns with other studies that have demonstrated reduced TLR/NF-κB signaling and NLRP3 inflammasome activation following long-term treadmill training in other disease states, including Parkinson's disease and diet-induced obesity in neuronal hippocampal cells and adipose tissue respectively (18, 33). Furthermore, aging was also associated with an increased expression of STING and BAX, which could further augment the inflammatory profile within muscle by promoting the release of DAMPs and activating other immune signaling

cascades that contribute towards the changes in protein expression. Another study also demonstrated a basal increase in STING protein in 24-26 month old mice, however, when assessing downstream activation through the phosphorylation of IRF3, they saw no differences within skeletal muscle, which further encourages us to elucidate the activation of this pathway within the context of aging (34). Most importantly, following the same trend that was observed with muscle mass and mitochondrial function adaptations, aged skeletal muscle displays a larger attenuation of inflammatory signaling despite a lower exercise capacity, suggesting that innate immune signaling in aged muscle is increasingly responsive to endurance exercise compared to young, healthy controls. This effect was also evident after assessing STING and BAX protein expression, which also demonstrated a larger capacity for attenuation due to the basal increase present in aged muscle. Within literature, there is still conflicting evidence surrounding the adaptive potential of aging skeletal muscle. While some groups have demonstrated that aging muscle can possess the same capacity for improvement as young muscle (35), other work has demonstrated a reduced adaptive response specifically in mitochondrial changes with age (36). However, consistent with our results, aged muscle has been shown to undergo increased reductions in pro-apoptotic signaling (36).

To assess upstream DAMPs that could link the mitochondrial and innate immune adaptations, we also investigated changes in mtDNA release and ROS production. Surprisingly, we did not observe an effect of age or training on mtDNA release or ROS emission, which suggests that other DAMPs play a larger role. For instance, another study demonstrated increases in plasma ATP levels in sarcopenic muscle that was associated with NLRP3 inflammasome activation (37), which emphasizes the need to investigate alternative DAMPs to better understand the effects of aging on NLRP3 inflammasome activation.

While this study highlights several findings, there are some limitations to consider for future work. For instance, as a whole-body stimulus, it is critical to recognize that various other tissue types could be contributing to the observed results when assessing both age and endurance training. Furthermore, voluntary wheel running was an as low-stress exercise modality, however, it was difficult to control the quantity of exercise, especially within the aged animals due to reduced volition. Using another model of exercise such as chronic contractile activity could help ensure that the aged animals undergo the same extent of exercise training and minimize variability within the results.

In summary, this study demonstrates that skeletal muscle disuse promotes NLRP3 inflammasome activation and mitochondrial deteriorations, contributing towards a pro-inflammatory environment within skeletal muscle. Furthermore, this work emphasizes the anti-inflammatory effects of chronic endurance training in attenuating the age-related increases in NLRP3 inflammasome protein expression and improving mitochondrial function. However, more work is still required to identify the specific stimuli involved in mediating this process. Surprisingly, these results also suggest an increased adaptive response to endurance training within aged skeletal muscle, allowing a larger degree of adaptation despite the lower exercise quantity compared to young mice. As overstimulated NLRP3 inflammasome activation is associated with a variety of disease states, this work helps establish exercise training as a promising intervention for combatting inflammation within skeletal muscle. Furthermore, this emphasizes that exercise intolerant populations, such as the aged population, can still benefit from the anti-inflammatory effects of low-intensity endurance training, increasing its feasibility as an intervention.

ACKNOWLEDGEMENTS

This work was supported by funding from the Natural Sciences and Engineering Research Council of Canada (NSERC) to D.A. Hood. D.A. Hood is also the holder of a Canada Research Chair in Cell Physiology. P. Khemraj is a recipient of the Ontario Graduate Scholarship.

REFERENCES

1. Hood DA, Memme JM, Oliveira AN, Triolo M. Maintenance of Skeletal Muscle Mitochondria in Health, Exercise, and Aging. *Annu Rev Physiol* 81: 19–41, 2019. doi: 10.1146/annurev-physiol-020518-114310.
2. Delves PJ, Roitt IM. The Immune System. *N Engl J Med* 343: 37–49, 2000. doi: 10.1056/NEJM200007063430107.
3. Brunelli S, Roverequerini P. The immune system and the repair of skeletal muscle. *Pharmacological Research* 58: 117–121, 2008. doi: 10.1016/j.phrs.2008.06.008.
4. Chen Y-F, Lee C-W, Wu H-H, Lin W-T, Lee OK. Immunometabolism of macrophages regulates skeletal muscle regeneration [Online]. *Frontiers in Cell and Developmental Biology* 10, 2022. https://www.frontiersin.org/articles/10.3389/fcell.2022.948819 [15 Oct. 2022].
5. De Paepe B, De Bleecker JL. Cytokines and Chemokines as Regulators of Skeletal Muscle Inflammation: Presenting the Case of Duchenne Muscular Dystrophy. *Mediators of Inflammation* 2013: 1–10, 2013. doi: 10.1155/2013/540370.
6. Loell I, Lundberg IE. Can muscle regeneration fail in chronic inflammation: a weakness in inflammatory myopathies?: Review: Muscle weakness in myositis. *Journal of Internal Medicine* 269: 243–257, 2011. doi: 10.1111/j.1365-2796.2010.02334.x.
7. Kelley N, Jeltema D, Duan Y, He Y. The NLRP3 Inflammasome: An Overview of Mechanisms of Activation and Regulation. *Int J Mol Sci* 20: E3328, 2019. doi: 10.3390/ijms20133328.
8. Zhang W, Li G, Luo R, Lei J, Song Y, Wang B, Ma L, Liao Z, Ke W, Liu H, Hua W, Zhao K, Feng X, Wu X, Zhang Y, Wang K, Yang C. Cytosolic escape of mitochondrial DNA triggers cGAS-STING-NLRP3 axis-dependent nucleus pulposus cell pyroptosis. *Exp Mol Med* 54: 129–142, 2022. doi: 10.1038/s12276-022-00729-9.
9. Li D, Wu M. Pattern recognition receptors in health and diseases. *Sig Transduct Target Ther* 6: 291, 2021. doi: 10.1038/s41392-021-00687-0.
10. He W, Wan H, Hu L, Chen P, Wang X, Huang Z, Yang Z-H, Zhong C-Q, Han J. Gasdermin D is an executor of pyroptosis and required for interleukin-1β secretion. *Cell Res* 25: 1285–1298, 2015. doi: 10.1038/cr.2015.139.
11. Gurung P, Lukens JR, Kanneganti T-D. Mitochondria: diversity in the regulation of the NLRP3 inflammasome. *Trends in Molecular Medicine* 21: 193–201, 2015. doi: 10.1016/j.molmed.2014.11.008.
12. Triolo M, Slavin M, Moradi N, Hood DA. Time-dependent changes in autophagy, mitophagy and lysosomes in skeletal muscle during denervation-induced disuse. *The Journal of Physiology* 600: 1683–1701, 2022. doi: 10.1113/JP282173.
13. You Z, Huang X, Xiang Y, Dai J, Xu L, Jiang J, Xu J. Ablation of NLRP3 inflammasome attenuates muscle atrophy via inhibiting pyroptosis, proteolysis and apoptosis following denervation. *Theranostics* 13: 374–390, 2023. doi: 10.7150/thno.74831.
14. Eggelbusch M, Shi A, Broeksma BC, Vázquez-Cruz M, Soares MN, de Wit GMJ, Everts B, Jaspers RT, Wüst RCI. The NLRP3 inflammasome contributes to inflammation-induced morphological and metabolic alterations in skeletal muscle. *Journal of Cachexia, Sarcopenia and Muscle* n/a, 2022. doi: 10.1002/jcsm.13062.
15. Franceschi C, Bonafè M, Valensin S, Olivieri F, De Luca M, Ottaviani E, De Benedictis G. Inflamm-aging: An Evolutionary Perspective on Immunosenescence. *Annals of the New York Academy of Sciences* 908: 244–254, 2000. doi: 10.1111/j.1749-6632.2000.tb06651.x.
16. McBride MJ, Foley KP, D'Souza DM, Li YE, Lau TC, Hawke TJ, Schertzer JD. The NLRP3 inflammasome contributes to sarcopenia and lower muscle glycolytic potential in old mice. *Am J Physiol Endocrinol Metab* 313: E222–E232, 2017. doi: 10.1152/ajpendo.00060.2017.
17. Chen CCW, Erlich AT, Hood DA. Role of Parkin and endurance training on mitochondrial turnover in skeletal muscle. *Skeletal Muscle* 8: 10, 2018. doi: 10.1186/s13395-018-0157-y.
18. Wang W, Lv Z, Gao J, Liu M, Wang Y, Tang C, Xiang J. Treadmill exercise alleviates neuronal damage by suppressing NLRP3 inflammasome and microglial activation in the MPTP mouse model of Parkinson's disease. *Brain Res Bull* 174: 349–358, 2021. doi: 10.1016/j.brainresbull.2021.06.024.

19. Lee J, Lee Y, LaVoy EC, Umetani M, Hong J, Park Y. Physical activity protects NLRP3 inflammasome-associated coronary vascular dysfunction in obese mice. *Physiol Rep* 6: e13738, 2018. doi: 10.14814/phy2.13738.
20. Bongers KS, Fox DK, Ebert SM, Kunkel SD, Dyle MC, Bullard SA, Dierdorff JM, Adams CM. Skeletal muscle denervation causes skeletal muscle atrophy through a pathway that involves both Gadd45a and HDAC4. *American Journal of Physiology-Endocrinology and Metabolism* 305: E907–E915, 2013. doi: 10.1152/ajpendo.00380.2013.
21. Adhihetty PJ, O'Leary MFN, Chabi B, Wicks KL, Hood DA. Effect of denervation on mitochondrially mediated apoptosis in skeletal muscle. *Journal of Applied Physiology* 102: 1143–1151, 2007. doi: 10.1152/japplphysiol.00768.2006.
22. Zhou R, Yazdi AS, Menu P, Tschopp J. A role for mitochondria in NLRP3 inflammasome activation. *Nature* 469: 221–225, 2011. doi: 10.1038/nature09663.
23. Shimada K, Crother TR, Karlin J, Dagvadorj J, Chiba N, Chen S, Ramanujan VK, Wolf AJ, Vergnes L, Ojcius DM, Rentsendorj A, Vargas M, Guerrero C, Wang Y, Fitzgerald KA, Underhill DM, Town T, Arditi M. Oxidized mitochondrial DNA activates the NLRP3 inflammasome during apoptosis. *Immunity* 36: 401–414, 2012. doi: 10.1016/j.immuni.2012.01.009.
24. Russell-Guzmán J, Américo-Da Silva L, Cadagan C, Maturana M, Palomero J, Estrada M, Barrientos G, Buvinic S, Hidalgo C, Llanos P. Activation of the ROS/TXNIP/NLRP3 pathway disrupts insulin-dependent glucose uptake in skeletal muscle of insulin-resistant obese mice. *Free Radical Biology and Medicine* 222: 187–198, 2024. doi: 10.1016/j.freeradbiomed.2024.06.011.
25. Nakahira K, Haspel JA, Rathinam VAK, Lee S-J, Dolinay T, Lam HC, Englert JA, Rabinovitch M, Cernadas M, Kim HP, Fitzgerald KA, Ryter SW, Choi AMK. Autophagy proteins regulate innate immune responses by inhibiting the release of mitochondrial DNA mediated by the NALP3 inflammasome. *Nat Immunol* 12: 222–230, 2011. doi: 10.1038/ni.1980.
26. Irazoki A, Martinez-Vicente M, Aparicio P, Aris C, Alibakhshi E, Rubio-Valera M, Castellanos J, Lores L, Palacín M, Gumà A, Zorzano A, Sebastián D. Coordination of mitochondrial and lysosomal homeostasis mitigates inflammation and muscle atrophy during aging. *Aging Cell* 21: e13583, 2022. doi: 10.1111/acel.13583.
27. Yamazaki T, Galluzzi L. BAX and BAK dynamics control mitochondrial DNA release during apoptosis. *Cell Death Differ* 29: 1296–1298, 2022. doi: 10.1038/s41418-022-00985-2.
28. Xian H, Watari K, Sanchez-Lopez E, Offenberger J, Onyuru J, Sampath H, Ying W, Hoffman HM, Shadel GS, Karin M. Oxidized DNA fragments exit mitochondria via mPTP- and VDAC-dependent channels to activate NLRP3 inflammasome and interferon signaling. *Immunity* 55: 1370-1385.e8, 2022. doi: 10.1016/j.immuni.2022.06.007.
29. López-Otín C, Blasco MA, Partridge L, Serrano M, Kroemer G. The Hallmarks of Aging. *Cell* 153: 1194–1217, 2013. doi: 10.1016/j.cell.2013.05.039.
30. Wong JC, Oliveira AN, Khemraj P, Hood DA. The role of TFE3 in mediating skeletal muscle mitochondrial adaptations to exercise training. *Journal of Applied Physiology* 136: 262–273, 2024. doi: 10.1152/japplphysiol.00484.2023.
31. Crilly MJ, Tryon LD, Erlich AT, Hood DA. The role of Nrf2 in skeletal muscle contractile and mitochondrial function. *J Appl Physiol (1985)* 121: 730–740, 2016. doi: 10.1152/japplphysiol.00042.2016.
32. Chabi B, Ljubicic V, Menzies KJ, Huang JH, Saleem A, Hood DA. Mitochondrial function and apoptotic susceptibility in aging skeletal muscle. *Aging Cell* 7: 2–12, 2008. doi: 10.1111/j.1474-9726.2007.00347.x.
33. Mardare C, Krüger K, Liebisch G, Seimetz M, Couturier A, Ringseis R, Wilhelm J, Weissmann N, Eder K, Mooren F-C. Endurance and Resistance Training Affect High Fat Diet-Induced Increase of Ceramides, Inflammasome Expression, and Systemic Inflammation in Mice. *J Diabetes Res* 2016: 4536470, 2016. doi: 10.1155/2016/4536470.
34. Jiménez-Loygorri JI, Villarejo-Zori B, Viedma-Poyatos Á, Zapata-Muñoz J, Benítez-Fernández R, Frutos-Lisón MD, Tomás-Barberán FA, Espín JC, Area-Gómez E, Gomez-Duran A, Boya P. Mitophagy

curtails cytosolic mtDNA-dependent activation of cGAS/STING inflammation during aging. *Nat Commun* 15: 830, 2024. doi: 10.1038/s41467-024-45044-1.
35. Škorjanc D, Traub I, Pette D. Identical responses of fast muscle to sustained activity by low-frequency stimulation in young and aging rats. *Journal of Applied Physiology* 85: 437–441, 1998. doi: 10.1152/jappl.1998.85.2.437.
36. Ljubicic V, Joseph A-M, Adhihetty PJ, Huang JH, Saleem A, Uguccioni G, Hood DA. Molecular basis for an attenuated mitochondrial adaptive plasticity in aged skeletal muscle. *Aging* 1: 818–830, 2009. doi: 10.18632/aging.100083.
37. Antuña E, Potes Y, Baena-Huerta FJ, Cachán-Vega C, Menéndez-Coto N, Álvarez Darriba E, Fernández-Fernández M, Burgos Bencosme N, Bermúdez M, López Álvarez EM, Gutiérrez-Rodríguez J, Boga JA, Caballero B, Vega-Naredo I, Coto-Montes A, Garcia-Gonzalez C. NLRP3 Contributes to Sarcopenia Associated to Dependency Recapitulating Inflammatory-Associated Muscle Degeneration. *IJMS* 25: 1439, 2024. doi: 10.3390/ijms25031439.
38. Oliveira AN, Memme JM, Wong J, Hood DA. Dimorphic effect of TFE3 in determining mitochondrial and lysosomal content in muscle following denervation. *Skeletal Muscle* 14: 7, 2024. doi: 10.1186/s13395-024-00339-1.
39. Jaillon S, Berthenet K, Garlanda C. Sexual Dimorphism in Innate Immunity. *Clinic Rev Allerg Immunol* 56: 308–321, 2019. doi: 10.1007/s12016-017-8648-x.

FUTURE DIRECTIONS

1. Further investigate the presence of DAMPs and upstream signaling. While we are observing an impact of both skeletal muscle disuse and use on innate immune adaptations, the specific stimuli involved in mediating these changes need to be further elucidated. For instance, by investigating other DAMPS such as extracellular ATP, the release of lysosomal enzymes such as Cathepsin B, or structural components of the mitochondrial membrane, we can create more targeted interventions to alleviate this pro-inflammatory phenotype. Furthermore, investigating earlier timepoints prior to inflammasome activation will provide insight into the upstream patterns of activation.
2. Investigate the source of NLRP3 inflammasome activation within skeletal muscle. Since this study was performed using whole muscle skeletal muscle samples, the contribution of immune cells in promoting NLRP3 inflammasome following aging, muscle denervation and exercise training remains unknown. By measuring the extent of immune cell infiltration into skeletal muscle following these stimuli, this could offer insight into the crosstalk between immune cells and myofibers, as well as the source of immune signaling.
3. Evaluating sex differences in innate immune adaptations in response to these metabolic alternations. Within the current body of literature, there is sufficient evidence to suggest that males and females experience different mitochondrial and innate immune adaptations which emphasizes the need to expand this study to female mice (12, 38, 39) . These findings could help inform sex-specific exercise interventions to alleviate muscle-disuse induced inflammation.

APPENDIX A: DATA AND STATISTICAL ANALYSIS

Table A1: Pre-post Denervation Body weights

	Body Weight (g)	
N	CON	DEN
1	33.70	30.60
2	35.09	36.50
3	31.21	31.50
4	31.21	29.30
5	25.72	25.93
6	28.76	28.95
7	36.03	34.07
8	35.88	29.80
9	28.43	28.40
10	27.90	28.30
11	28.58	28.48
12	30.26	29.71
13	30.93	30.51
14	37.60	36.78
X	31.52	30.63
SD	3.60	3.14

Paired T-Test: CON vs DEN	
P-value	0.1015
P-value Summary	ns
Significantly different (P<0.05)?	No

Table A2: Hindlimb Muscle Mass

	Hindlimb Muscle Weight (mg)	
N	CON	DEN
1	202.00	176.60
2	197.70	184.20
3	194.60	176.10
4	205.60	181.30
5	196.90	176.00
6	224.70	199.10
7	208.50	193.90
8	219.00	210.90
9	220.90	174.20
10	224.50	185.70
11	219.50	168.30
12	215.90	205.10
13	205.30	196.70
14	236.00	182.20
X	212.22	186.45
SD	12.48	12.74

Paired T-Test: CON vs DEN	
P-value	<0.0001
P-value Summary	****
Significantly different (P<0.05)?	Yes

Table A3: TA Muscle Mass

	TA Muscle Weight (mg)	
N	CON	DEN
1	40.40	37.80
2	43.80	41.70
3	42.60	39.30
4	46.50	41.30
5	49.30	39.00
6	51.40	46.20
7	44.80	41.40
8	42.60	37.90
9	48.80	36.10
10	47.30	39.80
11	49.10	43.60
12	47.90	45.40
13	52.90	48.10
14	50.80	44.10
X	47.01	41.55
SD	3.72	3.53

Paired T-Test: CON vs DEN	
P-value	<0.0001
P-value Summary	****
Significantly different (P<0.05)?	Yes

Table A4: Soleus Muscle Mass

	Soleus Muscle Weight (mg)	
N	CON	DEN
1	6.90	5.20
2	7.30	7.00
3	7.70	5.30
4	6.80	4.20
5	7.60	4.90
6	7.30	5.30
7	8.00	5.30
8	7.10	4.20
9	7.50	5.70
10	6.20	5.30
11	6.80	4.70
12	6.50	5.20
13	7.60	5.40
14	9.10	5.50
X	7.31	5.23
SD	0.72	0.68

Paired T-Test: CON vs DEN	
P-value	<0.0001
P-value Summary	****
Significantly different (P<0.05)?	Yes

Table A5: GAST Muscle Mass

	GAST Muscle Weight (mg)	
N	CON	DEN
1	145.40	123.90
2	136.40	126.00
3	133.50	121.00
4	142.30	126.50
5	129.60	123.10
6	153.20	137.50
7	144.50	136.60
8	158.80	158.90
9	153.30	123.40
10	158.40	130.10
11	151.50	111.00
12	150.00	143.20
13	132.40	131.10
14	163.50	122.30
X	146.63	129.61
SD	10.70	11.66

Paired T-Test: CON vs DEN	
P-value	0.0004
P-value Summary	***
Significantly different (P<0.05)?	Yes

Table A6: MURF-1 Protein Expression

	MURF-1 Protein (a.u.)	
N	CON	DEN
1	0.60	1.35
2	0.52	1.32
3	0.38	1.14
4	0.58	1.27
5	0.64	1.39
6	0.61	0.99
X	0.55	1.24
SD	0.10	0.15

Paired T-Test: CON vs DEN	
P-value	0.0001
P-value Summary	***
Significantly different (P<0.05)?	Yes

Table A7: GADD-45α Protein Expression

	GADD45α Protein (a.u.)	
N	CON	DEN
1	0.43	1.05
2	1.45	1.33
3	0.34	0.67
4	0.70	1.37
5	0.75	1.24
6	0.55	1.35
X	0.70	1.17
SD	0.40	0.27

Paired T-Test: CON vs DEN	
P-value	0.0173
P-value Summary	*
Significantly different (P<0.05)?	Yes

Table A8: COX-IV Protein Expression

	COX-IV Protein (a.u.)	
N	CON	DEN
1	0.71	0.33
2	0.52	0.32
3	0.48	0.41
4	0.47	0.34
5	0.49	0.39
6	0.47	0.36
X	0.52	0.36
SD	0.09	0.03

Paired T-Test: CON vs DEN	
P-value	0.0164
P-value Summary	*
Significantly different (P<0.05)?	Yes

Table A9: VDAC Protein Expression

	VDAC Protein (a.u.)	
N	CON	DEN
1	3.09	1.88
2	2.58	1.63
3	2.96	2.43
4	3.26	2.59
5	3.04	2.81
6	3.69	3.28
X	3.10	2.44
SD	0.37	0.60

Paired T-Test: CON vs DEN	
P-value	0.0063
P-value Summary	**
Significantly different (P<0.05)?	Yes

Table A10: Complex I Inactive O_2 Consumption

	Complex I O_2 Consumption	
N	CON	DEN
1	45.87	23.33
2	47.75	29.29
3	63.09	28.35
X	52.24	26.99
SD	9.44	3.21

Paired T-Test: CON vs DEN	
P-value	0.0355
P-value Summary	*
Significantly different (P<0.05)?	Yes

Table A11: Complex I Active O_2 Consumption

	Complex I Active O_2 Consumption	
N	CON	DEN
1	235.63	117.77
2	196.75	151.38
3	249.67	165.38
X	227.35	144.84
SD	27.41	24.46

Paired T-Test: CON vs DEN	
P-value	0.0588
P-value Summary	ns
Significantly different (P<0.05)?	No

Table A11: Complex I+II Active O_2 Consumption

	Complex I + II Active O_2 Consumption	
N	CON	DEN
1	299.88	146.15
2	596.75	159.88
3	227.94	191.93
X	374.86	165.99
SD	195.50	23.50

Paired T-Test: CON vs DEN	
P-value	0.2212
P-value Summary	ns
Significantly different (P<0.05)?	No

Table A13: NLRP3 Protein Expression

	NLRP3 Protein (a.u.)	
N	CON	DEN
1	0.18	0.35
2	0.17	0.37
3	0.16	0.42
4	0.26	0.44
5	0.42	0.53
6	0.49	0.54
X	0.28	0.44
SD	0.14	0.08

Paired T-Test: CON vs DEN	
P-value	0.0029
P-value Summary	**
Significantly different (P<0.05)?	Yes

Table A14: Procaspase-1 Protein Expression

	Procaspase-1 Protein (a.u.)	
N	CON	DEN
1	0.19	0.57
2	0.36	0.86
3	0.30	0.98
4	0.25	0.57
5	0.67	0.83
6	0.22	0.36
X	0.33	0.69
SD	0.18	0.23

Paired T-Test: CON vs DEN	
P-value	0.0076
P-value Summary	**
Significantly different (P<0.05)?	Yes

Table A15: Caspase-1 Protein Expression

	Caspase-1 Protein (a.u.)	
N	CON	DEN
1	0.59	0.96
2	0.58	0.80
3	0.58	0.57
4	0.94	0.99
5	0.43	0.86
6	0.59	0.89
X	0.62	0.85
SD	0.17	0.15

Paired T-Test: CON vs DEN	
P-value	0.0263
P-value Summary	*
Significantly different (P<0.05)?	Yes

Table A16: GSDMD Protein Expression

	GSDMD Protein (a.u.)	
N	CON	DEN
1	0.67	1.03
2	0.55	0.81
3	0.60	1.13
4	0.55	0.95
5	0.80	1.15
6	0.49	0.90
X	0.61	1.00
SD	0.11	0.13

Paired T-Test: CON vs DEN	
P-value	0.0001
P-value Summary	***
Significantly different (P<0.05)?	Yes

Table A17: GSDMD-N Protein Expression

	GSDMD-N Protein (a.u.)	
N	CON	DEN
1	0.17	0.97
2	0.25	0.84
3	0.20	0.36
4	0.29	0.75
5	0.46	0.55
6	0.17	0.42
X	0.26	0.65
SD	0.11	0.24

Paired T-Test: CON vs DEN	
P-value	0.0172
P-value Summary	*
Significantly different (P<0.05)?	Yes

Table A18: NF-κB p65 Protein Expression

	NF-κB p65 Protein (a.u.)	
N	CON	DEN
1	0.35	0.94
2	0.47	1.15
3	0.38	1.02
4	0.28	1.04
5	0.36	1.08
6	0.33	1.11
X	0.36	1.06
SD	0.06	0.08

Paired T-Test: CON vs DEN	
P-value	<0.0001
P-value Summary	****
Significantly different (P<0.05)?	Yes

Table A19: IL-1β Fold Change

	IL-1β Protein (pg/mL)	
N	CON	DEN
1	28.24	36.80
2	19.60	32.58
3	33.16	52.76
X	27.00	40.71
SD	6.86	10.64

Paired T-Test: CON vs DEN	
P-value	0.0505
P-value Summary	ns
Significantly different (P<0.05)?	No

Table A20: Complex I ROS Emission

	Complex I ROS Emission	
N	CON	DEN
1	0.021	0.485
2	0.044	0.330
3	0.014	0.424
X	0.026	0.41
SD	0.016	0.08

Paired T-Test: CON vs DEN	
P-value	0.018
P-value Summary	*
Significantly different (P<0.05)?	Yes

Table A21: Complex I Active ROS Emission

	Complex I Active ROS Emission	
N	CON	DEN
1	0.003	0.058
2	0.009	0.040
3	0.002	0.046
X	0.005	0.05
SD	0.003	0.01

Paired T-Test: CON vs DEN	
P-value	0.0242
P-value Summary	*
Significantly different (P<0.05)?	Yes

Table A22: Complex I + II Active ROS Emission

	Complex I + II Active ROS Emission	
N	CON	DEN
1	0.002	0.051
2	0.004	0.036
3	0.003	0.038
X	0.003	0.04
SD	0.001	0.01

Paired T-Test: CON vs DEN	
P-value	0.0167
P-value Summary	*
Significantly different (P<0.05)?	Yes

Table A23: GAST mtDNA levels

	GAST mtDNA	
N	CON	DEN
1	68.45	64.51
2	76.32	34.36
3	20.55	20.12
4	90.28	33.65
5	95.41	47.12
6	24.60	13.51
7	13.96	12.76
8	26.06	10.95
X	51.95	29.62
SD	33.96	19.07

Paired T-Test: CON vs DEN	
P-value	0.0283
P-value Summary	*
Significantly different (P<0.05)?	Yes

Table A24: Cytosolic mtDNA levels

	Cytosolic mtDNA	
N	CON	DEN
1	32.20	4.80
2	16.10	8.00
3	10.22	6.79
4	59.52	18.51
5	23.60	16.76
6	20.78	5.54
7	8.77	4.09
8	12.11	5.51
X	22.91	8.75
SD	16.71	5.63

Paired T-Test: CON vs DEN	
P-value	0.02
P-value Summary	*
Significantly different (P<0.05)?	Yes

Table A25: Cytosolic/GAST mtDNA ratio

	Cyto/Gast Rati	
N	CON	DEN
1	32.20	4.80
2	16.10	8.00
3	10.22	6.79
4	59.52	18.51
5	23.60	16.76
6	20.78	5.54
7	8.77	4.09
8	12.11	5.51
X	22.91	8.75
SD	16.71	5.63

Paired T-Test: CON vs DEN	
P-value	0.072
P-value Summary	ns
Significantly different (P<0.05)?	No

Table A26: STING Protein Expression

	STING Protein (a.u.)	
N	CON	DEN
1	0.57	1.25
2	0.61	1.41
3	0.54	1.36
4	0.62	1.59
5	0.79	1.46
6	0.67	1.44
X	0.63	1.42
SD	0.09	0.11

Paired T-Test: CON vs DEN	
P-value	<0.0001
P-value Summary	****
Significantly different (P<0.05)?	Yes

Table A27: BAX Protein Expression

	BAX/COX-IV Protein (a.u.)	
N	CON	DEN
1	0.34	4.82
2	5.06	7.35
3	2.33	4.64
4	4.53	8.73
5	3.04	5.05
6	2.16	8.94
X	2.91	6.59
SD	1.72	2.00

Paired T-Test: CON vs DEN	
P-value	0.0046
P-value Summary	**
Significantly different (P<0.05)?	Yes

Table A28: AIF Protein Expression

	AIF/COX-IV Protein (a.u.)	
N	CON	DEN
1	3.66	7.63
2	4.02	6.09
3	5.97	6.91
4	6.84	8.69
5	5.81	6.97
6	6.03	6.52
X	5.39	7.13
SD	1.26	0.92

Paired T-Test: CON vs DEN	
P-value	0.0179
P-value Summary	*
Significantly different (P<0.05)?	Yes

Table A29: Voluntary Wheel Running Distances

	VWR Distances (km)	
N	Young	Aged
1	377.20	48.86
2	386.29	62.28
3	249.28	96.31
4	362.11	170.03
5	408.69	154.40
6	315.65	28.96
X	349.87	94.37
SD	58.26	54.25

Unpaired T-Test: CON vs DEN	
P-value	<0.0001
P-value Summary	****
Significantly different (P<0.05)?	Yes

Table A30: Body Weight (% change)

	Body Weight (% change)			
	Young		Aged	
N	UT	T	UT	T
1	14.18	2.46	14.22	1.63
2	22.68	6.37	14.61	-12.29
3	13.12	9.51	5.50	8.50
4	18.86	8.53	10.73	5.67
5	29.05	20.45	27.39	
6	21.98	3.83	10.57	
7			19.37	
X	19.98	8.52	13.84	0.88
SD	5.93	6.43	7.40	9.22

2-WAY ANOVA			
Source of Variation	P value	P value Summary	Significant
Interaction	0.7053	ns	No
Age	0.0428	*	Yes
Training	0.0005	***	Yes

POST-HOC TEST				
Tukey	Mean difference	Significant?	P-value summary	P-value
Young:Untrained vs. Young:Trained	11.45	Yes	*	0.0487
Young:Untrained vs. Aged:Untrained	5.35	No	ns	0.5328
Young:Untrained vs. Aged:Trained	19.1	Yes	**	0.0024
Young:Trained vs. Aged:Untrained	-6.104	No	ns	0.4225
Young:Trained vs. Aged:Trained	7.648	No	ns	0.3575
Aged:Untrained vs. Aged:Trained	13.75	Yes	*	0.0263

Table A31: GAST Muscle Mass

	GAST Muscle Mass/Body Weight			
	Young		Aged	
N	UT	T	UT	T
1	0.00366	0.00586	0.00286	0.00451
2	0.00506	0.00581	0.00274	0.00431
3	0.00497	0.0053	0.0040	0.0042
4	0.00480	0.0051	0.0030	0.0051
5	0.00421	0.0043	0.0033	
6	0.0037	0.0051	0.0037	
7			0.0047	
X	0.00441	0.00524	0.00327	0.00454
SD	0.00062	0.00057	0.00050	0.00040

2-WAY ANOVA			
Source of Variation	P value	P value Summary	Significant
Interaction	0.6366	ns	No
Age	0.005	**	Yes
Training	0.0015	**	Yes

POST-HOC TEST				
Tukey	Mean difference	Significant?	P-value summary	P-value
Young:Untrained vs. Young:Trained	-0.0008306	No	ns	0.1151
Young:Untrained vs. Aged:Untrained	0.0009398	No	ns	0.0517
Young:Untrained vs. Aged:Trained	-0.0001381	No	ns	0.9843
Young:Trained vs. Aged:Untrained	0.00177	Yes	***	0.0002
Young:Trained vs. Aged:Trained	0.0006926	No	ns	0.3151
Aged:Untrained vs. Aged:Trained	-0.001078	Yes	*	0.0467

Table A32: TA Muscle Mass

	TA Muscle Mass/Body Weight			
	Young		Aged	
N	UT	T	UT	T
1	0.0011	0.0009	0.0017	0.0014
2	0.0015	0.0009	0.0017	0.0014
3	0.0015	0.0011	0.0015	0.0013
4	0.0016	0.0011	0.0017	0.0015
5	0.0016	0.0009	0.0014	
6	0.0012	0.0012	0.0016	
7		0.0014		
X	0.00143	0.00104	0.00160	0.00142
SD	0.00021	0.00014	0.00013	0.00009

2-WAY ANOVA			
Source of Variation	P value	P value Summary	Significant
Interaction	*0.4154*	*ns*	*No*
Age	*0.0022*	**	*Yes*
Training	*0.0011*	**	*Yes*

POST-HOC TEST				
Tukey	Mean difference	Significant?	P-value summary	P-value
Young:Untrained vs. Young:Trained	-0.0002101	No	ns	0.1521
Young:Untrained vs. Aged:Untrained	0.0003041	Yes	*	0.0165
Young:Untrained vs. Aged:Trained	-0.00002203	No	ns	0.9967
Young:Trained vs. Aged:Untrained	0.0005143	Yes	***	0.0001
Young:Trained vs. Aged:Trained	0.0001881	No	ns	0.312
Aged:Untrained vs. Aged:Trained	-0.0003262	Yes	*	0.0232

Table A33: SOL Muscle Mass

	SOL Muscle Mass/Body Weight			
	Young		Aged	
N	UT	T	UT	T
1	0.00016	0.00014	0.00031	0.00028
2	0.00021	0.00012	0.00035	0.00022
3	0.00018	0.00021	0.00033	0.00027
4	0.00018	0.00017	0.00027	0.00032
5	0.00023	0.00021	0.00028	
6	0.00023	0.00019	0.00034	
7		0.00021		
X	0.00020	0.00017	0.00031	0.00027
SD	0.00003	0.00004	0.00003	0.00004

2-WAY ANOVA			
Source of Variation	P value	P value Summary	Significant
Interaction	*0.4812*	*ns*	*No*
Age	*0.0393*	*	*Yes*
Training	*<0.0001*	****	*Yes*

POST-HOC TEST				
Tukey	Mean difference	Significant?	P-value summary	P-value
Young:Untrained vs. Young:Trained	-0.0001152	Yes	****	<0.0001
Young:Untrained vs. Aged:Untrained	0.0000222	No	ns	0.6671
Young:Untrained vs. Aged:Trained	-0.00007163	Yes	*	0.0231
Young:Trained vs. Aged:Untrained	0.0001374	Yes	****	<0.0001
Young:Trained vs. Aged:Trained	0.00004353	No	ns	0.247
Aged:Untrained vs. Aged:Trained	-0.00009383	Yes	**	0.002

Table A34: Heart Muscle Mass

	Heart Muscle Mass/Body Weight			
	Young		Aged	
N	UT	T	UT	T
1	0.00292	0.00283	0.00447	0.00337
2	0.00495	0.00278	0.00441	0.00372
3	0.00376	0.00353	0.00425	0.00334
4	0.00373	0.00309	0.00423	0.00370
5	0.00341	0.00315	0.00365	
6	0.00323	0.00321	0.00430	
7		0.0040		
X	0.00367	0.00310	0.00422	0.00353
SD	0.00070	0.00027	0.00030	0.00020

2-WAY ANOVA			
Source of Variation	P value	P value Summary	Significant
Interaction	*0.541*	*ns*	*No*
Age	*0.0109*	*	*Yes*
Training	*0.0451*	*	*Yes*

POST-HOC TEST				
Tukey	Mean difference	Significant?	P-value summary	P-value
Young:Untrained vs. Young:Trained	-0.0005506	No	ns	0.2079
Young:Untrained vs. Aged:Untrained	0.0004371	No	ns	0.3596
Young:Untrained vs. Aged:Trained	0.0001343	No	ns	0.9697
Young:Trained vs. Aged:Untrained	0.0009877	Yes	**	0.0061
Young:Trained vs. Aged:Trained	0.0006848	No	ns	0.1401
Aged:Untrained vs. Aged:Trained	-0.0003028	No	ns	0.7316

Table A35: Epididymal Fat

	Heart Muscle Mass/Body Weight			
	Young		Aged	
N	UT	T	UT	T
1	0.05062	0.05768	0.01716	0.03008
2	0.03472	0.04322	0.01531	0.02124
3	0.02907	0.03874	0.02825	0.03880
4	0.03331	0.07551	0.02012	0.02164
5	0.04922	0.05730	0.03636	
6	0.06367	0.04534	0.03160	
7		0.0507		
X	0.04343	0.05297	0.02480	0.02794
SD	0.01326	0.01345	0.00851	0.00831

2-WAY ANOVA			
Source of Variation	P value	P value Summary	Significant
Interaction	*0.53*	*ns*	*No*
Age	*0.2088*	*ns*	*No*
Training	*0.0002*	***	*Yes*

POST-HOC TEST				
Tukey	Mean difference	Significant?	P-value summary	P-value
Young:Untrained vs. Young:Trained	0.01863	Yes	*	0.042
Young:Untrained vs. Aged:Untrained	-0.009211	No	ns	0.4646
Young:Untrained vs. Aged:Trained	0.01549	No	ns	0.172
Young:Trained vs. Aged:Untrained	-0.02784	Yes	**	0.0013
Young:Trained vs. Aged:Trained	-0.003139	No	ns	0.9714
Aged:Untrained vs. Aged:Trained	0.02471	Yes	*	0.0108

Table A36: COX-IV Protein Expression

	COX-IV Protein Expression			
	Young		Aged	
N	UT	T	UT	T
1	2.22	2.03	1.70	2.40
2	2.22	3.00	1.74	1.69
3	2.07	2.44	1.80	2.83
4	2.89	2.31	1.91	1.50
5	1.77	2.05	1.60	
6	1.41	1.99	1.59	
X	2.10	2.30	1.72	2.11
SD	0.50	0.38	0.12	0.62

2-WAY ANOVA			
Source of Variation	P value	P value Summary	Significant
Interaction	0.6294	ns	No
Age	0.133	ns	No
Training	0.122	ns	No

POST-HOC TEST				
Tukey	Mean difference	Significant?	P-value summary	P-value
Young:Untrained vs. Young:Trained	-0.2065	No	ns	0.8304
Young:Untrained vs. Aged:Untrained	0.3766	No	ns	0.4311
Young:Untrained vs. Aged:Trained	-0.008998	No	ns	>0.9999
Young:Trained vs. Aged:Untrained	0.5831	No	ns	0.1134
Young:Trained vs. Aged:Trained	0.1975	No	ns	0.8853
Aged:Untrained vs. Aged:Trained	-0.3856	No	ns	0.5047

Table A37: COX-I Protein Expression

	COX-I Protein Expression			
	Young		Aged	
N	UT	T	UT	T
1	1.89	1.56	1.06	1.47
2	2.25	2.03	1.91	1.82
3	3.06	2.41	1.37	2.13
4	1.80	2.69	1.31	0.84
5	1.13	1.90	1.27	
6	1.95	2.50	1.05	
X	2.01	2.18	1.33	1.56
SD	0.63	0.42	0.31	0.56

2-WAY ANOVA			
Source of Variation	P value	P value Summary	Significant
Interaction	0.8743	ns	No
Age	0.0065	**	Yes
Training	0.3567	ns	No

POST-HOC TEST				
Tukey	Mean difference	Significant?	P-value summary	P-value
Young:Untrained vs. Young:Trained	-0.1664	No	ns	0.9341
Young:Untrained vs. Aged:Untrained	0.6858	No	ns	0.1072
Young:Untrained vs. Aged:Trained	0.4515	No	ns	0.4979
Young:Trained vs. Aged:Untrained	0.8522	Yes	*	0.034
Young:Trained vs. Aged:Trained	0.6178	No	ns	0.2406
Aged:Untrained vs. Aged:Trained	-0.2343	No	ns	0.8788

Table A38: Complex I Inactive O_2 Consumption

	Complex I O_2 Consumption			
	Young		Aged	
N	UT	T	UT	T
1	23.64	47.20	48.59	42.13
2	42.60	66.71	29.46	54.90
3	49.60	49.68	42.18	53.14
4	47.47	72.96	23.62	96.01
5	49.47		32.37	82.99
6			37.67	
7			66.44	
8			31.48	
X	42.56	59.14	38.98	65.84
SD	10.95	12.65	13.55	22.62

2-WAY ANOVA			
Source of Variation	P value	P value Summary	Significant
Interaction	0.4595	ns	No
Age	0.821	ns	No
Training	0.005	**	Yes

POST-HOC TEST				
Tukey	Mean difference	Significant?	P-value summary	P-value
Young:Untrained vs. Young:Trained	-16.58	No	ns	0.403
Young:Untrained vs. Aged:Untrained	3.578	No	ns	0.9766
Young:Untrained vs. Aged:Trained	-23.28	No	ns	0.1163
Young:Trained vs. Aged:Untrained	20.16	No	ns	0.1808
Young:Trained vs. Aged:Trained	-6.698	No	ns	0.9153
Aged:Untrained vs. Aged:Trained	-26.86	Yes	*	0.0318

Table A39: Complex I Active O_2 Consumption

	Complex I Active O_2 Consumption			
	Young		Aged	
N	UT	T	UT	T
1	99.49	140.71	152.10	214.45
2	118.42	169.31	81.95	170.07
3	172.89	168.24	111.82	151.70
4	132.77	190.03	112.57	396.09
5	134.16		147.91	408.36
6			152.35	
7			157.94	
8			75.57	
X	131.55	167.07	124.03	268.14
SD	27.01	20.24	33.19	124.59

2-WAY ANOVA			
Source of Variation	P value	P value Summary	Significant
Interaction	0.0703	ns	No
Age	0.1147	ns	No
Training	0.0051	**	Yes

POST-HOC TEST				
Tukey	Mean difference	Significant?	P-value summary	P-value
Young:Untrained vs. Young:Trained	-35.53	No	ns	0.8413
Young:Untrained vs. Aged:Untrained	7.521	No	ns	0.9968
Young:Untrained vs. Aged:Trained	-136.6	Yes	*	0.0164
Young:Trained vs. Aged:Untrained	43.05	No	ns	0.6959
Young:Trained vs. Aged:Trained	-101.1	No	ns	0.1235
Aged:Untrained vs. Aged:Trained	-144.1	Yes	**	0.0048

Table A40: Complex I + II Active O_2 Consumption

	Complex I Active O_2 Consumption			
	Young		Aged	
N	UT	T	UT	T
1	97.17	172.69	144.58	222.62
2	115.83	173.73	84.16	163.81
3	202.15	163.99	122.83	158.95
4	135.67	143.47	138.32	313.79
5	127.09		151.46	402.08
6			142.94	
7			144.85	
8			80.39	
X	135.58	163.47	126.19	252.25
SD	39.91	14.03	28.36	104.45

2-WAY ANOVA			
Source of Variation	P value	P value Summary	Significant
Interaction	0.0614	ns	No
Age	0.124	ns	No
Training	0.0058	**	Yes

POST-HOC TEST				
Tukey	Mean difference	Significant?	P-value summary	P-value
Young:Untrained vs. Young:Trained	-27.89	No	ns	0.878
Young:Untrained vs. Aged:Untrained	9.39	No	ns	0.9908
Young:Untrained vs. Aged:Trained	-116.7	Yes	*	0.0189
Young:Trained vs. Aged:Untrained	37.28	No	ns	0.7003
Young:Trained vs. Aged:Trained	-88.78	No	ns	0.1197
Aged:Untrained vs. Aged:Trained	-126.1	Yes	**	0.0047

Table A41: NF-κB p65 Protein Expression

	NF-kB p65 Protein (a.u.)			
	Young		Aged	
N	UT	T	UT	T
1	0.41	0.78	1.22	1.01
2	1.03	1.07	0.97	1.13
3	0.26	0.72	1.46	0.64
4	0.17	0.35	0.28	0.57
X	0.47	0.73	0.98	0.84
SD	0.39	0.30	0.51	0.27

2-WAY ANOVA			
Source of Variation	P value	P value Summary	Significant
Interaction	0.3013	ns	No
Age	0.1261	ns	No
Training	0.7625	ns	No

POST-HOC TEST				
Tukey	Mean difference	Significant?	P-value summary	P-value
Young:Untrained vs. Young:Trained	-0.2624	No	ns	0.7618
Young:Untrained vs. Aged:Untrained	-0.5145	No	ns	0.2682
Young:Untrained vs. Aged:Trained	-0.3689	No	ns	0.5333
Young:Trained vs. Aged:Untrained	-0.2521	No	ns	0.7824
Young:Trained vs. Aged:Trained	-0.1065	No	ns	0.9776
Aged:Untrained vs. Aged:Trained	0.1456	No	ns	0.9461

Table A42: NLRP3 Protein Expression

	NLRP3 Protein (a.u.)			
	Young		Aged	
N	UT	T	UT	T
1	0.54	0.34	1.01	0.49
2	0.42	0.47	1.22	0.48
3	0.52	0.57	0.87	0.53
4	0.28	0.35	1.36	0.46
5	1.01	1.07	1.06	
6	0.52	0.63	0.91	
X	0.55	0.57	1.07	0.49
SD	0.25	0.27	0.19	0.03

2-WAY ANOVA			
Source of Variation	P value	P value Summary	Significant
Interaction	0.0046	**	Yes
Age	0.0298	*	Yes
Training	0.0081	**	Yes

POST-HOC TEST				
Tukey	Mean difference	Significant?	P-value summary	P-value
Young:Untrained vs. Young:Trained	-0.02415	No	ns	0.9973
Young:Untrained vs. Aged:Untrained	-0.5238	Yes	**	0.0028
Young:Untrained vs. Aged:Trained	0.05747	No	ns	0.9758
Young:Trained vs. Aged:Untrained	-0.4997	Yes	**	0.0042
Young:Trained vs. Aged:Trained	0.08162	No	ns	0.9355
Aged:Untrained vs. Aged:Trained	0.5813	Yes	**	0.003

Table A43: Procaspase-1 Protein Expression

	Procaspase-1 Protein (a.u.)			
	Young		Aged	
N	UT	T	UT	T
1	0.35	0.21	0.41	0.17
2	0.45	0.41	0.37	0.43
3	0.23	0.13	0.44	0.14
4	0.05	0.13	1.73	0.11
5	0.34	0.97	0.83	
6	0.61	1.09	0.92	
X	0.34	0.49	0.78	0.21
SD	0.19	0.43	0.52	0.15

2-WAY ANOVA			
Source of Variation	P value	P value Summary	Significant
Interaction	0.0385	*	Yes
Age	0.6086	ns	No
Training	0.2139	ns	No

POST-HOC TEST				
Tukey	Mean difference	Significant?	P-value summary	P-value
Young:Untrained vs. Young:Trained	-0.1532	No	ns	0.8924
Young:Untrained vs. Aged:Untrained	-0.4466	No	ns	0.2019
Young:Untrained vs. Aged:Trained	0.1244	No	ns	0.9545
Young:Trained vs. Aged:Untrained	-0.2934	No	ns	0.5406
Young:Trained vs. Aged:Trained	0.2776	No	ns	0.6654
Aged:Untrained vs. Aged:Trained	0.571	No	ns	0.1209

Table A44: Caspase-1 Protein Expression

	Caspase-1 Protein (a.u.)			
	Young		Aged	
N	UT	T	UT	T
1	1.03	0.72	1.14	1.04
2	0.77	0.48	1.41	1.21
3	0.31	0.28	1.46	0.75
4	0.40	0.56	1.06	0.66
5	0.50	0.51	1.24	
6	0.56	0.55	1.13	
X	0.60	0.52	1.24	0.92
SD	0.27	0.14	0.16	0.26

2-WAY ANOVA			
Source of Variation	P value	P value Summary	Significant
Interaction	0.1894	ns	No
Age	<0.0001	****	Yes
Training	0.0381	*	Yes

POST-HOC TEST				
Tukey	Mean difference	Significant?	P-value summary	P-value
Young:Untrained vs. Young:Trained	0.07899	No	ns	0.9122
Young:Untrained vs. Aged:Untrained	-0.6455	Yes	***	0.0002
Young:Untrained vs. Aged:Trained	-0.32	No	ns	0.1181
Young:Trained vs. Aged:Untrained	-0.7245	Yes	****	<0.0001
Young:Trained vs. Aged:Trained	-0.399	Yes	*	0.0381
Aged:Untrained vs. Aged:Trained	0.3255	No	ns	0.1096

Table A45: GSDMD-N Protein Expression

	GSDMD-N Protein (a.u.)			
	Young		Aged	
N	UT	T	UT	T
1	0.61	0.28	0.35	0.84
2	0.27	0.33	0.49	0.52
3	0.30	0.32	1.45	0.39
4	0.25	0.28	0.44	0.43
X	0.36	0.30	0.68	0.54
SD	0.17	0.02	0.52	0.20

2-WAY ANOVA			
Source of Variation	P value	P value Summary	Significant
Interaction	0.7798	ns	No
Age	0.076	ns	No
Training	0.5219	ns	No

POST-HOC TEST				
Tukey	Mean difference	Significant?	P-value summary	P-value
Young:Untrained vs. Young:Trained	0.05422	No	ns	0.9932
Young:Untrained vs. Aged:Untrained	-0.3232	No	ns	0.4272
Young:Untrained vs. Aged:Trained	-0.186	No	ns	0.8017
Young:Trained vs. Aged:Untrained	-0.3774	No	ns	0.303
Young:Trained vs. Aged:Trained	-0.2402	No	ns	0.6553
Aged:Untrained vs. Aged:Trained	0.1372	No	ns	0.9069

Table A46: GSDMD Protein Expression

GSDMD protein (a.u.)				
	Young		Aged	
N	UT	T	UT	T
1	0.43	1.06	1.23	1.12
2	1.17	1.06	1.20	1.03
3	0.68	0.74	1.75	0.66
4	0.65	0.67	1.46	0.93
X	0.74	0.88	1.41	0.93
SD	0.31	0.21	0.25	0.20

2-WAY ANOVA			
Source of Variation	P value	P value Summary	Significant
Interaction	0.0271	*	Yes
Age	0.0123	*	Yes
Training	0.2064	ns	No

POST-HOC TEST				
Tukey	Mean difference	Significant?	P-value summary	P-value
Young:Untrained vs. Young:Trained	-0.1459	No	ns	0.8373
Young:Untrained vs. Aged:Untrained	-0.6749	Yes	*	0.0105
Young:Untrained vs. Aged:Trained	-0.1988	No	ns	0.6749
Young:Trained vs. Aged:Untrained	-0.5291	Yes	*	0.0453
Young:Trained vs. Aged:Trained	-0.05294	No	ns	0.9899
Aged:Untrained vs. Aged:Trained	0.4761	No	ns	0.0761

Table A47: Fold change/Distance Ran

Fold change/Distance ran		
N	Young	Aged
1	-0.09	-1.04
2	0.03	-0.98
3	0.04	-0.40
4	0.06	-0.39
5	-0.08	-0.17
6	-0.10	-0.23
7	-0.04	-0.51
8	0.11	-0.22
9	-0.11	-1.19
10	-0.02	0.28
11	-0.16	-0.72
12	0.44	-0.55
X	0.01	-0.51
SD	0.16	0.42

Unpaired T-Test: Young vs Aged	
P-value	0.0006
P-value Summary	***
Significantly different (P<0.05)?	Yes

Table A48: Complex I ROS Emission

Complex I ROS Emission				
	Young		Aged	
N	UT	T	UT	T
1	0.15	0.05	0.11	0.07
2	0.11	0.11	0.21	0.12
3	0.03	0.01	0.04	0.08
4	0.04	0.02	0.12	0.02
5	0.03		0.05	0.04
6			0.08	
7			0.02	
8			0.05	
X	0.07	0.05	0.09	0.07
SD	0.05	0.04	0.06	0.04

2-WAY ANOVA			
Source of Variation	P value	P value Summary	Significant
Interaction	0.9178	ns	No
Age	0.4889	ns	No
Training	0.3474	ns	No

POST-HOC TEST				
Tukey	Mean difference	Significant?	P-value summary	P-value
Young:Untrained vs. Young:Trained	0.0246	No	ns	0.895
Young:Untrained vs. Aged:Untrained	-0.01384	No	ns	0.9658
Young:Untrained vs. Aged:Trained	0.005943	No	ns	0.9979
Young:Trained vs. Aged:Untrained	-0.03844	No	ns	0.6338
Young:Trained vs. Aged:Trained	-0.01865	No	ns	0.9501
Aged:Untrained vs. Aged:Trained	0.01978	No	ns	0.9091

Table A49: Complex I Active ROS Emission

Complex I Active ROS Emission				
	Young		Aged	
N	UT	T	UT	T
1	0.04	0.01	0.03	0.02
2	0.03	0.03	0.06	0.04
3	0.01	0.01	0.03	0.03
4	0.02	0.01	0.02	0.00
5	0.01		0.01	0.02
6			0.02	
7			0.01	
8			0.02	
X	0.02	0.01	0.03	0.02
SD	0.01	0.01	0.02	0.01

2-WAY ANOVA			
Source of Variation	P value	P value Summary	Significant
Interaction	0.8173	ns	No
Age	0.2948	ns	No
Training	0.4848	ns	No

POST-HOC TEST				
Tukey	Mean difference	Significant?	P-value summary	P-value
Young:Untrained vs. Young:Trained	0.006029	No	ns	0.9237
Young:Untrained vs. Aged:Untrained	-0.005373	No	ns	0.9134
Young:Untrained vs. Aged:Trained	-0.002326	No	ns	0.994
Young:Trained vs. Aged:Untrained	-0.0114	No	ns	0.5816
Young:Trained vs. Aged:Trained	-0.008355	No	ns	0.8241
Aged:Untrained vs. Aged:Trained	0.003046	No	ns	0.9822

Table A50: Complex I + II Active ROS Emission

Complex I+II Active ROS Emission				
	Young		Aged	
N	UT	T	UT	T
1	0.06	0.03	0.06	0.01
2	0.06	0.04	0.08	0.05
3	0.01	0.01	0.04	0.04
4	0.01	0.01	0.03	0.01
5	0.01		0.02	0.03
6			0.04	
7			0.01	
8			0.04	
X	0.03	0.02	0.04	0.03
SD	0.02	0.02	0.02	0.02

2-WAY ANOVA			
Source of Variation	P value	P value Summary	Significant
Interaction	0.925	ns	No
Age	0.4369	ns	No
Training	0.3286	ns	No

POST-HOC TEST				
Tukey	Mean difference	Significant?	P-value summary	P-value
Young:Untrained vs. Young:Trained	0.008467	No	ns	0.5584
Young:Untrained vs. Aged:Untrained	-0.008296	No	ns	0.5005
Young:Untrained vs. Aged:Trained	0.001949	No	ns	0.8858
Young:Trained vs. Aged:Untrained	-0.01676	No	ns	0.2122
Young:Trained vs. Aged:Trained	-0.006518	No	ns	0.6517
Aged:Untrained vs. Aged:Trained	0.01025	No	ns	0.407

Table A51: GAST mtDNA levels

	GAST mtDNA			
	Young		Aged	
N	UT	T	UT	T
1	70.95	87.19	67.52	170.28
2	66.21	101.22	23.83	72.05
3	27.66	37.41	10.40	66.63
4	38.72	55.15	21.78	41.37
5	37.66		30.27	
X	48.24	70.24	30.76	87.58
SD	19.14	29.17	21.76	56.73

2-WAY ANOVA			
Source of Variation	P value	P value Summary	Significant
Interaction	0.2896	ns	No
Age	0.9964	ns	No
Training	0.0259	*	Yes

POST-HOC TEST				
Tukey	Mean difference	Significant?	P-value summary	P-value
Young:Untrained vs. Young:Trained	-22	No	ns	0.7609
Young:Untrained vs. Aged:Untrained	17.48	No	ns	0.8399
Young:Untrained vs. Aged:Trained	-39.34	No	ns	0.3323
Young:Trained vs. Aged:Untrained	39.48	No	ns	0.3294
Young:Trained vs. Aged:Trained	-17.34	No	ns	0.8813
Aged:Untrained vs. Aged:Trained	-56.82	No	ns	0.0964

Table A52: Cytosolic mtDNA levels

	Cytosolic mtDNA			
	Young		Aged	
N	UT	T	UT	T
1	20.89	12.01	62.37	14.53
2	10.41	11.40	6.29	13.00
3	6.40	34.15	3.34	11.47
4	30.31	36.01	20.07	9.07
5	27.28		9.16	
X	19.06	23.39	20.25	12.02
SD	10.40	13.52	24.38	2.33

2-WAY ANOVA			
Source of Variation	P value	P value Summary	Significant
Interaction	0.408	ns	No
Age	0.5004	ns	No
Training	0.7953	ns	No

POST-HOC TEST				
Tukey	Mean difference	Significant?	P-value summary	P-value
Young:Untrained vs. Young:Trained	-4.334	No	ns	0.9748
Young:Untrained vs. Aged:Untrained	-1.188	No	ns	0.9993
Young:Untrained vs. Aged:Trained	7.042	No	ns	0.9044
Young:Trained vs. Aged:Untrained	3.146	No	ns	0.99
Young:Trained vs. Aged:Trained	11.38	No	ns	0.7317
Aged:Untrained vs. Aged:Trained	8.23	No	ns	0.8577

Table A53: Cytosolic/Gast mtDNA ratio

	Cytosolic/Whole muscle mtDNA			
	Young		Aged	
N	UT	T	UT	T
1	0.29	0.14	0.92	0.09
2	0.16	0.11	0.26	0.18
3	0.23	0.91	0.32	0.17
4	0.78	0.65	0.92	0.22
5	0.72		0.30	
X	0.44	0.45	0.55	0.16
SD	0.29	0.39	0.34	0.06

2-WAY ANOVA			
Source of Variation	P value	P value Summary	Significant
Interaction	0.1886	ns	No
Age	0.5396	ns	No
Training	0.2243	ns	No

POST-HOC TEST				
Tukey	Mean difference	Significant?	P-value summary	P-value
Young:Untrained vs. Young:Trained	-0.01591	No	ns	0.9998
Young:Untrained vs. Aged:Untrained	-0.1085	No	ns	0.9409
Young:Untrained vs. Aged:Trained	0.2738	No	ns	0.5521
Young:Trained vs. Aged:Untrained	-0.09261	No	ns	0.9676
Young:Trained vs. Aged:Trained	0.2897	No	ns	0.5492
Aged:Untrained vs. Aged:Trained	0.3823	No	ns	0.2814

Table A54: STING Protein Expression

	STING Protein (a.u.)			
	Young		Aged	
N	UT	T	UT	T
1	1.17	0.94	1.18	1.09
2	1.01	0.86	1.02	0.83
3	0.74	0.74	3.47	0.54
4	0.95	0.69	1.98	1.10
X	0.97	0.81	1.91	0.89
SD	0.18	0.11	1.12	0.27

2-WAY ANOVA			
Source of Variation	P value	P value Summary	Significant
Interaction	0.1661	ns	No
Age	0.1042	ns	No
Training	0.066	ns	No

POST-HOC TEST				
Tukey	Mean difference	Significant?	P-value summary	P-value
Young:Untrained vs. Young:Trained	0.1603	No	ns	0.9793
Young:Untrained vs. Aged:Untrained	-0.9463	No	ns	0.156
Young:Untrained vs. Aged:Trained	0.07746	No	ns	0.9975
Young:Trained vs. Aged:Untrained	-1.107	No	ns	0.0828
Young:Trained vs. Aged:Trained	-0.08289	No	ns	0.997
Aged:Untrained vs. Aged:Trained	1.024	No	ns	0.1155

Table A55: BAX Protein Expression

	BAX/COX-IV protein (a.u.)			
	Young		Aged	
N	UT	T	UT	T
1	0.41	0.30	1.07	0.23
2	0.29	0.14	0.35	0.42
3	0.12	0.17	1.17	0.22
4	0.08	0.14	0.92	0.27
X	0.22	0.19	0.88	0.28
SD	0.15	0.08	0.37	0.09

2-WAY ANOVA			
Source of Variation	P value	P value Summary	Significant
Interaction	0.0188	*	Yes
Age	0.0036	**	Yes
Training	0.0101	*	Yes

POST-HOC TEST				
Tukey	Mean difference	Significant?	P-value summary	P-value
Young:Untrained vs. Young:Trained	0.03456	No	ns	0.9951
Young:Untrained vs. Aged:Untrained	-0.6537	Yes	**	0.0037
Young:Untrained vs. Aged:Trained	-0.05761	No	ns	0.9783
Young:Trained vs. Aged:Untrained	-0.6883	Yes	**	0.0025
Young:Trained vs. Aged:Trained	-0.09218	No	ns	0.9204
Aged:Untrained vs. Aged:Trained	0.5961	Yes	**	0.0073

APPENDIX B: SUPPLEMENTARY DATA

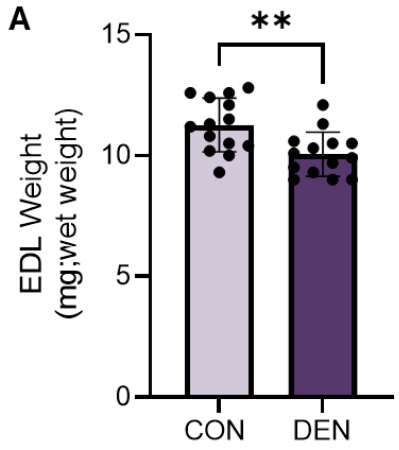

Figure B1: Change in EDL muscle weight following 7 days of muscle denervation (n=14). Measurements underwent a paired student's t-test (A). **, p<0.01. EDL, Extensor Digitorum Longus; CON, control; DEN, denervated. Values are expressed as mean ± SD.

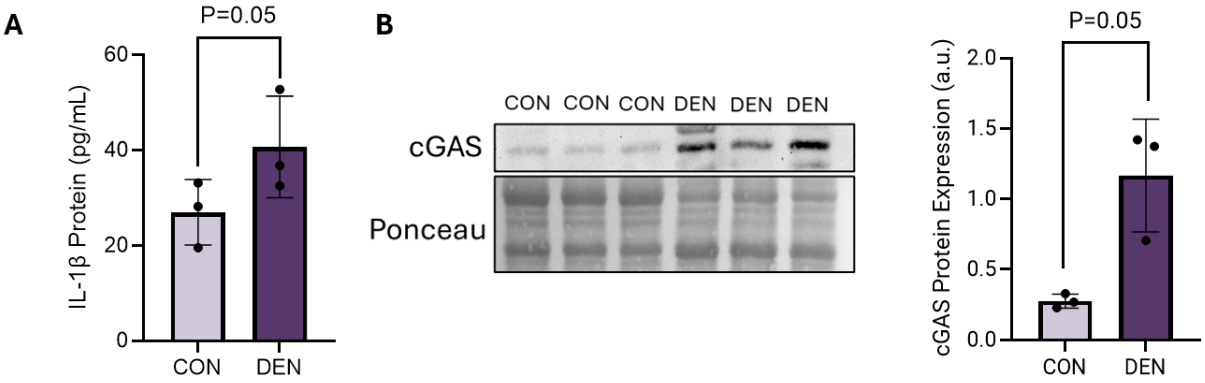

Figure B2: IL-1β ELISA results in the denervated gastrocnemius compared to the sham-operated control (A) (n=3). Representative western blot of cGAS protein expression and the corresponding quantification (B) (n=3). All measurements underwent a paired student's t-test. CON, control; DEN, denervated. Values are expressed as mean ± SD.

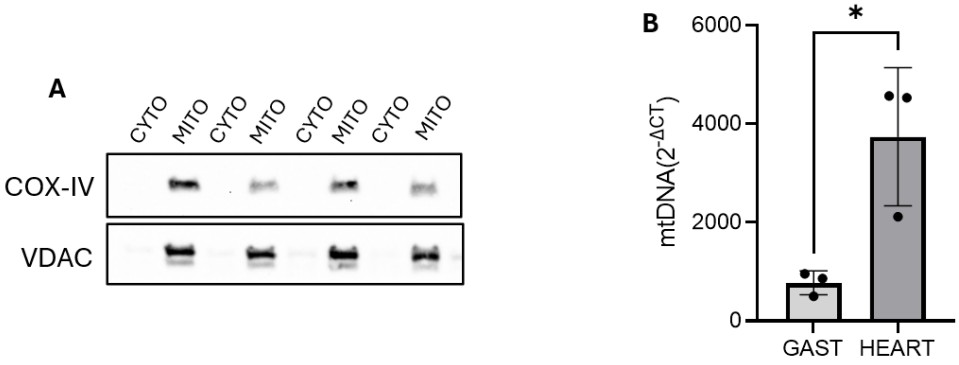

Figure B3: Representative western blots for purity of mitochondrial and cytosolic fractions. COX-IV and VDAC were used as markers of mitochondrial contamination (A). Positive control for 16s rRNA primer in gastrocnemius and heart tissues. Values were corrected to Actin-B (B). mtDNA measurement underwent an unpaired student's t-test. CON, control; DEN, denervated; Cyto, cytosolic fraction; Mito, mitochondrial fraction. Values are expressed as mean ± SD.

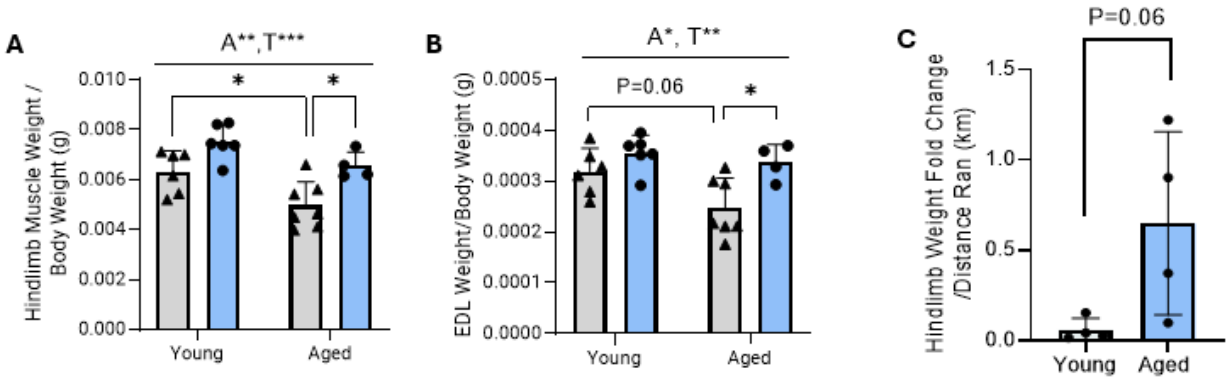

Figure B4: Changes in total hindlimb weight [GAST, EDL, TA, SOL] (A) and EDL (B) corrected to body weight (n=4-7). Fold change in pooled hindlimb muscle mass corrected to the total running distance (km) (C) (n=4). Body composition was analyzed using a two-way ANOVA. Fold change was analyzed using a student's unpaired t-test. A, main effect of age; T, main effect of training. *, p<0.05; **, p<0.01; ***, p<0.001;TA, tibialis anterior; SOL, soleus; GAST, gastrocnemius; EDL, Extensor Digitorum Longus; Values are expressed as mean ± SD.

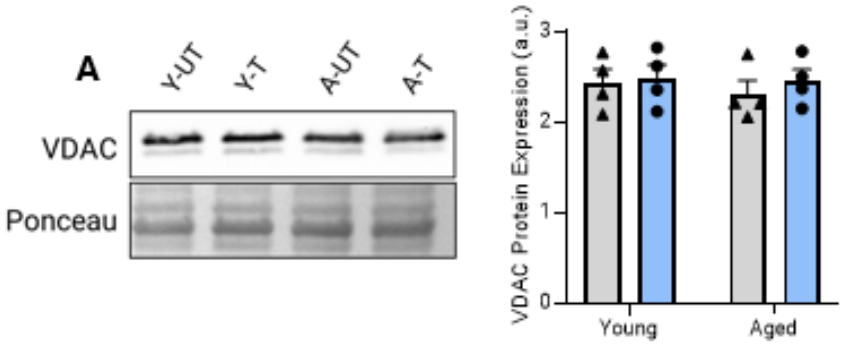

Figure B5: Representative western blot and the graphical representation of VDAC protein expression within young and aged animals following the 6-week exercise protocol (A) (n=4). Western blot was analyzed used a two-way ANOVA. Values are expressed as mean ± SD.

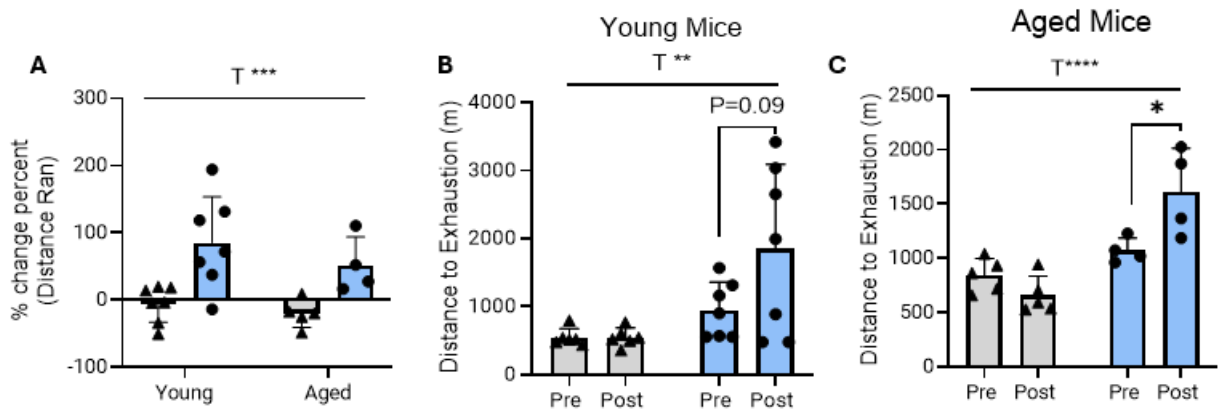

Figure B6: Percent change of the distance ran during an acute treadmill test before and after the 6-week training protocol within young and aged animals (A) (n=4-7). Absolute values of distance to exhaustion during the pre- and post-test within young (B) and aged (C) mice. All data was analyzed using a two-way ANOVA. A, main effect of age; T, main effect of training. *, $p<0.05$, **, $p<0.01$; ***, $p<0.001$; ****, $p<0.0001$. Pre, pre-intervention; Post, post-intervention; Values are expressed as mean ± SD.

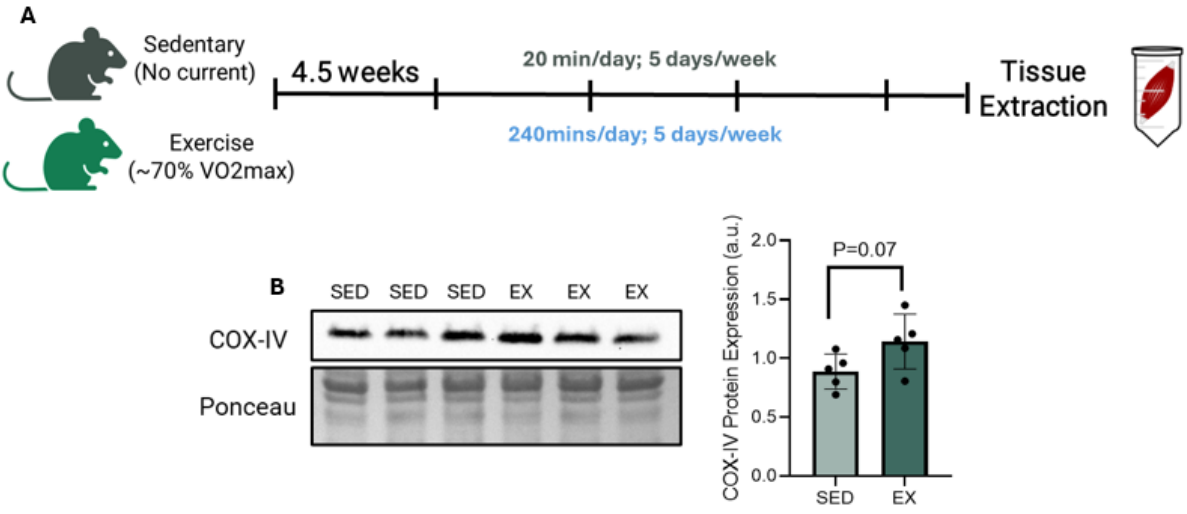

Figure B7: Study design of a pilot swim exercise protocol for 7-week-old mice (A). Changes in mitochondrial content marker, COX-IV following 4.5 weeks of exercise training (B) (n=5). All data underwent an unpaired student's t-test. SED, sedentary group; EX, exercise group. Values are expressed as mean ± SD.

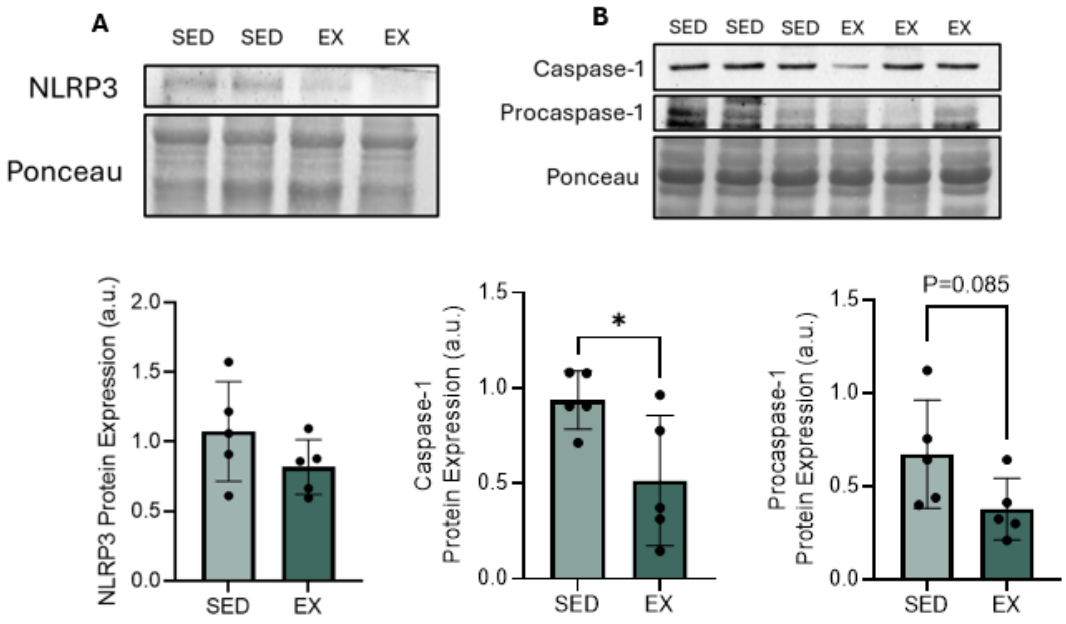

Figure B8: Representative western blots of NLRP3 (n=5) (A), and downstream targets, Caspase-1 P20 and Procaspase-1 (B) (n=5), alongside their graphical quantifications. Data was analyzed using an unpaired student's t-test. *, $p<0.05$. SED, sedentary group; EX, exercise group. All values are expressed as mean ± SD.

APPENDIX C: LABORATORY METHODS AND PROTOCOLS

ACUTE TREADMILL ENDURANCE TEST

Young Mice		Aged Mice	
Treadmill speed (m/min)	**Duration (min)**	**Treadmill speed (m/min)**	**Duration (min)**
0	5	0	5
5	5	5	5
10	10	7	10
11	2	10	20
12	2	11	20
Increasing speed by 1 m/min every 2 minutes until exhaustion		12 m/min until exhaustion	

Table C1: Acute treadmill endurance test for young and aged mice.

SAMPLE CALCULATION FOR VOLUNTARY WHEEL RUNNING DISTANCE

Wheel diameter: 12cm; Example revolutions: 1405

1) km/rev = wheel diameter x pi

   = 0.00012 km x 3.14159….
   =0.000376991 km/revolution
2) km ran = km/rev x # of revolutions

   =0.000376991 x 1405
   = 0.529672355 km

SCIATIC NERVE TRANSECTION

Sterilize surgical instruments through autoclaving prior to surgery

1. Collect all surgical instruments and sterilize with 70% ethanol. All surgical tools should be kept in 70% ethanol when not in use.

2. After the mouse is anesthetized and weighed, place tear gel on the eyes to avoid dryness throughout the duration of the surgery.

3. Landmark incision site by locating the femur, and the incision will be parallel with the femur, approximately half-way between the hip and knee joint. Wipe down the incision site using a kimwipe soaked with 70% ethanol and shave the incision area with an electric razor.

4. After shaving, wipe the site with iodine, followed by 70% ethanol to prep the skin for surgery.

5. Using small scissors, make a small incision in the skin, below the femur bone, and locate the sciatic nerve through the muscle. It should appear as a thick white band below the surface of the muscle.

6. Following this, make another incision into the muscle, perpendicular to the first cut to reveal the nerve.

7. Using blunt scissors, remove a 3-5mm section of the sciatic nerve to denervate the hindlimb muscles.

8. Suture the incision in the muscle closed by tying two knots, ensuring that they are tied in opposite directions.

9. To close the incision in the skin, use 2-3 surgical staples, ensuring to fully squeeze the staples closed.

10. Sham-operate the opposite leg, as an internal control, by performing steps 3-9, without transecting the nerve. If the tear gel has dissipated, reapply as needed throughout the procedure.

11. Following the surgery, use a 29g syringe to inject Metacam (2µg/g of body weight), subcutaneously. Create the working stock of Metacam by adding 1mL to 9mL of 0.9% saline solution. In brief, pinch the skin along the spine to create a "tent' shape and inject it into the center of the skin.

12. Put the mouse in a new, fresh cage and keep a heat lamp on the animal to help normalize body temperature. The heat lamp should be left on even after the animal regains consciousness, until any abnormal behaviour subsides. If abnormal behaviour persists for over 20 minutes, crush up a piece of chow with tap water in a small petri dish and place in cage.

13. To help avoid the risk of infection, Baytril is incorporated into the water for the remainder of the denervation period. In brief, 1mL of Baytril is added to 200mL of water.

The following day:

14. Give a second Metacam injection (1µg/g of body weight) approximately 24 hours after the surgery.

15. Continue to carefully monitor the animal throughout the duration of the denervation period.

WHOLE MUSCLE PROTEIN EXTRACTION

1. Muscle Extraction Buffer (Sakamoto Buffer)
    a. 20mM Hepes (ph 7.4); 2.383g/500ml
    b. 2mM EGTA; 0.3804g/500ml
    c. 1% Trition-X100; 5ml/500ml
    d. 50% Glycerol; 10ml/500ml
    e. 50mM b-Glycerophosphate; 5.4g/500ml
    Volume up to 500ml with double distilled water (ddH_2O); pH to 7.4

2. Make up buffer with Protease and phosphatase inhibitors:
In a 15ml tube, mix the following at the appropriate ratio as outlined below and keep on ice:
a. 1 ml Sakamoto Muscle Extraction Buffer
b. 10 µl Protease Inhibitor Stock
c. 10 µl Cocktail 2 Phosphatase Inhibitor
d. 10 µl Cocktail 3 Phosphatase Inhibitor

Procedure:
1. Add 200µl of Sakamoto Muscle Extraction Buffer to a set of 2mL Eppendorf tubes.

2. Weigh out 25-30mg of tissue into the first set of Eppendorf tubes and record the exact weight of each sample in a table.

3. Add the appropriate volume of buffer solution to each Eppendorf to produce a 15x dilution [(Equation: weight of muscle (mg) x 14 - 200µL = Additional buffer volume added (µL)]

4. Insert a metal bead into each Eppendorf.

5. Place Eppendorfs in balanced manner in metal brackets (kept in -20ºC freezer).

6. Insert brackets into TissueLyser and homogenize (shake) at 30 Hz for 1 min at a time.

7. Remove blocks, check for homogeneity and repeat if necessary (flip orientation of blocks for each cycle).

8. Remove beads with a magnet and centrifuge at 14000g for 10 minutes at 4°C.

9. Completely withdraw the supernatant and pipette the solution into the new Eppendorf tubes.

10. Store at -80°C.

MITOCHONDRIAL-CYTOSOLIC FRACTIONATION

Reagents:
1. Mitochondrial Isolation Buffer (MIB)
a. 64mM Sucrose (323.3g/mol); 22.93g
b. 50mM Tris (121.14g/mol); 6.06g

c. 50mm KCl (74.55g/mol); 3.73g
d. 10mM EDTA (292.24g/mol); 2.92g
e. 0.2% BSA; 2.0g
Volume up to 1L with double distilled water (ddH_2O); pH to 7.4

2. Make up buffer with Protease and phosphatase inhibitors:
In a 15ml tube, mix the following at the appropriate ratio as outlined below and keep on ice:
a. 1 ml Mitochondrial Isolation Buffer
b. 10 µl Protease Inhibitor Stock (1 tablet in 500µL ddH_2O)
c. 10 µl Cocktail 2 Phosphatase Inhibitor
d. 10 µl Cocktail 3 Phosphatase Inhibitor
→Approximately 2 mls required per hindlimb.

Procedure:
1. Collect gastrocnemius into a labeled tube with 1ml pure MIB (no inhibitors).

2. Mince on a glass plate over ice.

3. Add minced tissue to Dounce Homogenizer tube with 1ml of MIB with inhibitor and homogenize until it is a uniform mixture.

4. Centrifuge the sample at 1200g for 15 mins at 4°C and transfer the resulting supernate to a new Eppendorf tube.

5. Centrifuge at 21000g for 20 minutes at 4°C. The resulting supernate will become the cytosolic fraction, while the pellet retains the mitochondrial fraction.

For the cytosolic fraction:

6. Centrifuge at 21000g for 20 minutes at 4°C, for two more cycles, transferring to a new Eppendorf tube each time.

7. Store the cytosolic fraction at -80°C.

For the mitochondrial fraction:

8. Resuspend the pellet obtained in step 5 in 100µl MIB with inhibitors.

9. Centrifuge the sample at 21,000g for 20 mins at 4°C.

10. Resuspend the pellet in 20-50ul of MIC with inhibitors, depending on the size of the pellet.

11. Store at -80°C.

WESTERN BLOTTING PROTOCOL

GEL ELECTROPHORESIS-SDS PAGE (PROTEIN BIORAD SYSTEM)

Reagents:

1. Acrylamide/Bis-Acrylamide, 30% Solution 37.5:1 (BioShop 10.502)
    a. Store at 4°C
2. Under Tris Buffer
    a. 1M Tris, pH 8.8 (60.5g/500ml)
    b. Store at 4°C
3. Over Tris Buffer
    a. 1M Tris, pH 6.8 (12.1g/100ml)
    b. Bromophenol Blue (for colour)
    c. Store at 4°C
4. Ammonium Persulfate (APS)
    a. 10% (w/v) APS in ddH_20 (1g/10ml)
    b. Stored at 4°C
5. Sodium Dodecyl Sulfate (SDS)
    a. 10% (w/v) in ddH_20 (1g/10ml)
    b. Store at room temperature
6. TEMED (Sigma T-9281)
7. Electrophoresis Buffer, pH 8.3 (10L)
    a. 25mM Tris 30.34g, 192mM Glycine 144g, 0.1% SDS 10g
    b. Volume to 10L with ddH_20
    c. Store at room temperature
8. 6X SDS
    a. Warm 100% glycerol in water bath at 65°C for 30 minutes
    b. Combine 1.2g SDS, 0.06g Bromophenol Blue, 3mls of 1M Tris, pH 6.8 and 1ml of ddH_20 and stir at 4°C for 5 minutes
    c. Add 3mls of 100% glycerol, stir and aliquot mixture.
    d. Store at -20°C
    e. Add 5% (v/v) ß-mercaptoethanol (Sigma M6250) to 6X SDS <u>just prior</u> to use
9. *tetra*-Amyl alcohol ReagentPlus, 99% (Sigma 152463)

Procedure:

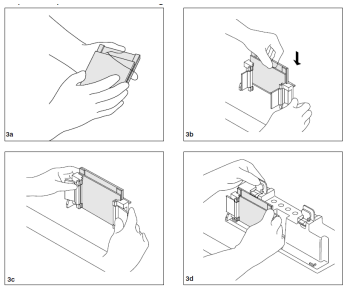

1. *Prepare gel electrophoresis rack:*
    a. Clean glass plates thoroughly with soap followed by 95% ethanol then ddH_20.
    b. Dry carefully with a kimwipe.
    c. Assemble glass plates as shown below:
    d. Check the seal by adding a small volume of ddH_20 then pour off and let dry.
2. *Prepare separating gels:*

a. Mini Protean 3 Bio-Rad System volumes:

	8%	10%	12%	15%	18%
Acrylamide	2.7 ml	3.3 ml	4.0 ml	5.0 ml	6.0 ml
ddH_20	4.1 ml	3.5 ml	2.8 ml	1.8 ml	0.8 ml
Under Tris	3.0 ml	3.0 ml	3.0 ml	3.0 ml	3.0 ml
SDS	100µl	100µl	100µl	100µl	100µl
APS	100µl	100µl	100µl	100µl	100µl
TEMED	10µl	10µl	10µl	10µl	10µl

b. Mix the contents of the separating gel without adding APS or TEMED. Stir.

c. Add APS and TEMED. Stir.

d. Slowly pour the entire volume of the solution into the space between the two plates while keeping plates tilted to prevent bubble formation.

e. Add *tert*-Amyl alcohol to coat top surface of gel solution.

f. Allow 30 minutes for gel polymerization.

g. Remove *tert*-Amyl alcohol by pouring it off and remove any remainder with a kimwipe. Rinse with ddH_20.

3. *Prepare stacking gel:*

Acrylamide	500 µl
Over Tris	625 µl
ddH_20	3.75 ml
SDS	50 µl
APS	50 µl
TEMED	7.5 µl

a. For a single mini gel use the following volumes →

b. Mix the contents of the stacking gel without adding APS or TEMED. Stir.

c. Add APS and TEMED. Stir.

d. Using a Pasteur pipette slowly add the entire volume from the beaker in between the plates.

e. Add comb for desired number of wells.

f. Allow 30 minutes for gel polymerization.

4. *Prepare samples:*

a. Turn on the block heater to 95ºC.

b. Pipette required volume of sample into new eppendorf with same amount of lysis buffer and 5 µl of sample dye. Keep samples on ice until all samples are prepared (use pipette plan).

c. Briefly spin each sample to bring volume to the bottom of the eppendorf.

d. Incubate each sample at 95 ºC for 5 minutes in the heating block to denature the proteins.

e. Briefly spin again to return volume to the bottom of the eppendorf.

5. *Assemble Mini-PROTEAN gel caster system:*

   a. If you are only running one gel a rectangular plastic pseudo plate must be clamped on the other side of the caster.

   b. Fill with electrophoresis buffer between the plates and outside of the plates in the chamber.

   c. Slowly remove the comb using both hands (one on each side) by pulling the comb straight upwards.

   d. Fix any wells that are deformed using a small spatula.

   e. Clean out the wells using a syringe filled with electrophoresis buffer.

   f. Withdraw the entire volume of the sample using a Hamilton syringe. Inject volume slowly into the bottom of the well.

6. *Gel electrophoresis:*

   a. Immediately after all samples are loaded place the lid on the gel chamber.

   b. Place positive and negative plugs into the power supply and turn on power supply.

   c. Set power supply to 120V. Gel will run for ~2 hours depending on percent gel made.

   d. When the bromophenol blue has run off the bottom of the gel (or when gel has separated the desire amount) turn off the power supply. Remove plugs from power supply and remove lid.

   e. Prepare for electrotransfer of proteins from the gel to nitrocellulose membrane.

WESTERN BLOTTING – TRANSFER AND IMMUNODETECTION

Reagents:

1. Transfer Buffer
   a. 0.025M Tris-HCl pH 8.3; 12.14g
   b. 0.15M Glycine ; 45.05g
   c. 20% Methanol; 800ml
   d. make up to 4L with ddH_20
   e. store at 4°C
2. Ponceau S stain
   a. 0.1% (w/v) Ponceau S

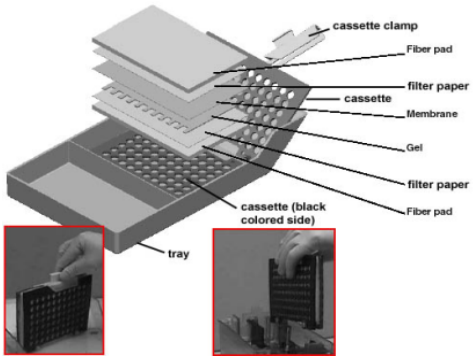

   b. 0.5% (v/v) Acetic Acid
   c. Store at room temperature
3. Wash Buffer
   a. Tris-HCl pH 7.5; 12g
   b. NaCl; 58.5g
   c. 0.1% Tween; 10ml
   d. Store at room temperature
4. Blocking Solution
   a. 5% (w/v) skim milk power in wash buffer OR
   b. 5% (w/v) BSA in wash buffer
5. Enhanced Chemiluminescence Fluid (ECL; Santa Cruz sc-2048)
6. Film/Developer/Fixer

Procedure:

1. *Transfer Procedure:*

   a. Remove electrophoresis plates from chamber and separate the plates.

   b. Cut away unnecessary parts of the gel using a spatula and measure remaining gel size.

   c. Using a paper cutter cut 6 pieces of Whatman paper per gel to the same size as the gel. Wearing gloves cut nitrocellulose membrane (GE Healthcare RPN303D) to the dimensions of the gel.

   d. Assemble Whatman paper, nitrocellulose membrane and gel as shown above:

   e. Close the cassette and place in the transfer chamber with the black side of the cassette facing the back side of the chamber.

   f. Place ice pack in the chamber.

   g. Place lid on the chamber and connect the leads to the power supply.

   h. Turn on the power supply and run at 120V for 2 hours. This can vary depending on the size of the protein of interest.

2. *Removal of transfer membrane:*

   a. Turn off the power supply and disconnect leads from the power supply then remove the lid from the chamber.

   b. Remove the cassette from the chamber.

   c. With gloves on, remove the Whatman paper and gel and place the nitrocellulose membrane in a plastic dish.

   d. Add Ponceau S stain on the membrane and gently swirl.

   e. Drain off the remaining Ponceau S and save for reuse.

f. Rinse the membrane with ddH_20 to reduce the red background. Wrap membrane in saran wrap and scan image.

g. Cut the membrane while protein bands are still visible at the desired molecular weight.

h. Rotate membrane at room temperature in wash buffer until remaining Ponceau S has been removed.

i. Incubate membrane for 1 hour with rotation in blocking solution.

j. Incubate membrane with desired antibody diluted in blocking solution overnight at 4ºC. Membrane is placed face up into the solution on a glass plate covered in parafilm. To maintain a moist environment overnight, wet a small kimwipe and form it into a ball and place in each corner of the dish. Cover the dish with saran wrap.

3. *Immunodetection:*

   a. Wash the blots in wash buffer with gentle rotation for 5 minutes 3X.

   b. Incubate the blots for 1 hour in room temperature with the appropriate secondary antibody diluted in blocking solution.

   c. Membrane is placed face up in solution on a glass plate covered with parafilm. Place moist kimwipes in each corner of the dish and cover the dish with saran wrap.

   d. Following the incubation, wash the membrane 3X for 5 minutes with wash buffer.

4. *Enhanced Chemiluminescence Detection:*

   a. Mix ECL fluids "A" and "B" in a 1:1 ratio in a disposable Rohr tube.

   b. Place blots on saran wrap face up and apply ECL solution for 2 minutes.

   c. Dab off excess ECL on a kimwipe and place blots face down on a fresh piece of saran wrap and wrap tightly.

   d. Expose blot to film (time will vary depending on protein and antibody).

   e. Place film into developer (time will vary).

   f. Once image appears place film into fixer for 2 minutes. Wash with fresh water when complete.

ENZYME-LINKED IMMUNOSORBENT ASSAY (ELISA)

Reagents

- Mouse IL-1 beta/IL-1F2 DuoSet ELISA (cat #: DY401) was used for the measurement of IL-1β in denervated muscle. All reagents were included in the DuoSet ELISA Ancillary Reagent Kit 2 (cat #: DY008B)

Procedure

Day 1:

1. Obtain a 96-well microplate.
2. For first time use, reconstitute the capture antibody and detection antibody accordingly.
    a. Capture Antibody: Reconstitute with 0.5 ml PBS and mix gently. Let it sit for 15 minutes before preparing the working concentration or aliquoting.
    b. Detection Antibody: Reconstitute with 1 ml of Reagent Diluent and mix gently. Let it sit overnight at 4ºC before using or aliquoting.
3. Dilute the capture antibody to the working concentration in PBS.
4. Coat a 96-well microplate with 100 µl per well of the diluted Capture Antibody using a multi-channel pipette.
5. Seal the plate and incubate overnight at room temperature.

Day 2:

6. Ensure that all reagents are equilibrated to room temperature before using.
7. Aspirate each well with Wash Buffer using a squirt bottle, by filling each well fully and decanting on a kimwipe until dry. Repeat 3 sets of washes.
8. Block plates by adding 300 µl of Reagent Diluent to each well. Incubate at room temperature for 1 hour.
    a. During this incubation, prepare samples for testing. Volumes can be diluted in reagent diluent so that they have volumes sufficient to add 100 uL to each well if required. For skeletal muscle lysates, 6-fold dilution lysates were added directly without diluting further due to low abundance of proteins.
    b. Prepare standard curve using the provided IL-1β standard using a standard serial dilution. The final well in the standard should contain only reagent diluent as a negative blank. Standard curve should be prepared last, as it needs to be added with minimal delay.
9. Repeat aspiration as in step 7.
10. Add 100 µl of sample and standards per well. Cover with an adhesive plate sealer and incubate for 2 hours at room temperature.
    a. During this incubation, dilute the Detection Antibody to the working concentration using reagent diluent.

11. Repeat the aspiration as in step 7.
12. Add 100 µl of the Detection Antibody to each well. Cover with a new adhesive strip and incubate for 2 hours at room temperature.
    a. During this incubation, dilute the Streptavidin-HRP to the working concentration in Reagent Diluent.
13. Repeat the aspiration as in step 7.
14. Add 100 µl of the working dilution of Streptavidin-HRP to each well. Cover the plate and incubate for 20 minutes at room temperature. Avoid placing the plate in direct light.
15. Repeat the aspiration as in step 7.
16. Add 100 µl of Substrate Solution (1:1 mixture of hydrogen peroxide and tetramethyl benzadine) to each well. Incubate for 20 minutes at room temperature. Avoid placing the plate in direct light.
17. Add 50 µl of Stop Solution to each well. Gently tap the plate to ensure thorough mixing and no bubbles.
18. Determine the optical density of each well immediately, using a microplate reader set to 450 nm and 570nm. To correct for optical imperfections in the place, subtract readings at 570 nm from the readings at 450 nm.
19. Correct these values to the blank well to obtain the final values used for interpolation.
20. Following interpolation, correct the samples by their dilution factors to obtain the final quantity of IL-1β.

gDNA Extraction from Cytosolic and Whole Muscle Extracts

Reagents

- All reagents were included in the Qiagen DNeasy Blood and Tissue Kit (cat #: 69504)
- All Eppendorf tubes and supplies should be sterile. In between steps, ensure to sterilize surfaces, pipettes and gloves with 70% ethanol.

gDNA isolation from frozen tissue

1. Allow frozen tissue to equilibrate to room temperature before starting.
2. Cut up to 25mg of tissue into small pieces using a glass plate and small surgical scissors, and place in a sterile 1.5 ml Eppendorf tube.
3. Add 180µl of Buffer ATL and 20µl of Proteinase K and vortex until thoroughly combined.

4. Incubate the tubes in a water bath at 56ºC for 1 hour and 20 minutes. During incubation, ensure to vortex tubes approximately every 20 minutes to aid in lysis.
5. Vortex samples for 15 seconds.
6. Add 200µl of Buffer AL and absolute ethanol to each tube, and mix thoroughly with vortex.
    a. Note: A white precipitate may form following the addition of the ethanol, which will not interfere with the DNA extraction.
7. Pipet mixture from step 6 into the provided DNeasy spin column placed in a 2ml collection tube (including any white precipitate that may have formed)
8. Centrifuge at 6000g at room temperature for 1 minute.
9. Discard the flow-through in the collection tube and replace with a 2ml collection tube.
10. Add 500µl of Buffer AW1 to the spin column, and centrifuge at 6000g at room temperature for 1 minute.
11. Discard flow-through as indicated in step 9.
12. Add 500µl of Buffer AW2 to the spin column and centrifuge at 20000g at room temperature for 3 minutes to get rid of any excess ethanol.
    a. When removing the column, ensure it does not come in contact with any of the flow-through. If this occurs, centrifuge for an additional minute at 20000g before continuing.
13. To elute DNA, pipet 120µl of Buffer AE directly onto the membrane, and allow it to sit for 1 minute at room temperature.
14. Centrifuge at 6000g at room temperature for 1 minute to elute DNA.
15. Store extracted DNA at -20ºC until later analysis.

gDNA isolation from cytosolic fractions

1. Combine 200µl of cytosolic fraction with 20µl of Proteinase K and 200µl of Buffer AL.
2. Incubate the tubes in a water bath at 56ºC for 10 minutes.
3. Add 200µL of absolute ethanol and mix by vortex.
4. Repeat steps 7-9 as described in the gDNA isolation from frozen tissue.
5. To elute DNA, pipet 60-70µl of Buffer AE directly onto the membrane and allow it to sit for 1 minute.
6. Repeat steps 14-16 as indicated in the gDNA isolation from frozen tissue.

7. Store at -20ºC until further analysis.

REAL-TIME qPCR

Reaction settings:
• 25µL reaction volume.
• Initial holding stage (95°C for 10 min).
• Amplification cycles (40x: 60°C for 1 min, 95°C for 15 secs).

HIGH-RESOLUTION RESPIROMETRY AND ROS EMISSION IN PERMEABILIZED FIBERS

Reagents:

1. Buffer Z, for 500ml:
   a. 105mM K-MES; 12.26g
   b. 30mM KCl; 1.12g
   c. 10mM KH_2PO4; 0.7g
   d. 5mM $MgCl_2 \cdot 6H_2O$; 0.51g
   e. 1mM EGTA; 0.19g
   f. 5mg/ml BSA; 2.5
   pH 7.4; Store at -20°C

2. BIOPS Buffer, for 1L:

   a. 2.77mM CaK_2EGTA; 27.7ml
   b. 7.23mM K_2EGTA; 72.3ml
   c. 5.77mM Na_2ATP; 3.14g
   d. 6.56mM $MgCl_2 \cdot 6H_2O$; 1.335g
   e. 20mM Taurine; 2.51g
   f. 15mM Na_2Phosphocreatine; 3.825g
   g. 20mM Imidazole; 1.36g
   h. 0.5mM Dithiothreitol (DTT); 0.077g
   i. 50mM MES Hydrate; 9.76g
   pH 7.1; Store at -20°C

3. Permeabilization Buffer
   a. BIOPS Buffer; 1.5ml
   b. Saponin (10mg/ml); 6µl
   c. 10.5mM CDNB; 5µl

4. Amplex Ultra Red Buffer
   a. Buffer Z; 1.5mL
   b. 5mM AUR; 650µL
      i. 666.6µL DMSO
      ii. 1mg AUR
   c. 5000IU/ml SOD1; 1625µl
      i. pH 7.0

d. 10mM BLEB; 32.5µl
e. 0.5M EGTA
    i. pH 7.5-8.0
f. Store in black 5ml tubes at -20°C.

5. Horseradish peroxidase; 0.5U/mL (HRP)
    a. Store at -20ºC.

6. 0.1µM H_2O_2

7. Pyruvate (P2256, Sigma)
    a. 27.5mg/125µl
    b. Make fresh each day

8. Malate (M1000, Sigma), for 10ml stock:
    a. 1.073g
    b. pH 7.1
    c. Store at -20°C

9. ADP (A2754, Sigma), for 10ml stock:
    a. 2.13g
    b. pH 7.1
    c. Store at -20°C

10. Succinate (S2378, Sigma), for 10ml stock:
    a. 2.7014g
    b. pH 7.1
    c. Store at -20°C

Procedure:

1. Collect medial portion of the TA and store in ice cold BIOPS Buffer

2. Gently tease apart muscle fibers with fine-tip forceps in BIOPS Buffer over ice

3. Place bundles in Permeabilization Buffer and permeabilize on orbital for 30 mins at 4°C

4. Transfer bundles to Eppendorf with Buffer Z and wash for 7.5mins

5. Transfer bundles to another Eppendorf with Buffer Z and was for 7.5 mins

6. Measure wet weight muscle bundle (~2-5mg)

7. Set up experiment using O2K

    a. Set up chamber by rinsing with 3x ddH_2O then 1x 70% EtOH. Repeat 3 times ending with ddH_2O. Remove all liquid with suction

b. Add 3x710ul AUR Buffer into the chamber and close part-way

c. Wait for oxygen reading to level out and adjust for background detection

d. Add 1ul BLEB to chamber with p10

e. Stop stir bar and add muscle bundle

f. Close chamber part-way and start stir bar

g. Add 50ml O_2 and close chamber fully for an O_2 reading of ~380

h. Once O_2 stabilizes, turn on fluorescence

i. Add 4ul HRP

j. Calibrate ROS signal

8. Run experiment

a. Add 5ul pyruvate and 5ul malate to the chamber and wait until O_2 levels stabilize

b. Add 20ul ADP to the chamber and wait until O_2 levels stabilize

c. Add 20ul succinate to the chamber and wait until O_2 levels stabilize

APPENDIX D: OTHER CONTRIBUTIONS TO LITERATURE

Peer-Reviewed Publications

1. Wong, J., Oliveira, A., **Khemraj, P**., & Hood, D.A. (2023). The Role of TFE3 in Mediating Skeletal Muscle Mitochondrial Adaptations to Exercise Training. *Journal of Applied Physiology. (DOI: 10.1152/japplphysiol.00484.2023)*

2. Slavin, M.B., **Khemraj, P.,** & Hood, D.A. (2023). Exercise, mitochondrial dysfunction and inflammasomes in skeletal muscle. Biomedical Journal (DOI: 10.1016/j.bj.2023.100636)

Presentations and Published Abstracts

1. **Khemraj, P.,** Hood, D.A. (July 2024). NLRP3 Inflammasome signaling is responsive to skeletal muscle mitochondrial perturbations following muscle use and disuse. [Poster Presentation]. International Biochemistry of Exercise Conference, 2024. University of Limerick, Ireland.

2. Kuznyetsova, A., Sanfrancesco, V. C., **Khemraj, P**., & Hood D.A. (May 2024). The effects of Aging on Mitochondrial Stress Responses in Skeletal Muscle Following Acute Exercise. [Poster Presentation]. Muscle Health Awareness Day, 2024. York University, Toronto, ON.

3. **Khemraj, P**., Sanfrancesco, V. C., Oliveira, A. N., Gorman, R. A., Backx, P. H., & Hood, D. A. (May 2024). [Published abstract] Impact of chronic muscle use and disuse on innate immune signaling in skeletal muscle. Physiology (39). (DOI:10.1152/physiol.2024.39.S1.1289)

4. **Khemraj, P.,** Sanfrancesco, V. C., Oliveira, A. N., Gorman, R. A., Backx, P. H., & Hood, D. A. (April 2024). [Poster Presentation] American Physiological Summit, 2024. Long Beach, CA, United States.

5. **Khemraj, P.,** Sanfrancesco, V. C., Oliveira, A. N., Gorman, R. A., Backx, P. H., & Hood, D. A. (October 2023). Effect of Denervation and Exercise Training on NLRP3 Inflammasome Activation in Skeletal Muscle. [Poster Presentation] CSEP. Journal of Applied Physiology, Nutrition and Metabolism. In Press, 2023. Calgary, Alberta, Canada.

6. **Khemraj, P.,** Sanfrancesco V.C., Oliveira A.N., Gorman, R.A., Backx, P., & Hood D. A. (July 2023). The Relationship between Mitochondria and NLRP3 Inflammasome signaling following Denervation and Exercise Training in Skeletal Muscle. [Oral Presentation] Ontario Exercise Physiology Conference. Kingston, ON.

7. **Khemraj, P**., Sanfrancesco V.C., Oliveira A.N., Gorman, R.A., Backx, P., & Hood D. A. (May 2023). Investigating NLRP3 Inflammasome Activation in response to Chronic Denervation and Exercise Training. [Poster Presentation]. Muscle Health Awareness Day, 2023. York University, Toronto, ON.